universität wien

DISSERTATION / DOCTORAL THESIS

Titel der Dissertation /Title of the Doctoral Thesis

„Characterizing the role of Toddler signaling during zebrafish gastrulation“

verfasst von / submitted by

Jessica Stock, B.Sc. MRes

angestrebter akademischer Grad / in partial fulfilment of the requirements for the degree of

Doctor of Philosophy (PhD)

Wien, 2022

Studienkennzahl lt. Studienblatt / degree programme code as it appears on the student record sheet:	UA 794 685 490
Dissertationsgebiet lt. Studienblatt / field of study as it appears on the student record sheet:	Molekulare Biologie
Betreut von / Supervisor:	Dr. Andrea Pauli

“It is not birth, marriage, or death, but gastrulation which is truly the most important time in your life.”

- Lewis Wolpert

Acknowledgments

This work was only possible with the support of many people, that I would like to acknowledge here.
First and foremost, I would like to thank my supervisor, Andrea Pauli, for giving me the possibility to work in the Pauli Lab, and for trusting me to continue her postdoctoral work and seeing it through to the end. Thank you, Andi, for providing me with a little gastrulation corner in the lab, for your continuous enthusiasm, for giving me endless opportunities to explore and present this project, and for supporting me every step of the way to becoming an independent and confident scientist.
Thank you to the wonderful people in the Pauli Lab, past and present, that have filled every day with joy, support, and wonderfully diverse science. In particular, I would like to thank Krista Gert, for being the Bouncer to my Toddler. Thank you for being by my side for the last 5 years, for making every morning in the injection room the best part of the day and for being a wonderful friend. Thank you to Karin Panser and Victoria Deneke, for being the most supportive and genuine friends anyone can hope for, in and outside of the lab.
A big thank you goes to the collaborators on this project and the support I had in the scientific community. I would like to thank Edouard Hannezo, who has been essential to this project, for his expertise and support along the way. Thank you to the Heisenberg lab, in particular Diana Pinheiro, for our joint lab meetings, their input, and enthusiasm about the project. Thank you to all the VBC core facilities on campus, in particular the BioOptics facility, without whom this project would not have been possible.
A special mention goes to all the people that managed to pull me out of the scientific bubble, whenever needed. Thank you, Paco, for there throughout the highs and lows of the PhD, for always finding the right thing to say and for filling my life with joy, laughter, and music. Thank you to Sandra, Steffi and Anthony, for all the phone calls and voice notes that made me feel connected to home, even when far away.
Thank you to my grandparents for filling my childhood with books, stories and knowledge about plants and nature, that sparked my love for science.
Finally, thank you to my parents. Mum, dad, this would not have been possible without you. Your never-ending support throughout life is how I made it this far. Thank you for always believing in me and making me believe that I can do whatever I set my mind to. Thank you for everything.

Table of Contents

Abstract

The process of gastrulation is essential for the specification and assembly of germ layers during embryonic development and depends on the coordination of directed cell migration. In gastrulating zebrafish embryos, mesodermal progenitors are specified at the margin and then undergo directed migration to the animal pole. While the main regulators of mesoderm specification have been identified, the molecular mechanisms underlying mesoderm guidance have remained a mystery.

The most commonly known mechanism to guide directional cell migration is chemotaxis based on chemokine gradients that arise from a localized source. In contrast to this idea, I found that mesoderm migration is guided by a self-generated gradient of the small protein Toddler/Apela/ELABELA, and that the gradient formation is coordinated by its own receptor, the Apelin receptor (Aplnr), which is expressed in the responding mesodermal cells. In this thesis I show that Toddler acts as a chemoattractant for Aplnr-expressing cells, yet the rescue of mesoderm migration defects in *toddler* mutants is independent of the site of Toddler expression. To reconcile these seemingly contradicting results, we combined computational modeling and experimental approaches to show that (i) the location of the Aplnr-mediated sink, not the Toddler source, determines direction of mesoderm migration, (ii) a collective of Aplnr-expressing cells, but not an individual cell, can undergo directed migration in a uniform Toddler environment, and (iii) Aplnr takes on a dual role by providing a sink for Toddler and sensing the self-generated gradient to drive mesoderm migration.

Taken together, this work provides a compelling explanation for the long-standing question of how mesodermal cells are directed to the animal pole during zebrafish gastrulation. This mechanism of a self-generated gradient, in which generation and reading of the guidance cue are mediated by a single receptor, provides a simple yet robust mechanism for mesodermal cells to steer their own directional migration.

Zusammenfassung

Der Prozess der Gastrulation ist essenziell für die Spezifizierung und Anordnung der Keimblätter während der Embryonalentwicklung. Insbesondere die räumliche Organisation der Keimblätter ist von kontrollierten und gerichteten Zellbewegungen abhängig. Während der Gastrulation in Zebrafischembryonen werden die Vorläufer der Mesodermzellen am Rand des Blastoderms spezifiziert und migrieren anschließend zum Animalpol. Obwohl die primären Regulatoren der Mesodermspezifizierung bereits identifiziert sind, sind die molekularen Mechanismen, die die gerichtete Zellbewegung des Mesoderms dirigieren, noch weitgehend unbekannt.

Es wurde lang angenommen, dass gerichtete Zellbewegungen durch Chemokingradienten dirigiert werden, die von einer lokalen Chemokinquelle ausgehen. Jedoch zeige ich hier, dass die Migration des Mesoderms durch einen selbstgenerierten Gradienten des kleinen Proteins Toddler/Apela/ELABELA dirigiert wird und die Entstehung dieses Gradienten durch den Apelin Rezeptor (Aplnr) koordiniert wird, der spezifisch in Mesodermzellen exprimiert wird. In dieser Doktorarbeit zeige ich einerseits, dass Toddler als ein Chemokin für Aplnr-exprimierende Zellen wirkt, jedoch andererseits, dass die gerichtete Bewegung von Mesodermzellen im Embryo unabhängig von der Lage der Toddler-Quelle ist. Durch die Anwendung von numerischen Simulationen in Kombination mit Experimenten vereinbaren wir diese, auf den ersten Blick widersprüchlichen Resultate und zeigen, dass (i) die Lage des Chemokin-Fängers (Aplnr) und nicht der Chemokin-Quelle (Toddler) die Richtung der Zellbewegung definiert, (ii) ein Kollektiv an Aplnr-exprimierenden Zellen, jedoch nicht eine einzelne Zelle, in der Lage ist sich effektiv und gerichtet in einer homogenen Toddler-Umgebung zu bewegen, und (iii) Aplnr eine doppelte Aufgabe hat, indem der Rezeptor einerseits als Chemokin-Fänger für Toddler agiert und andererseits als Chemokinrezeptor den selbstgenerierten Gradienten erkennt und die gerichtete Bewegung führt.

Zusammenfassend liefert diese Arbeit eine überzeugende Antwort auf eine offenstehende Frage in der Entwicklungsbiologie: Wie ist die gerichtete Bewegung von Mesodermzellen während der Gastrulation in Zebrafischembryonen auf einer molekularen Ebene reguliert? Der hier beschriebene Mechanismus eines selbstgenerierenden Chemokingradientens, bei dem die Entstehung und das Erkennen des Gradientens durch ein und denselben Rezeptor ausgeführt wird, bietet einen einfachen jedoch robusten Mechanismus, durch den Mesodermzellen ihre eigene Migration steuern können.

1. Introduction

1.1. Gastrulation

1.1.1. Universal concepts of gastrulation

At the beginning of development, an embryo consists of undifferentiated cells that were established through several rounds of cell cleavages after fertilization. To give rise to a fully functional, multicellular organism, these undifferentiated blastomeres are subsequently specified and shaped into three different germ layers. This process is called gastrulation and is characterized by two major events: cell specification and cell migration. While specific details differ between species, the fundamental signaling mechanisms and cell movements are conserved across the animal kingdom.

The specification of the three germ layers as well as patterning of the body axes is mediated by morphogen gradients. The most important morphogen signals during vertebrate gastrulation are canonical Wnt signaling, which initiates the formation of the dorsal organizer shortly after fertilization (Hikasa and Sokol, 2013; Schneider et al., 1996), BMP signaling, which is responsible for dorsoventral patterning (Dosch et al., 1997; Neave et al., 1997; Zinski et al., 2018), and Nodal signaling, the master regulator of mesodermal and endodermal germ layer induction (Conlon et al., 1994; Schier and Shen, 2000). The Nodal signaling pathway is highly conserved and has been extensively studies over the past decades. The segregation between mesodermal and endodermal cell fate, however, remains poorly understood (Kotkamp et al., 2014; Zhang and Klymkowsky, 2007).

Cell migration is required to spatially arrange the germ layers in a characteristic manner. The prospective ectoderm is the outermost layer of the future embryo, eventually forming the epidermis and building the nervous system. The mesodermal and endodermal germ layers move beneath the ectoderm before being shaped along the dorsoventral and anteroposterior axis. As the middle layer, mesoderm is situated between the ectoderm and endoderm and will give rise to muscles and the cardiovascular system, while the endoderm, the innermost layer, builds the foundation for the gastrointestinal, respiratory, and endocrine systems (Solnica-Krezel, 2005; Solnica-Krezel and Sepich, 2012). These spatial arrangements are achieved through three conserved morphogenetic cell movements. (1) Epiboly drives the isotropic thinning and spreading of tissues and is responsible for blastopore closures in the classic examples of zebrafish and *Xenopus*. (2) Emboly moves prospective mesodermal and endodermal cells beneath the overlaying ectoderm. This internalization can be achieved either through invagination, the folding of a coherent sheet of mesendodermal progenitor cells into the embryo (e.g., *Drosophila*), involution, the “rolling” of a mesodermal cells sheet into the embryo like a conveyer belt (e.g. *Xenopus*), or ingression, the autonomous and individual migration of

cells into the embryo after they have broken away from the overlying epithelium (e.g. amniotes). (3) Convergence and extension (C&E) narrow and elongate the tissue, respectively, which shapes the germ layers along the different body axes (Solnica-Krezel, 2005; Solnica-Krezel and Sepich, 2012).

1.1.2. Germ layer specification in zebrafish

1.1.2.1. Mesoderm and endoderm

Embryonic patterning of germ layers and body axes is achieved through morphogen signals. As mentioned above, Nodal signaling is the main determinant of germ layer specification in vertebrates. In zebrafish, the Nodal ligands Cyclops and Squint, which are initially expressed in the yolk syncytial layer (YSL) (Chen and Kimelman, 2000; Fan et al., 2007; Hong et al., 2011) and dorsally in the future embryonic shield (Dougan et al., 2003; Feldman et al., 1998), bind to a triple-receptor complex comprised of Activin receptors type I and II as well as the co-receptor Oep (Figure 1) (Gritsman et al., 1999; Reissmann et al., 2001; Schier et al., 1997; Zhang et al., 1998). Activation of the receptor complex leads to the phosphorylation of Smad2/3 and its subsequent association with Smad4 and other transcription factors. Upon translocation to the nucleus, this complex induces the expression of Nodal target genes (Attisano and Wrana, 2002; Jia et al., 2008; Shi and Massagué, 2003), including the Nodal ligands themselves (Chen and Schier, 2002; Juan and Hamada, 2001), Nodal inhibitors Lefty1 and Lefty2 (Chen and Schier, 2002; Hagos and Dougan, 2007; Juan and Hamada, 2001; Meno et al., 1999) as well as germ layer specific markers, such as *goosecoid (gsc)*, *t-box transcription factor t (tbxt)* and *sox32* (Figure 1) (Dougan et al., 2003; Hagos and Dougan, 2007; Jia et al., 2008; Thisse et al., 1994; Thisse et al., 2000).

The Nodal signaling gradient arises at the blastoderm margin adjacent to the YSL and extends over a range of 6 to 10 cell tiers towards the animal pole to define mesendodermal progenitors (Figure 1) (Chen and Schier, 2002). How the Nodal signaling domain is established, though, remains the subject of ongoing research. It is thought to be generated through a reaction-diffusion patterning system (Almuedo-Castillo et al., 2018; Chen and Schier, 2002; Gierer and Meinhardt, 1972; Juan and Hamada, 2001). Nodal ligands are initially expressed and secreted by the YSL, but as Nodal induces the expression of its own ligands in adjacent cells the signaling range extends. Due to their low diffusivity, Nodal ligands act as local activators over a short range. Meanwhile, the concomitant Nodal-induced expression of rapidly diffusing Nodal inhibitors Lefty1 and Lefty2 leads to a long-range inhibition of Nodal signaling in regions closer to the animal pole (Müller et al., 2012). However, this model continues to be questioned and adjusted. Technological advances over recent years hinted at more

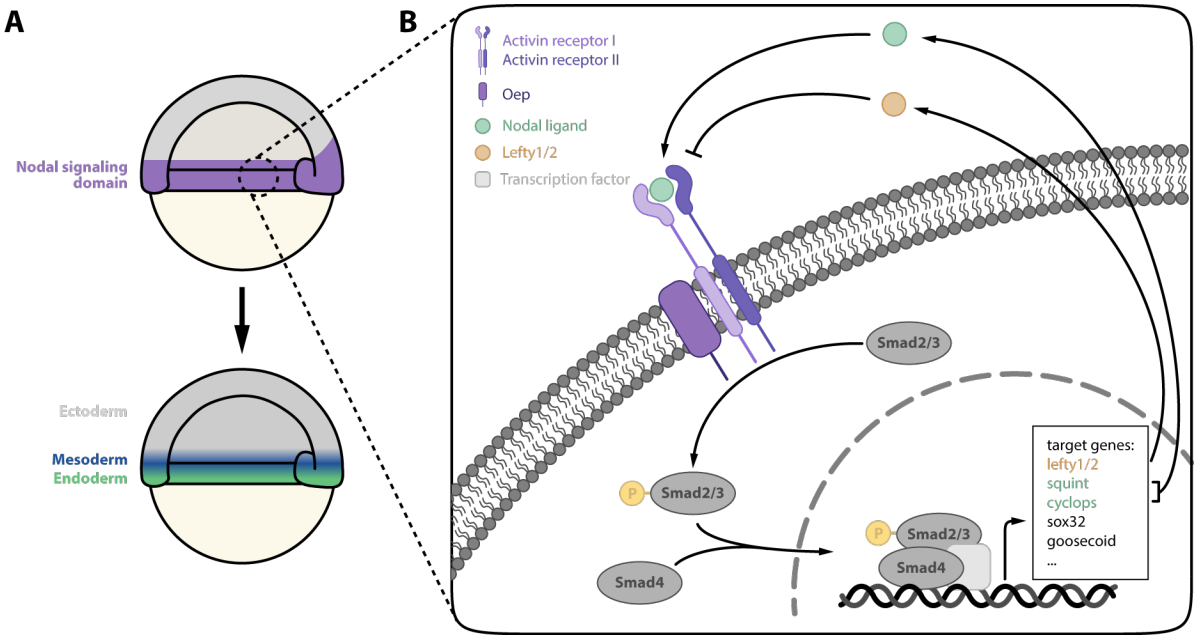

Fig. 1 | Schematic of Nodal signaling in the zebrafish embryo. (A) Nodal ligands are secreted from the YSL, which establishes the Nodal signaling domain from the margin spanning 6 to 10 cell tiers towards the animal pole, where it induces the specification of the endodermal and mesodermal germ layers. (B) Nodal ligands signal through a triple-receptor complex (Activin receptors type I/II and the co-receptor Oep), which leads to the phosphorylation of Smad2/3, which in association with Smad4 induces the expression of Nodal target genes, including Nodal ligands (Cyclops and Squint) and Nodal inhibitors (Lefty1/2).

complex mechanisms, with the duration of Nodal signaling, a time delay in Nodal inhibitor expression and additional regulatory factors and mechanisms influencing the Nodal signaling range and germ layer specification (Dubrulle et al., 2015; Hagos and Dougan, 2007; Lord et al., 2021; Montague and Schier, 2017; van Boxtel et al., 2015). Furthermore, it remains to be understood how Nodal signaling separates mesodermal and endodermal cell fates. While this is still subject of ongoing research, the duration of exposure to Nodal signaling has been implicated to play a significant role during germ layer segregation (Hagos and Dougan, 2007). Nodal signaling is initiated at the margin and expands over time, consequently cells closest to the margin receive a higher and longer exposure to Nodal signaling than cells further away from the margin. This correlates with marginal cells primarily giving rise to the endodermal lineage, while the mesodermal cells arise further away from the margin (Figure 1A). In fact, recent research has revealed that prolonged Nodal signaling at the margin leads to the expression of Fgf ligands and Dusp4. Secreted Fgf ligands act over a long range and were shown to induce mesodermal cell fate, while Dusp4 only acts in marginal cells to inhibit Fgf signaling locally, therefore promoting the endodermal lineage close to the margin (van Boxtel et al., 2018).

1.1.2.2. Ectoderm

In contrast to mesoderm and endoderm, the ectoderm is often considered as the default cell state, that forms when Nodal signaling is absent or actively inhibited and therefore arises at the animal pole

of the zebrafish embryo (Ho and Kimmel, 1993; Kotkamp et al., 2014; Zhang and Klymkowsky, 2007). In fact, block of mesoderm specification leads to the expansion of the ectodermal domain (Feldman et al., 2000; Gritsman et al., 1999; Thisse et al., 2000). Nonetheless, towards the end of gastrulation the ectoderm is patterned into neural and non-neural ectoderm, which does require the activity of other morphogens including BMP, Fgf, RA and Wnt signaling (Schier and Talbot, 2005).

1.1.3. Gastrulation movements in zebrafish

1.1.3.1. Epiboly

At the beginning of gastrulation, the embryo proper of a zebrafish is located on top of the yolk and consists of three layers: a superficial enveloping layer (EVL), a multilayer array of loosely packed deep cells (blastomeres) and a yolk syncytial layer (YSL) located between the blastomeres and the yolk (Kimmel et al., 1995). During epiboly all three layers spread out towards the vegetal pole until the blastopore is closed and the yolk is fully engulfed by the embryo (Kimmel et al., 1995).

Even though the movements of EVL, YSL and blastomeres occur concomitantly, each of them undergoes epiboly independently and is regulated by distinct mechanisms. While epiboly of the EVL is partially driven by being passively pulled towards the vegetal pole through its tight connection to the YSL (Heisenberg and Bellaïche, 2013), the flattening and division of EVL cells along the animal-vegetal pole axis partially releases the tension created by the pulling force of the YSL and further supports spreading of the EVL (Figure 2) (Campinho et al., 2013; Xiong et al., 2014). Epiboly of the YSL in turn is accomplished by actomyosin contractility (Figure 2). At approximately 40% epiboly an actomyosin band forms within the YSL spanning the entire circumference of the embryo. Retrograde actin flow within the YSL establishes a force to pull the YSL margin towards the vegetal pole, while actomyosin contractility additionally contributes to the blastopore closure once epiboly has surpassed 50% (Behrndt et al., 2012; Cheng et al., 2004). Epiboly of the blastoderm is triggered during the final synchronous cell cycles, when central, but not marginal blastomeres lose their viscosity in a Wnt11-dependent manner (Petridou et al., 2019), allowing the underlying yolk to dome upwards (Figure 2). The external force of the doming yolk and the tension created by the overlaying EVL pushes the blastomeres to undergo radial intercalation of deep cells into more superficial layers (Bensch et al., 2013; Kimmel et al., 1995; Morita and Heisenberg, 2013), which results in the thinning and extension of the cell cap towards the vegetal pole.

1.1.3.2. Emboly

At approximately 50% epiboly, emboly movements are initiated, which drive the internalization of mesendodermal progenitors at the margin to move beneath the prospective ectoderm and form the hypoblast (Figure 2). The onset is marked by the appearance of the germ ring, a thickening along the

margin that is formed as movement of the most vegetally located cells starts to slow down in preparation of their internalization (Keller et al., 2008; Kimmel et al., 1995; Rohde and Heisenberg, 2007). The inwards movement of mesendoderm is first initiated at the dorsal side, marked by the formation of the embryonic shield (Montero et al., 2005), and subsequently extends towards the most ventral regions. The mode of internalization in zebrafish embryos can be described as synchronized ingression as mesendodermal progenitors internalize autonomously as individual cells but do so in a highly coordinated and synchronized manner (Keller et al., 2008).

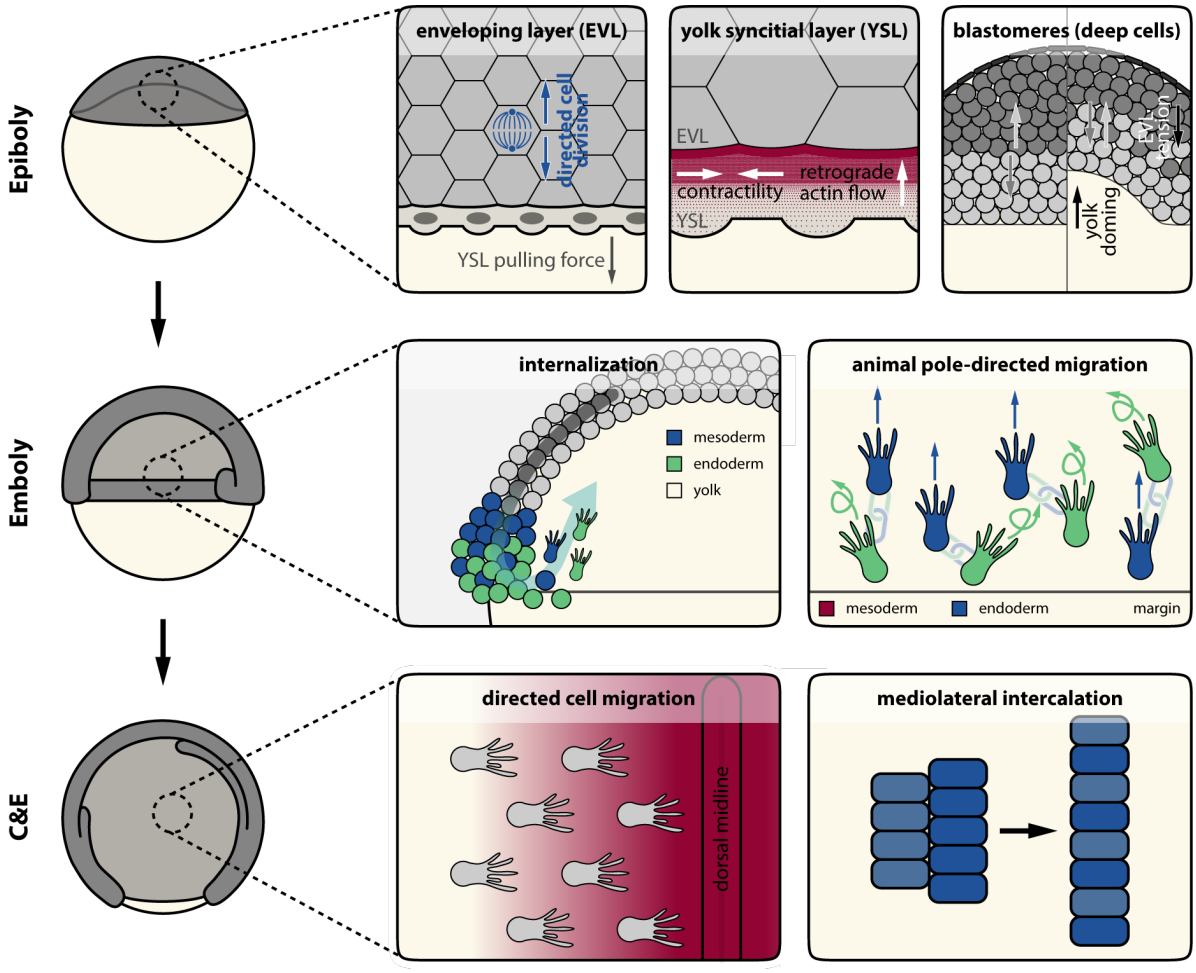

Fig. 2 | Gastrulation movements in the zebrafish embryo. During epiboly, which is driven by directed cell division (EVL), actomyosin contractility (YSL) and radial intercalation (blastomeres), the embryonic cells spread across the yolk until the blastopore is closed at the vegetal pole. Emboly sets in at 50% epiboly with mesendodermal progenitors internalizing at the margin and migrating towards the animal pole. At 70% epiboly convergence and extension (C&E) movements drive narrowing of the germ layers along the dorsoventral axis and stretching along the anteroposterior axis through directed cell migration and mediolateral intercalation.

Unlike for cell specification, the molecular drivers that initiate and direct internalization of mesendodermal progenitor cells are largely unknown. As the master regulator of germ layer specification, Nodal has long been suspected to play a role in their spatial organization as well. However, while Nodal signaling-deficient *MZoep* mutant embryos lack cell internalization, they also

lack mesendodermal progenitors entirely, precluding the analysis of Nodal's role in internalization. In support of a cell specification-independent role during emboly, Nodal has been suggested to be involved in cell internalization by inducing the expression of cytoskeletal remodeling factors, such as Ezrin or Fascin, and regulating endocytosis and recycling of E-Cadherin (Diz-Muñoz et al., 2010; Giger and David, 2017; Krieg et al., 2008; Ogata et al., 2007), that could influence cell-cell contact formation. However, its exact involvement in cell internalization remains to be fully understood. On the other hand, Nodal receptor-deficient cells have been shown to be able to internalize at the margin when placed in a wild-type embryo, albeit afterwards not contributing to the hypoblast or engaging in animal pole-directed migration (Carmany-Rampey and Schier, 2001). This indicates the presence of additional, Nodal-independent, and so far elusive mediators of cell internalization as well as directional cues to guide mesendodermal cells to the inside of the embryo.

After successful internalization mesendodermal progenitors migrate away from the margin (Keller et al., 2008; Kimmel et al., 1995). The mode and regulation of animal-pole directed migration differs greatly between the germ layers and areas of the embryo. Canonical Wnt signaling induces the formation of the embryonic shield and the dorsal side. Additionally, it was implicated to also be involved in the migration of dorsal mesendodermal progenitors to the animal pole, both in an instructive and a permissive function. In an instructive role, Wnt signaling through ligand Wnt5b can induce the directed polarization and protrusion formation as a chemorepellent (Kilian et al., 2003; Lin et al., 2010). In a permissive role, Wnt11 is involved in regulating the dynamics of E-Cadherin-based adhesions (Čapek et al., 2019; Ulrich et al., 2003; Ulrich et al., 2005). The axial mesoderm migrates as a coherent sheet of mesenchymal cells. E-Cadherin based adhesions between cells and their posterior neighbors are required to establish a directional front-rear polarity and protrusion formation in the leading cells, while they need to be released for the cell to move forward. Through the interaction with Rab5, Wnt11 influences the dynamic endocytosis, recycling, and establishment of E-Cadherin-based adherens junctions to enable efficient and directional migration towards the animal pole (Diz-Muñoz et al., 2010; Heisenberg et al., 2000).

Ventrally internalizing progenitors are characterized by two distinct migration patterns (Figure 2). Endodermal progenitors spread across the embryo cap in a random, non-directional migration pattern (Keller et al., 2008). Their unconstrained expansion, however, is contained by the overlying mesoderm. The endoderm expresses the G protein-coupled receptor Cxcr4a, that binds the mesoderm-secreted ligand Cxcl12b. Cxcr4a activity increases the levels of Integrin β-1, which tethers the endoderm to the extracellular matrix through its interaction with fibronectin (Nair and Schilling, 2008). Mesodermal progenitor cells, on the other hand, display a directional migration with cells clearly polarized towards the animal pole (Keller et al., 2008; Row et al., 2011). The nature of the molecular mechanisms driving

the directional migration of mesodermal cells has been one of the biggest open questions of zebrafish gastrulation that remained to be solved. While several mechanisms, including chemoattractant signals at the animal pole, self-organizing principles, and mechanical forces could in principle be responsible for the observed directional migration, direct experimental evidence has been lacking. The discovery of Toddler (Chng et al., 2013; Pauli et al., 2014), a short and secreted protein (further discussed below) that is essential for the migration of mesodermal cells, has provided a new lead towards understanding this mechanism. The investigation of the Toddler-mediated mechanisms guiding mesodermal cell migration is the subject of this thesis.

1.1.3.3. Convergence and extension

At approximately 70% epiboly convergence and extension (C&E) movements are initiated to narrow the germ layers along the dorsoventral axis and extend them in anteroposterior direction (Figure 2) (Kimmel et al., 1995). While all germ layers undergo C&E to a certain extent, the most prominent active movements can be detected in the mesoderm. However, only dorsal and lateral mesendoderm converge, while ventral mesoderm does not undergo C&E after internalization and instead continues to move vegetally to contribute to blastopore closure and tail bud formation (Myers et al., 2002).

C&E is mainly driven through directional migration and planar cell polarity (PCP). Directional migration of the dorsal mesoderm contributes to extension of the tissue in anterior direction. As described above, anterior migration of axial mesoderm is driven by directional polarization and extension of actin-rich protrusions, mediated by the cell-cell contact to posterior neighbors (Diz-Muñoz et al., 2010; Heisenberg et al., 2000). In lateral mesoderm directional migration supports the convergence to the dorsal midline (Figure 2). Due to lower cell density on the ventrolateral side, lateral mesoderm undergoes individual cell migration and displays a clear front-rear polarity by extending actin-rich protrusions towards the dorsal midline (Diz-Muñoz et al., 2016; Sepich et al., 2005). The molecular mechanism driving this directional migration remains unclear. While such migratory behavior suggests the expression of a chemoattractant at the dorsal midline that can guide convergence of lateral mesoderm, the molecular factor(s) driving such a mechanism have yet to be identified.

PCP-mediated cell intercalation drives C&E in chorda- and presomitic mesoderm. Driven by non-canonical Wnt signaling (Heisenberg et al., 2000; Kilian et al., 2003), core components of the PCP signaling network are asymmetrically distributed within the cell (Ciruna et al., 2006; Roszko et al., 2015; Yin et al., 2008), which allows for the mediolateral intercalation of cells between their dorsal neighbors, separating them along the anteroposterior axis (Figure 2) (Yin et al., 2008). Given that intercalation of mesodermal cells between their neighbors still takes place even in the absence of PCP signaling with only the directional bias being lost, the main role of PCP is to provide a compass that

gives mesodermal cells the necessary directional information to elongate, align and extend protrusions towards the dorsal midline (Gray et al., 2011; Yin et al., 2008).

1.2. Toddler and Apelin receptor signaling

1.2.1. Identification of the Toddler/Aplnr signaling axis

The Apelin receptor (Aplnr) is a conserved seven transmembrane domain G protein-coupled receptor (GPCR) first described in human cells as Angiotensin II receptor-like 1 (Agtrl1). Despite its sequence similarity to Angiotensin II receptor, the ligand Angiotensin II did not bind to Aplnr, leaving Aplnr's endogenous ligand unknown, categorizing it as an "orphan" receptor (O'Dowd et al., 1993). However, a screen for orphan receptor ligands revealed Apelin, a 77 amino acid long secreted protein (55 amino acids in its mature form), to bind to Aplnr (Tatemoto et al., 1998). Due to genome duplication, zebrafish harbors two paralogues of this gene, *aplnra* and *aplnrb* (collectively referred to as *aplnr*). *Aplnrb* was first characterized as the gene mutated in the *grinch* mutant, which was discovered in a forward genetic screen, searching for mediators of cardiovascular development (Scott et al., 2007). The mutant name stems from the reduction in heart size, pericardial edema, and absence of cardiac progenitors observed in these larvae (Scott et al., 2007; Zeng et al., 2007). *Aplnra* and *aplnrb* are both zygotically expressed and peak during the time of gastrulation (Pauli et al., 2014). However, expression of *apelin* only sets in at the end of gastrulation (Pauli et al., 2014). These observations, together with a gastrulation phenotype in *aplnr* mutants that is absent in *apelin* mutants (further discussed below) already suggested the existence of an additional ligand binding to Aplnr.

Toddler/Elabela/Apela (for simplification referred to as Toddler throughout this thesis, unless indicated otherwise) is a short, secreted protein of only 36 amino acids in its mature form that was first identified in a screen for non-annotated, translated open reading frames (ORFs) during early development of zebrafish embryos (Pauli et al., 2014). Toddler was found to be highly conserved across vertebrates, with its C-terminus practically unchanged between different species (Figure 3) (Chng et al., 2013; Pauli et al., 2014). *Toddler* is a zygotically expressed gene, which peaks during gastrulation, and like *aplnr* mutants, *toddler* mutants show a strong gastrulation phenotype that is further discussed below, as well as severe defects in cardiovascular development (Figure 3): small or absent hearts, pericardial edema, and a lack of proper blood circulation, along with malformation and faulty left-right positioning of the liver and occasional posterior truncations (Chng et al., 2013; Pauli et al., 2014). These observations, together with the *in vitro* detection of Toddler binding to Aplnrb (Chng et al., 2013), revealed a functional connection between Toddler and Aplnr during gastrulation.

1.2.2. Functional implications of the Toddler/Aplnr signaling pathway

1.2.2.1. Migration of mesendodermal progenitors during zebrafish gastrulation

The potential causes for the cardiovascular phenotype in *aplnr* and *toddler* mutants are manifold. However, the expression peak during gastrulation of both the receptor and the ligand as well as the defective mesendodermal cell migration in both *aplnr* and *toddler* mutants suggested a role in gastrulation (Chng et al., 2013; Pauli et al., 2014). Instead of moving towards the animal pole after internalization, mesendodermal cells accumulate at the margin in mutant embryos (Figure 3). Interestingly, this phenotype is specific to lateral and ventral mesendoderm, while animal pole-directed migration on the dorsal side shows no defect in *toddler* mutants, further supporting the idea that dorsal and ventral emboly are mediated by different mechanisms. During the early phases of gastrulation *toddler* is expressed ubiquitously, and later on primarily by the ectoderm (based on scRNA-seq data (Farrell et al., 2018)), leading to its uniform distribution along the animal-vegetal and dorsoventral axis, while *aplnrb* is restricted to mesoderm and specifically enriched at the lateral and ventral side (Pauli et al., 2014; Scott et al., 2007; Tucker et al., 2007; Zeng et al., 2007). Not only is this in line with the ventrolateral-specific phenotype, but also suggests that Toddler mainly influences mesoderm migration. Indeed, recent results confirmed that the defect in endodermal cell migration in *toddler* mutant embryos is merely secondary due to the endoderm's connection to the mesoderm through Cxcr4a expression (Norris et al., 2017).

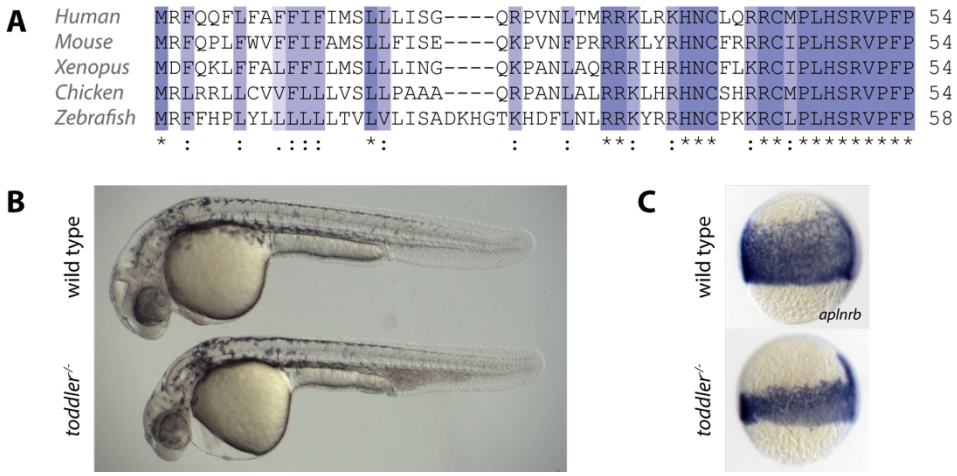

Fig. 3 | Toddler is a conserved protein essential for gastrulation. (A) Sequence alignment of full-length Toddler protein sequences in different vertebrates, highlighting the conservation of Toddler, in particular the C-terminus, across vertebrates (Pauli et al., 2014). (B) Wild-type and *toddler*$^{-/-}$ larvae 30 hpf. *Toddler*$^{-/-}$ larvae display an pericardial edema, blood accumulation in the tail and lack a functional heart. (C) Examples for *in situ* hybridization staining of wild-type and *toddler*$^{-/-}$ embryos against *aplnrb* (marking mesodermal cells). *Toddler*$^{-/-}$ embryos display a decrease in mesodermal spread towards the animal pole.

While these findings established Toddler and Aplnr as key mediators of animal-pole directed migration of mesodermal progenitors, how they function mechanistically has remained elusive. Intuitively, there

are two possible roles for Toddler that could explain the observed phenotype. Toddler could either act as a motogen that stimulates the migration of mesodermal cells without providing directionality, or Toddler could provide a chemoattractant signal at the animal pole that guides mesodermal cells. Based on the ubiquitous expression of *toddler* and experiments that suggested that directed mesoderm migration is independent of the Toddler source location, Toddler was suggested to act as a motogen and not provide a directional signal during gastrulation (Pauli et al., 2014). However, additional investigations of cardiovascular development at later developmental stages (further discussed below) have suggested Aplnr-expressing cells to be attracted by a source of the Toddler signal (Helker et al., 2015). Therefore, the mechanism of how Toddler stimulates migration of mesodermal cells during gastrulation on a molecular level has remained an open question and is subject to this thesis.

1.2.2.2. Nodal signaling and endoderm differentiation during zebrafish gastrulation

Cardiac progenitors, that will eventually form the heart and cardiovascular system, are derived from anterior lateral plate mesoderm that has internalized at the margin and migrated to the animal pole (Keegan et al., 2004). Therefore, the defect in mesendodermal cell migration alone could explain the defects of *toddler* and *aplnr* mutants in cardiovascular development. However, additional involvement of the Aplnr/Toddler signaling axis in cell specification cannot be excluded and research for and against this theory has been brought forward in recent years. In fact, the observation that *toddler* mutants display a 20% reduction in endodermal cells (Norris et al., 2017; Pauli et al., 2014) and that Aplnr was able to cell non-autonomously induce cardiac fate in neighboring cells (Paskaradevan and Scott, 2012) sparked the discussion of whether Aplnr, while being a Nodal target gene itself, could act with Toddler to promote Nodal signaling in a positive feedback loop and therefore be involved in cell fate determination.

Assessment of global mRNA expression in *aplnr* morphants indicated a reduced expression of one third of the Nodal signaling target genes, including *floating head*, *goosecoid* and *sox32*, while Aplnr overexpression increased the expression of Nodal target genes in wild-type embryos. In line with these observations, the elevation of Nodal signaling was sufficient to rescue the heart phenotype in *aplnr* mutants, suggesting Aplnr to be an upstream regulator of Nodal signaling (Deshwar et al., 2016). In contrast, a study by the Schier lab indicated Toddler signaling to act exclusively downstream of Nodal signaling. Following endoderm development through *in situ* hybridization assays indicated that initial endoderm specification in *toddler* mutants was unaffected and the reduction in endodermal cell population was more likely due to an increase in cell apoptosis (Norris et al., 2017). In further support, extensive experimental evidence, including *in situ* hybridization assays and RNAseq analysis to determine level and localization of Nodal target gene expression, showed no change in the level or

function of Nodal signaling in *toddler* mutants, nor did an increase of Nodal signaling rescue any aspect of the *toddler* mutant phenotype (Norris et al., 2017). These contradicting results could have multiple reasons. It was previously observed that the use of morpholinos can reveal phenotypes that are compensated in the corresponding mutants (El-Brolosy and Stainier, 2017; Sztal and Stainier, 2020). On the other hand, morpholinos are also prone to inducing unspecific toxicity or developmental delays (Nornes et al., 2009; Stainier et al., 2017), that could lead to differences in staging between the two studies. Ultimately, further research is required to disentangle the connection between the Toddler/Aplnr axis and Nodal signaling. However, at this point it cannot be excluded that Aplnr regulates Nodal signaling independent of Toddler.

1.2.2.3. The role of Toddler/Apela in other cell migration events

Despite its essential role during gastrulation in zebrafish, the continuous, albeit lower, expression of *toddler* and *aplnr* after gastrulation along with their conservation in other vertebrates, that do not display a gastrulation phenotype in the absence of TODDLER/APELA or APLNR/APJ (Freyer et al., 2017), suggests additional functions for Toddler and Aplnr signaling beyond gastrulation. Throughout the last years extensive investigations of Toddler/Aplnr signaling in zebrafish, mice and human have revealed their involvement in different processes centered mainly around cell specification and cell migration during cardiovascular development.

Once emboly is completed in zebrafish, cardiovascular progenitors must converge to the dorsal midline to commence cardiovascular development. Cardiac progenitors that will give rise to the heart are derived from the anterior axial mesoderm and after convergence form two bilateral heart fields that will eventually fuse to give rise to a single heart tube (Keegan et al., 2004). On the other hand, angioblasts, which will give rise to the vasculature, are derived from more posterior regions, and will converge to the midline via migration through the somites (Helker et al., 2015). In the later stages of gastrulation *toddler* expression becomes restricted to the future notochord (Pauli et al., 2014), similar to *apelin* expression that sets in at the end of gastrulation (Zeng et al., 2007). On the other hand, *aplnr* becomes enriched in adaxial lateral plate mesoderm and eventually restricted to the forming heart (Zeng et al., 2007). In line with these expression patterns, convergence of cardiac progenitors has been shown to be supported by the secretion of Toddler and Apelin at the midline, which was suggested to attract Aplnr-expressing cells in this context (Helker et al., 2015; Zeng et al., 2007). In posterior regions the lack of either Aplnr or Toddler/Apelin inhibits angioblasts from successfully reaching the midline. Interestingly, Toddler provides the main directional signal, while Apelin only plays a minor additive role (Helker et al., 2015). Whether the dominant role of Toddler is the same for anterior cardiac progenitors remains to be investigated. Taken together, this was a first indication that, contrary to the believe that the Toddler/Aplnr signaling axis stimulates cell migration in general, Aplnr could indeed

act as a chemokine receptor guiding cell migration towards a chemoattractant signal provided either by Toddler, Apelin or both.

Despite their high conservation among vertebrates, Toddler (in other vertebrates referred to as APELA) and APLNR (also referred to as APJ) seem to be neglectable for gastrulation in murine organisms. Nonetheless, *Apela* mutant mouse models show mild yet significant cardiovascular defects, including irregularities in heart looping and vascular remodeling, that lead to tissue hypoxia and reduced embryo survival (Freyer et al., 2017). Together with other studies, this work revealed that APELA is required at later stages of cardiovascular development. For example, after initial specification of angioblasts and formation of first blood vessels, angiogenesis is required to expand the vasculature throughout the body to provide blood circulation to the developing mouse heart muscle (Sharma et al., 2017). Blood vessels around the heart originate from two sources: the sinus venous (SV) at the dorsal side and the endocardium at the inside (Chen et al., 2014; Red-Horse et al., 2010). *Aplnr* is specifically expressed in the SV, but not the endocardium, while *Apela* can be detected in the epicardium, the outer layer of the heart. SV-derived coronary vessels are absent in *Aplnr* mutants, leading to the conclusion that APELA and APLNR are required for the growth of coronary vessels by mediating the migration of SV sprouts across the heart (Sharma et al., 2017). The underlying mechanism of how APELA drives vessel growth, though, remains to be investigated. In support of this angiogenic sprouting phenotype, studies in pregnant mice have revealed the importance of APELA in placental development (Ho et al., 2017; Wang et al., 2019). Angioblasts arise in the extraembryonic mesoderm and invade the trophoblast and future placenta in response to pro-angiogenic signals. To undergo sprouting angiogenesis and colonize the placenta, new sprouts arise from a pre-existing blood vessel. Tip cells are specified to initiate a new sprout and are followed by stalk cells as the sprout extends. *Apela* mutant mice display many ectopically forming tip cells and a reduction of stalk cells, leading to a block in the extension of new angiogenic sprouts (Ho et al., 2017). This raises the question whether APELA could be actively repressing the expression of tip cell genes or mediate the growth of angiogenic sprouts through a so far unknown mechanism.

1.2.2.4. The role of Toddler/Apela in cell specification

Curiously, in human embryos *APELA* is highest expressed in the blastocyst before being rapidly downregulated once embryonic stem cells differentiate (Miura et al., 2004). Investigations into APELA's role in human embryos before the onset of gastrulation revealed that APELA is required for self-renewal of human embryonic stem cells (hESCs) in vitro. APELA signaling activates the PI3K/AKT signaling pathway (Ho et al., 2015), which subsequently promotes cell cycle progression and blocks cell apoptosis (Armstrong et al., 2006; Zhou et al., 2009). While the molecular connection between APELA and PI3K/AKT, as well as the further downstream signaling remains to be fully understood, this

indicates that APELA is required to maintain hESCs. Interestingly, hESCs do not express the APLNR (Ho et al., 2015), indicating the presence of another, so far unidentified APELA receptor or an alternative mode of APELA function. Curiously, APELA has been proposed to have a dual role in hESCs. While it seems to retain the pluripotency of hESC and block differentiation, once this blockage is released and cells differentiate, hESCs that were previously exposed to APELA signaling are likely to specify towards the mesendodermal lineage, indicating an additional role for APELA in priming cells for a certain cell fate (Ho et al., 2015). The underlying mechanisms for this dual role, however, remains to be understood.

In mouse embryonic stem cells (mESCs) no influence on stem cell self-renewal was detected in response to APELA signaling. In fact, APELA signaling seems to rather be promoting apoptosis in mESCs, albeit by a completely different mechanisms that is independent of *Apela*'s coding function (Li et al., 2015). In a tri-element feedback loop, P53 induces apoptosis of mESCs in response to DNA damage (Goh et al., 2012) to prevent transmission of the mutation to daughter cells. This action is antagonized by the binding of heterogenous nuclear ribonucleoprotein L (hnRNPL), which renders P53 inactive and prevents excessive cell apoptosis. However, this interaction can be interfered by the binding of the *Apela* mRNA 3'UTR to hnRNPL, negating the antagonizing effect of hnRNPL. Finally, to prevent excessive activity of *Apela* mRNA, high levels of free P53 can block the binding of *Apela* mRNA to hnRNPL in a negative feedback loop to avoid the uncontrolled induction of apoptosis (Li et al., 2015).

1.2.3. Downstream signaling of the Apelin receptor

As a GPCR, the intracellular domain of Aplnr interacts with G proteins upon activation to induce downstream signaling cascades (Hilger et al., 2018). Two G protein families have been observed to be activated downstream of Aplnr (reviewed by Chapman et al., 2014). First, $G\alpha_{i/o}$ is known for the downstream activation of ERK and Akt signaling, the inactivation of protein kinase A (PKA) and the concomitant decrease of cAMP production. In addition, the corresponding βɣ-subunit has been shown to indirectly signal through the small GTPase Ras, which thereby additionally feeds into the ERK signaling pathway. Second, $G\alpha_{q/11}$ has been implicated in promoting the PLCβ-PKC pathway downstream of the Apelin receptor (Chapman et al., 2014). In addition to and independently of G proteins, Aplnr has been indicated to activate β-Arrestin, that induces receptor internalization in a Clathrin-dependent way (Chapman et al., 2014). Interestingly, receptor internalization has been shown both in response to (Pauli et al., 2014) and independently of (Kwon et al., 2016) Toddler and Apelin, indicating that Aplnr might also be activated and internalized in response to mechanical stimuli.

1.3. Cell migration

Cell migration is crucial for development, physiology, and disease. As described above, it forms one of the pillars of gastrulation, as it is essential to spatially organize the three different germ layers during embryonic development and to lay the foundation for the development of a fully functional organism. Moreover, and as alluded to above, Toddler has a key role in regulating aspects of cell migration during gastrulation. Generally, migration can be influenced at two different levels: the intracellular machinery providing migratory ability, and guidance cues providing directionality to the migrating cell.

1.3.1. The migration machinery

1.3.1.1. Mesenchymal cell migration

Cells undergoing mesenchymal migration are characterized by an elongated cell shape, a front-rear polarity, and the extension of actin-rich protrusions, lamellipodia or filopodia, at the cell front (Figure 4). Lamellipodia are protrusions based on a branched network of thick actin filament bundles and are the main mediators of mesenchymal cell migration. Filopodia, on the other hand, are protrusions based on long parallel actin filament bundles, that support active cell migration and are also responsible for sensing of external stimuli (Ridley et al., 2003).

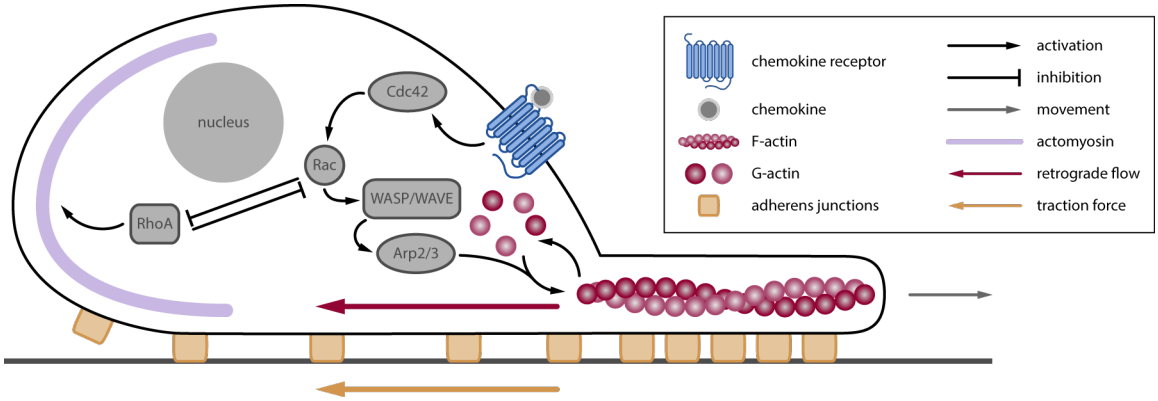

Fig. 4 | Molecular regulation of mesenchymal cell migration. The front of the cell is characterized by the Cdc42/Rac-mediated establishment of a branching actin network that leads to the formation of actin-rich protrusions, which can be initiated spontaneously or through activation of a chemokine receptor. The rear of the cell displays an increased actomyosin contractility due to RhoA activity. A retrograde actin flow in the cell imposes a traction force onto the substrate through adherens junctions that pulls the cell forward.

To initiate active migration the cell first has to establish a front-rear polarity. The establishment of the actin network and protrusions, characteristic for the front of the cell, are mediated by numerous molecular players and regulatory feedback loops that can differ between cell types (for reviews on this topic see Li and Gundersen, 2008; McCaffrey and Macara, 2012; Ridley et al., 2003; Stock and Pauli, 2021). However, the core machinery consists of a small number of key players. The small GTPase Cdc42 is often described as a master regulator of cell polarity (McCaffrey and Macara, 2012). Locally

activated, either spontaneously or through external guidance cues, it triggers the activity of Rac, which in turn stimulates WASP/WAVE complexes, a family of Arp2/3 activators. Arp2/3 ultimately promotes the polymerization of actin and extension of actin-rich protrusions (Figure 4) (Devreotes and Horwitz, 2015). The formation of protrusions is restricted to the front of the cell through active inhibition in the rear. RhoA acts in a mutually exclusive relationship with Rac, actively inhibiting its function in the rear, while itself being suppressed in the front (Figure 4). RhoA promotes the activity of myosin II through ROCK and MLC, therefore increasing the actomyosin contractility in the rear of the cell (Byrne et al., 2016). The mutually exclusive signaling model for RhoA and Rac has been questioned in recent studies, that observed a RhoA-dependent positive stimulation of Rac and the activity of RhoA and Rac in the front and rear domain, respectively, highlighting the importance of additional signaling pathways to maintain the front-rear polarity (Pertz et al., 2006).

To achieve active forward migration across a substrate, integrin-based adhesive contacts are established between the cell and the substrate. These adhesion sites tether the actin cytoskeleton to the underlying substrate through intracellular linkers (Ridley et al., 2003). In the front, integrin-based adhesion acts as an anchor for the cell to impose a traction force onto the substrate during migration (Figure 4). In the back, cell adhesion provides a drag force while the cell starts to move forward, which reinforces the front-rear polarity and protrusion formation (Theisen et al., 2012). Finally, the contractility gradient throughout the cell triggers a retrograde actin flow, that, through the adhesion sites, is translated into a traction force onto the substrate that pulls the cell forward (Figure 4). Ultimately, the adhesive contacts in the back are released, which triggers the retraction of the rear and the forward displacement of the migrating cell (Ridley et al., 2003).

1.3.1.2. Amoeboid cell migration

Amoeboid cell migration is based on the extension of actin-deficient cell blebs, rather than actin-rich lamellipodia. These cells are characterized by a less elongated and more roundish shape than mesenchymal cells, yet also display a front-rear polarity. A bleb-based migration requires a high intracellular pressure that imposes a pushing force onto the cell membrane. Bleb expansion is triggered by the occurrence of breaks within the actin cytoskeleton, followed by the detachment of the membrane from the cortex, which in response to the intracellular pressure bulges forward to form an actin-deficient, spherical bleb protrusion (Paluch and Raz, 2013).

Bleb-based migration can be driven by two mechanisms. An adhesion-dependent mechanism is mediated by Cadherin-based adhesive contacts that are established between the actin cortex at the base of the bleb and the underlying substrate. Like mesenchymal cell migration, the gradient of cell contractility induces a retrograde actin flow that imposes a traction force onto the substrate through these adhesive contacts pulling the cell forward (Paluch and Raz, 2013). Alternatively, bleb-based

migration can occur in an adhesion-independent manner. When navigating through a 3D environment, such as the extracellular matrix (ECM), blebs can be extended into gaps within the ECM. Through these cell shape changes the cytoplasm and entire cell body can then be translocated into gaps that are big enough, allowing the cell to navigate along the path of least resistance while usually still following a global guidance cue (Renkawitz et al., 2019; Yamada and Sixt, 2019).

1.3.2. Chemokine guidance of directional cell migration

The establishment of a front-rear polarity described above can be induced spontaneously, leading to the unbiased formation of protrusions around the cell, usually resulting in a random, non-directional migration of the cell. To acquire directionally persistent migration, front-rear polarity and protrusions must be established along a consistent axis. To a certain extent, this can be achieved through self-organizing intracellular mechanisms that re-enforce the polarity axis (Stock and Pauli, 2021). However, persistent migration usually requires the support by mechanochemical or biochemical guidance cues. Mechanochemical stimuli are provided through the physical interaction of cells with each other or their immediate surrounding. One of the most prominent examples for mechanical guidance is contact inhibition of locomotion (CIL). CIL entails the collapse of protrusions upon cell-cell collision and the reestablishment of polarity and therefore migration in the opposite direction. Thereby, cells can efficiently be directed from highest to lowest cell density (Mayor and Carmona-Fontaine, 2010; Roycroft and Mayor, 2016). Biochemical guidance cues are based on attracting cues in the form of chemokine gradients, that will be explored in more detail in the following sections.

1.3.2.1. Imposed chemokine gradients

Chemotaxis, the process of cell migration along a chemokine gradient (Figure 5), is based on detecting differences in chemokine levels between the front and the back of the cell, usually through differential chemokine receptor occupancy. Activation of chemokine receptors induces the activation of the actin polymerizing machinery described above. A network of regulatory feedback loops, that amplify the local activation while globally inhibiting ectopic protrusions, establishes the site of higher receptor occupancy as the front of the cell and maintains the front-rear polarity (Andrew and Insall, 2007; Stock and Pauli, 2021; van Haastert and Devreotes, 2004).

Traditionally, chemokine gradients were thought to be established by a local source secreting the chemokine, which then diffuses throughout the surrounding tissue, forming a concentration gradient that is imposed onto the migrating cell. Additionally, a chemokine sink can be established to clear the chemokine signal and prevent uncontrolled secretion of the chemokine ligand and flooding of the surrounded tissue (Figure 5). Despite the simplicity of the system, imposed chemokine gradients have multiple caveats (Tweedy and Insall, 2020) that can present major challenges, especially when

regulating directed cell migration in a more complex 3D environment, such as a developing embryo. For example, chemokine gradients are established over a defined length scale in the presence of a static source and sink location, which could create problems when cells need to navigate through the dynamically changing environment of an embryo. Furthermore, the length and chemokine levels of imposed gradients are limited. Chemokine levels secreted by the source must be high enough and the length scale short enough to generate a steep gradient in which the different chemokine levels can be reliably detected. On the other hand, chemokine levels must be low enough so that the cell is not saturated before reaching the source. If the distance covered by the gradient is too long, the gradient becomes too shallow to be read efficiently by the migrating cell. Due to these caveats, one major focus of research in recent years has been the exploration of mechanisms that present alternative and more versatile ways to generate a chemokine gradient.

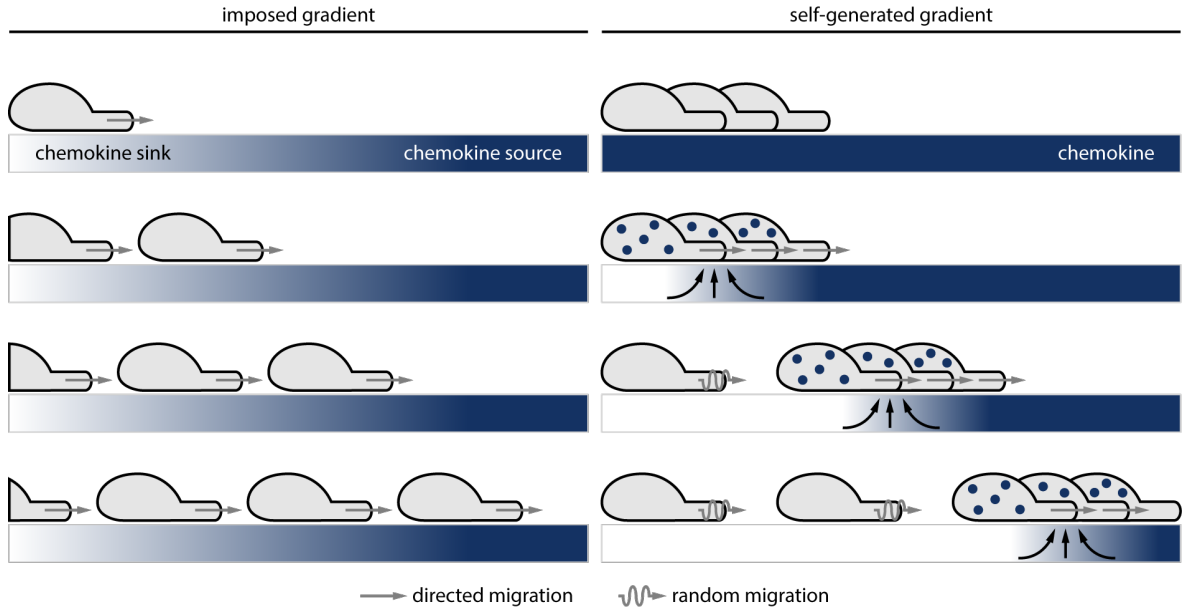

Fig. 5 | Imposed vs. self-generated chemokine gradients. Imposed chemokine gradients are generated by a localized chemokine source and sink. Self-generated gradients are established from an initially uniformly distributed chemokine. The sink activity is provided by the migrating cells themselves as they clear the chemokine from the environment to establish a local gradient. In a controlled environment self-generated gradients are characterized by the formation of a migratory wave.

1.3.2.2. Self-generated gradients

Instead of a localized chemokine source, self-generated chemokine gradients are based on an initially uniformly distributed chemokine signal that is converted into a directional guidance cue. The hallmark of self-generated chemokine gradients is a localized sink formed by a collective of cells that removes the chemokine locally, thereby establishing a gradient located in front of the leading cells. This provides a guidance signal that induces the directional migration of these cells. While cells follow this initial cue, more chemokine is continuously removed, which maintains a gradient and enables the

gradient to “move” with the cell collective (Figure 5). A self-generated gradient is therefore a feature of collective cell migration only; a single cell in this setting would quickly be saturated and not have the capacity to establish a gradient (Tweedy et al., 2016b).

In a simple 2D environment with a finite amount of chemokine, a characteristic migratory wave of cells is formed (Figure 5). The front of the migrating collective is characterized by an accumulation of directional cells, which have direct access to the chemokine gradient. As the chemokine is taken up by this wave, cells behind the migratory front are not exposed to the chemokine signal and follow in a more random migration pattern. This contrasts with imposed gradients, in which the cell migration behavior is more uniform as cells are exposed to a gradient at any point along the migratory path (Tweedy et al., 2016a; Tweedy et al., 2016b).

The mechanism of self-generated gradients has mainly been studied in *Dictyostelium discoideum*. Here, extracellular cAMP provides the chemokine and is broken down by extracellular deaminases to generate the chemokine gradient (Tweedy et al., 2016a; Tweedy et al., 2016b). The importance of self-generated gradients *in vivo*, in particular during embryogenesis, was first demonstrated during the formation of the lateral line in zebrafish. The lateral line primordium (LLP) arises just posterior to the developing ear of the zebrafish and has to migrate along the myoseptum towards the tail tip. The myoseptum uniformly secretes the chemokine ligand Cxcl12a, that guides LLP migration. The LLP is divided in two distinct domains, that each express a different receptor with specific roles. The rear domain expresses Cxcr7b, a scavenger receptor for Cxcl12a, that clears the chemokine through receptor binding and uptake, establishing a local gradient. The front domain, on the other hand, expresses the chemokine receptor Cxcr4b, that senses the established gradient and drives the migration of the tissue along the gradient (Donà et al., 2013; Haas and Gilmour, 2006; Venkiteswaran et al., 2013).

Compared to imposed gradients, self-generated gradients provide several advantages that are particularly important when navigating through a complex *in vivo* environment, such as a developing embryo. As mentioned above, imposed gradients are established over a defined, limited range. This challenge is overcome by a self-generated gradient that is continuously maintained in front of the migrating cells, making the distance that can be travelled theoretically unlimited. This also allows the self-generated gradient to compensate for dynamic changes in tissue size and length scale throughout development. Furthermore, self-generated gradients are more robust to fluctuations within the system, such as chemokine levels. As cells are breaking down the chemokine, guidance can be established within a larger range of chemokine concentration. However, even for self-generated gradients this range is limited. If the chemokine level is too low, the generated concentration difference would be too low to be detected. If the chemokine level is too high, it can surpass the

maximal chemokine degradation rate that the cell collective can provide, leading to the saturation of the chemokine receptors. It has been shown, however, that the latter case can be compensated through a time delay, if the pool of chemokine is limited and not replenished. Upon overexpression of the chemokine, the cell collective comes to a halt due to receptor saturation, yet the chemokine is continued to be broken down. Once enough chemokine has been cleared from the system, a detectable guidance cue is re-established and chemotaxis continues (Tweedy and Insall, 2020; Wong et al., 2020). Taken together these aspects make self-generated gradients an excellent mechanism to reliably guide cell migration through a developing embryo.

2. Aims and objective

Gastrulation is crucial for embryogenesis across the animal kingdom, as it ensures the proper formation and positioning of tissues, organs, and the entire body plan. While the key factors of germ layer specification have been identified, the molecular mediators controlling the morphogenetic movements are still largely unknown. In zebrafish, a characteristic cell movement of gastrulation is the migration of mesendodermal progenitor cells to the animal pole. The molecular guidance of this movement has been a long-standing open question and is of particular interest as the migration of mesodermal progenitors away from the point of internalization is conserved across animal kingdoms. Therefore, studying this process in zebrafish embryos, which are easily accessible and ideal for imaging-based approaches due to their transparency, can provide important insights into gastrulation movements for all vertebrate animals.

The observation of a directional migration of mesodermal progenitors to the animal pole has long suggested the presence of a chemokine guidance signal that would presumably be expressed in a gradual manner from animal pole to margin. However, to date no such differentially expressed candidate factor has been identified. In fact, advances in our understanding of cell migration in recent years has proposed alternative mechanisms that could be guiding the directional migration of a cell collective.

The first publication of this thesis (3.1. Self-organized cell migration across scales – from single cell movement to tissue formation) discusses the concept of self-organization in cell migration and how cell migration can be directed independently of a pre-defined chemokine gradient. In the second publication of this thesis (3.2. A self-generated Toddler gradient guides mesodermal cell migration), I aimed to understand how Toddler guides mesodermal cells to the animal pole. Toddler, a protein that plays a major role in ventrolateral mesoderm migration during zebrafish gastrulation, provided us with an entry point into understanding the molecular regulation of mesodermal cell migration. In particular, I investigated whether Toddler acts in a permissive role as a motogen that stimulates the migration of mesodermal cells, or in an instructive role as a directional cue that guides mesodermal cells to the animal pole.

3. Results

3.1. Self-organized cell migration across scales – from single cell movement to tissue formation

Authors:

Jessica Stock and Andrea Pauli

Preamble:

This publication explores self-organized principles that can mediate directed cell migration on different levels. This is directly linked to the scope of this thesis, which investigates the regulation of mesodermal cell migration during zebrafish gastrulation. This review provides an overview of cell guidance mechanisms that are based on self-organizing principles and provide an alternative to the traditional pre-defined chemokine gradients that are generated by a localized chemokine source.

Status:

published in Development, April 2021

My contributions:

- Conceptualizing the idea for the review
- Designing and discussing the content and structure of the manuscript
- Writing of the manuscript (text and figures, including original draft)
- Revising the manuscript together with Andrea Pauli
- Implementing reviewer's comments

© 2021. Published by The Company of Biologists Ltd | Development (2021) 148, dev191767. doi:10.1242/dev.191767

REVIEW

Self-organized cell migration across scales – from single cell movement to tissue formation

Jessica Stock and Andrea Pauli*

ABSTRACT

Self-organization is a key feature of many biological and developmental processes, including cell migration. Although cell migration has traditionally been viewed as a biological response to extrinsic signals, advances within the past two decades have highlighted the importance of intrinsic self-organizing properties to direct cell migration on multiple scales. In this Review, we will explore self-organizing mechanisms that lay the foundation for both single and collective cell migration. Based on *in vitro* and *in vivo* examples, we will discuss theoretical concepts that underlie the persistent migration of single cells in the absence of directional guidance cues, and the formation of an autonomous cell collective that drives coordinated migration. Finally, we highlight the general implications of self-organizing principles guiding cell migration for biological and medical research.

KEY WORDS: Cell migration, Self-organization, Symmetry breaking

Introduction

The ability of cells to migrate is an underlying principle that governs various biological processes ranging from development to physiology and disease. During embryonic development, for example, proper tissue arrangement, which lays the foundation for the future body architecture, crucially depends on large-scale migration events (Scarpa and Mayor, 2016; Solnica-Krezel and Sepich, 2012; Weijer, 2009). Similarly, an active immune response requires immune cells to migrate over large distances within an organism to fight off pathogens and reach sites of inflammation (Hampton and Chtanova, 2019; Krummel et al., 2016). Mechanisms regulating cell migration can also be repurposed by aberrant cells in the context of disease. Most noticeably, one cause of cancer progression is cells spreading from the primary tumor to populate secondary sites in the form of metastases (Chambers et al., 2002; Friedl and Wolf, 2003). In that regard, understanding the molecular regulation of cell migration will not only improve our understanding of how complex life is formed, but also our ability to tackle disease.

Cells can have different modes of migration (see Box 1). Importantly, they can switch between states in a highly dynamic and adaptable manner, as seen in both single cells and cell collectives. Despite this complexity, migrating cells share one main characteristic, i.e. a front-rear polarity along the axis of migration (de Pascalis and Etienne-Manneville, 2017; Mayor and Etienne-Manneville, 2016). Cell polarity and migration have long been thought to be initiated and guided exclusively through external signals (Roca-Cusachs et al., 2013; Schier, 2003; Wang and Knaut, 2014), yet in recent years the intrinsic ability of cells to establish and guide their own migration gained considerable attention (Carmona-Fontaine et al., 2008; Haas and Gilmour, 2006; Harris et al., 2012; Tweedy et al., 2016b).

The general concept of self-organization was first discussed towards the end of the 18th century by philosopher Immanuel Kant, who described an organism as a unit in which the origin of each part depends on the existence of the other parts (Kant, 1790). Today, self-organization has been defined as the emergence of order in a system based solely on the collective interaction of its individual components. In this way, each component on its own would not be able to account for the properties of the entire system. To achieve self-sustainability, individual components are functionally linked to each other in cause-and-effect relationships, and the entire system is built on a network of feedback loops, rather than linear connections (Karsenti, 2008; Sthijns et al., 2019).

Throughout the past two centuries, self-organizing systems have been described in various areas of science, ranging from social behavior in insects and mammals (Bonabeau et al., 1997; Couzin and Krause, 2003) to spontaneous folding of proteins (Gerstman and Chapagain, 2005; Molkenthin et al., 2020; Phillips, 2009) and self-assembly of nanoparticles (Kotov, 2017; Ponsinet et al., 2017). The first evidence of self-organization in tissue formation dates back to 1910, as Ross Harrison observed the directional outgrowth of *in vitro* cultured nerve fibers in the absence of external guidance signals. However, the self-organizing properties of this system were not clearly recognized at the time (Harrison, 1910). It was only in the 1970s that the autonomous migration of a single cell *in vitro* was appreciated as a self-organizing system (Albrecht-Buehler, 1979; Allan and Wilkinson, 1978; Gail and Boone, 1970; Potel and Mackay, 1979), and only in the 21st century that the importance of self-organizing aspects for cell migration was formally described *in vivo* (Carmona-Fontaine et al., 2008; Haas and Gilmour, 2006; Harris et al., 2012). At first glance, external regulation of cell migration, e.g. through a pre-shaped gradient that the cell merely needs to follow (Haeger et al., 2015), as opposed to self-organization, seems to be a more efficient mechanism and therefore the preferable mode of movement. However, research in recent decades has revealed the limitations and fragility of pre-defined external guidance cues, such as the sensitivity to fluctuations in chemokine levels (Fuller et al., 2010) or the challenge of guiding migration over long distances through a complex environment (Tweedy et al., 2016a). Self-organized migration, on the other hand, presents multiple advantages, including the surprising simplicity of the system, reduction of the network to a handful of key players, and a resilience to environmental fluctuations and genetic defects.

In this Review, we will explore how different levels of cell migration are self-organized, from the polarization of a single cell to the coordinated movement of a cell collective. We aim to highlight emerging concepts of self-organized regulation of cell migration *in vitro* and *in vivo*, focusing mainly on the developing embryo. In addition, we will shed light on the importance and advantages of self-sustainable systems in physiology and disease. It is important to

Research Institute of Molecular Pathology (IMP), Vienna BioCenter (VBC) Campus-Vienna-Biocenter 1, 1030 Vienna, Austria.

*Author for correspondence (andrea.pauli@imp.ac.at)

A.P., 0000-0001-9646-2303

Development (2021) 148, dev191767. doi:10.1242/dev.191767

Box 1. Different modes of cell migration

Mesenchymal migration

Generally considered the most prevalent mode of migration, mesenchymal migration is characterized by an elongated cell shape and actin polymerization at the leading edge, causing the extension of actin-rich protrusions. Integrin-mediated focal adhesions tether the frontal actin cortex to the substrate, while adhesive contacts in the rear detach. Rear contraction causes a retrograde actin flow that imposes a traction force, thereby pulling the cell forward (de Pascalis and Etienne-Manneville, 2017).

Amoeboid migration

A process characterized by a round cell shape and increased cellular contractility. Several different types of amoeboid migration have been characterized.

Adhesion dependent (e.g. primordial germ cells)

Breaks in the cortex cause the extension of hydrostatic, actin-depleted blebs. Cadherin-mediated adhesion occurs through the actin cortex at the base of the bleb. The high contractility in the cell triggers a retrograde actin flow that generates sufficient traction force to pull the cell forwards (Paluch and Raz, 2013).

Adhesion independent (e.g. leukocytes)

Amoeboid cells can use their ability to easily change shape to move through a three-dimensional environment by extending into gaps in the surrounding structures (e.g. extracellular matrix) (Yamada and Sixt, 2019). Using their nucleus as a mechanical sensor for gaps in the environment, they choose the path of least resistance while still following a global guidance cue (Renkawitz et al., 2019).

Cellular swimming (e.g. macrophages)

High contractility at the rear of a floating cell causes a rearward membrane flow that is further supported by a polarized vesicle trafficking from back to front. The membrane flow exhibits a rearward traction force against the surrounding medium that propels the cell forwards (O'Neill et al., 2018).

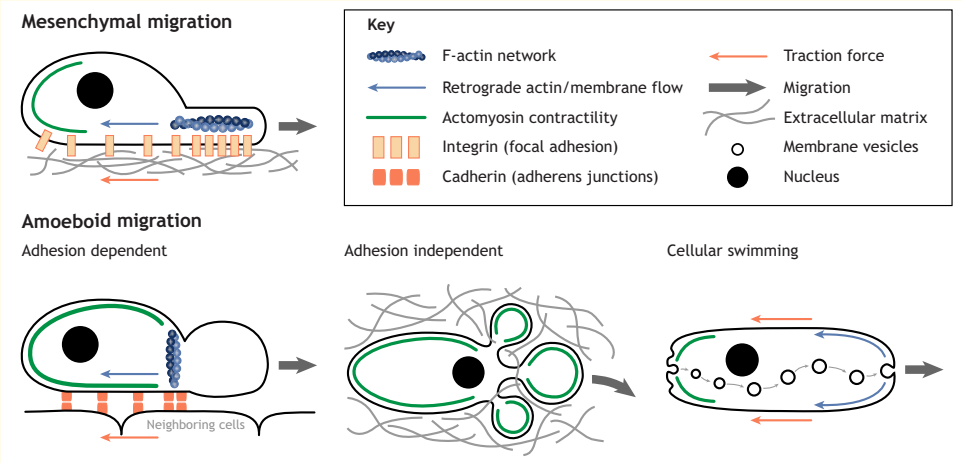

note that most aspects of self-organized cell migration discussed below have been studied in different systems and organisms. Hence, many open questions remain regarding the general applicability of these observations, the connection between individual aspects and the differences between systems.

Migration as a single cell

The migration of an individual cell can be subdivided into three steps: symmetry breakage, establishment of a front-rear axis and initiation of movement. These steps have long been thought to be governed by external cues such as chemoattractant gradients (Swaney et al., 2010; Wang and Knaut, 2014) or substrate rigidity (Angelini et al., 2010; Roca-Cusachs et al., 2013). However, studies in the past few decades have highlighted the ability of individual cells to initiate each of these steps autonomously and migrate independently of external signals (Sasaki et al., 2007; Takagi et al., 2008). Here, we will explore the intrinsic regulatory networks that allow single cells to self-organize to accomplish efficient and persistent migration.

Step 1: breaking symmetry

In order to migrate, an apolar cell first has to break symmetry and become polarized – with a distinct front and rear. Symmetry breaking is often triggered by an external stimulus, yet it can also occur spontaneously (Raynaud et al., 2016; Verkhovsky et al., 1999; Wedlich-Soldner and Li, 2003). Independent of its cause, symmetry breaking is governed by an underlying excitable network of intertwined feedback loops (Lindner et al., 2004; Nishikawa et al., 2014). An apolar cell resides in a quiescent state, characterized by continuous small oscillations between active and inactive states of the biochemical networks that regulate cell polarity, at a level that is not sufficient to excite the system. However, sufficiently large perturbations within the network can elevate the system above the activation threshold to an excited state where the cell becomes primed and polarized for migration. Owing to the self-amplifying nature of the feedback system, even small perturbations such as stochastic noise within the cell are, in principle, sufficient to trigger the active state, which can then be stabilized through the feedback network over a long period of time (Huang et al., 2013).

Development (2021) 148, dev191767. doi:10.1242/dev.191767

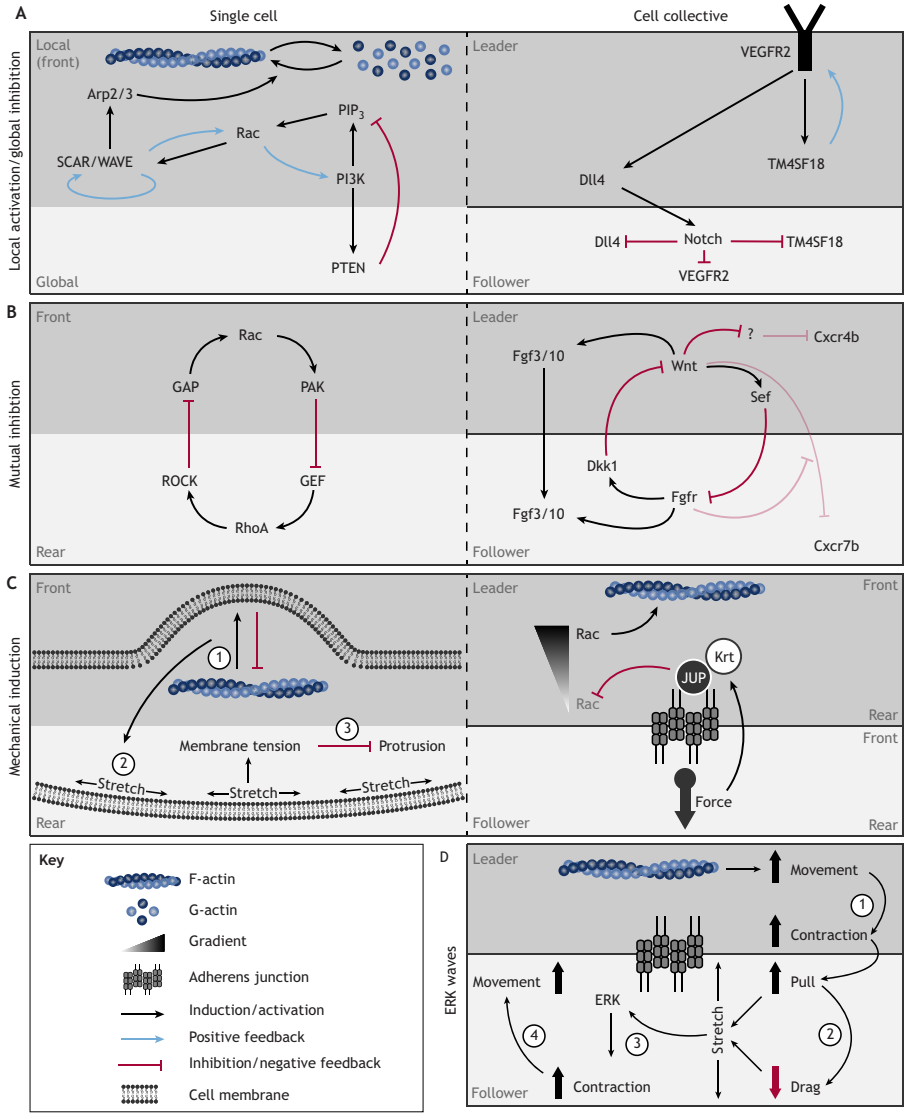

Fig. 1. Self-organized symmetry breaking and establishment of a front-rear axis. (A) Local activation and global inhibition. Single cell (left): the local-excitation-global-inhibition (LEGI) model allows for locally restricted formation of actin-rich protrusions. One example is based on two oscillating systems connected through Rac, centered around synthesis and degradation of PIP_3 on one side, and around actin polymerization and disassembly on the other side. Cell collective (right): lateral inhibition selects leader cells during angiogenesis through local activation of VEGFR2 signaling. The downstream target Dll4 is presented on the membrane and induces Notch signaling in neighboring cells (follower), suppressing VEGFR2 expression and leader fate. (B) Mutual inhibition. Single cell (left): mutual inhibition between Rac and RhoA, mediated by ROCK and PAK, respectively, maintains distinct front and rear domains. Cell collective (right): in the zebrafish lateral line primordium, Wnt and Fgf signaling define leader and follower domains, respectively. Wnt signaling indirectly induces leader-specific Cxcr4b expression and inhibits Fgfr (via Sef) and Cxcr7b expression. Fgf signaling in the follower domain blocks Wnt signaling via the Wnt inhibitor Dkk1, which allows expression of Cxcr7b. (C) Mechanical induction. Single cell (left): lamellipodia formation triggers local extension (1) and global stretching (2) of the plasma membrane. The concomitant increase in membrane tension prevents ectopic formation of additional protrusions (3). Cell collective (right): the drag force in follower cells of epithelial cell sheets, arising through stochastic fluctuations in cell-matrix interactions, or when the rear of leader cells is pulled forward, is transmitted through adherens junctions to the leader cells. Pulling forces at the rear recruit junctional plakoglobin (JUP) and keratin (Krt), which inhibit Rac activity, leading to a Rac activity gradient and subsequent protrusion formation in the front. (D) ERK waves. Forward migration of a leader cell in an epithelial cell sheet (1) pulls the front of the first follower cell forwards and induces its stretching along the migration axis, as the rear remains attached to the second follower cell (2). The cell deformation induces ERK signaling in the first follower cell, which triggers contraction of the rear (3) and forward migration (4). This induces a stretch in the next cell, triggering the propagation of the ERK wave through the tissue.

Symmetry breaking in the front

At the front of a cell, symmetry breaking is mediated through Rac activity, which connects two independently oscillating systems (Fig. 1A, left). Although still controversial with regard to its general importance (see below), the first network is based on the oscillation of PIP_3 levels. Formation of PIP_3 is mediated by PI3K signaling, while degradation is controlled by PTEN (Comer and Parent, 2002; Insall and Weiner, 2001; Matsuoka and Ueda, 2018). PIP_3 triggers Rac signaling (Huang et al., 2013), but the subtle oscillations in PIP_3 levels in a quiescent state are not sufficient for Rac activation. The second oscillating system is based on actin polymerization. Rac enhances SCAR/WAVE complex activity, which induces actin polymerization while also sustaining Rac activity, thus resulting in a positive-feedback loop (Devreotes and Horwitz, 2015). In the quiescent state, actin is blind to Rac signaling and oscillates between constant polymerization and depolymerization by recruiting its own negative regulator coronin (Brieher et al., 2006; Cai et al., 2007). Local stochastic perturbations in the PIP_3 signaling network, however, can drive Rac activity above the threshold and thus trigger a chain of positive-feedback loops leading to actin polymerization and the establishment of a stable actin network on one side of the cell that allows for cell polarization (Fukushima et al., 2019; Huang et al., 2013).

While PIP_3 signaling has been investigated in much detail, some studies question the necessity of this pathway in cell polarization. For example, experiments in *Dictyostelium discoideum* that block PI3K signaling and thereby PIP_3 production reported no impairment of cell polarization and only minor defects in chemotaxis in the presence of an external chemokine gradient (Hoeller and Kay, 2007; van Haastert et al., 2007; Veltman et al., 2014). This suggests the existence of alternative signaling pathways that can mediate symmetry breaking and polarization, e.g. PIP_5 kinase-dependent signaling, as has recently been described (Fets et al., 2014). Further research will be needed to fully understand the importance of PIP_3 signaling in cell migration, and to identify and characterize possible alternative pathways across different cell types.

Whether mediated by PIP_3 signaling or by alternative pathways, the probability of these spontaneous breaks in symmetry ultimately depends on the threshold level. Artificially decreasing or increasing the threshold by manipulating individual components of the excitable system has been shown to increase or reduce spontaneous initiation of cell migration, respectively (Miao et al., 2017). However, it remains to be determined how the threshold level is regulated *in vivo*.

Symmetry breaking in the rear

Symmetry breaking in the front of the cell was previously considered to be the only entry point into cell polarization, but in recent years the initiation of polarization has also been observed in the back of various cell types (Mseka et al., 2007; Yam et al., 2007). Although this indicates the presence of an excitable system capable of breaking symmetry at the rear of the cell, its molecular mechanisms are not as well understood.

According to current knowledge, an excitable system in the rear of the cell is most likely centered around a positive-feedback mechanism between actomyosin contractility and retrograde actin flow (Yam et al., 2007). Through recruiting its own inhibitor, myosin light chain phosphatase (MLCP), myosin II is thought to oscillate between active and inactive states. Although myosin II activity is known to display oscillating properties in tissue morphogenesis (He et al., 2010; Qin et al., 2018; Zhang et al., 2020), it has yet to be confirmed in the context of self-organized cell migration. In support of an excitable system centered around actomyosin contractility, recent studies have reported that fluctuations in actin dynamics and cell adhesion can induce spontaneous symmetry breaking in the rear (Barnhart et al., 2015).

Global symmetry breaking

The aforementioned molecular networks of spontaneous symmetry breaking in a specific domain mainly lead to the formation of an actin-rich lamellipodium as the defining protrusion of the front that pulls the cell forward (discussed further below). Nevertheless, various cell types are known to migrate based on the formation of blebs, rather than actin-rich protrusions, following an amoeboid-like cell migration behavior (Paluch and Raz, 2013) (see Box 1). The decision to migrate using lamellipodia or blebs depends on the balance between actin polymerization and contractility, with the latter favoring cell blebbing (Bergert et al., 2012). Blebs are caused by local breaks within the actin cortex that allow the membrane to detach and, with sufficient intracellular pressure, extend to form a spherical actin-deficient protrusion (Paluch and Raz, 2013). Owing to a general instability of the cell cortex, breaks can occur stochastically in both space and time, yet are subsequently repaired, resulting in dynamic blebbing around the cell periphery. However, mathematical models over the past decade have proposed that, at a crucial threshold of global cell contractility, a stochastic break in the cell cortex can lead to spontaneous symmetry breaking and polarization of the cell (Callan-Jones and Voituriez, 2013; Hawkins et al., 2011; Recho et al., 2013). Recently, this has been confirmed experimentally in both isolated zebrafish germ layer progenitor cells and human fibroblasts (Liu et al., 2015; Ruprecht et al., 2015). In culture, these cells undergo random blebbing behavior. Upon increase of global contractility, however, the cortical break underlying the bleb causes a local drop in contractility that leads to a steep contractility gradient. This gradient triggers a cortical actin flow that amplifies and stabilizes a single bleb, causing the transition to a polarized state (Liu et al., 2015; Ruprecht et al., 2015). Therefore, at a crucial point of global contractility, stochastic fluctuations in cortical stability can lead to spontaneous symmetry breaking. Importantly, contractility-mediated symmetry breaking acts on a global level and is tightly coupled with the formation of a front-rear polarity axis. Therefore, this bypasses the additional step of establishing a front-rear polarity axis further discussed below.

Step 2: establishing and maintaining front-rear polarity

Once symmetry is broken either at the front or the rear, the signal needs to be propagated to the other pole at the opposite end of the cell to establish a front-rear axis. Cell polarity can be generated through several self-organized signaling networks that are based on: (1) local excitation and global inhibition; (2) mutual inhibition; and/or (3) mechanical forces.

Local excitation and global inhibition

Key to self-organized cell polarity is that the pole at which polarity was initiated maintains its distinct state. This can be achieved through the local-excitation global-inhibition (LEGI) model. LEGI is based on a signal that induces both a short-range activator and a long-range inhibitor (Iglesias and Devreotes, 2012; Meinhardt, 1999). The activator acts fast and locally, and triggers additional positive-feedback mechanisms in close proximity to stabilize the established domain. The inhibitor, on the other hand, diffuses throughout the cell, where it inhibits the formation of ectopic 'front-like' domains (Xiong et al., 2010). Therefore, the LEGI model is crucial for maintaining and restricting an established domain but is incapable of inducing the opposing one without any additional signaling networks. The aforementioned PIP_3/PI3K/PTEN network that acts in the front of the cell, is an excellent example of LEGI, with PI3K being the local

Development (2021) 148, dev191767. doi:10.1242/dev.191767

activator and PTEN, after being released from the membrane and diffusing through the cell upon PIP_3 formation, acting as a global inhibitor (Fig. 1A, left) (Gerhardt et al., 2014).

Mutual inhibition

As mentioned above, each domain represses its own activity at the other side of the cell via globally acting feedback mechanisms. In addition, each domain locally blocks the activity of the opposing pole in a phenomenon called mutual inhibition. One well studied example of mutual inhibition in the context of a migrating cell is the opposing activities of Rac and RhoA (Fig. 1B, left). In a simplistic view, Rac is a key regulator of actin polymerization at the front of the cell, where it inhibits RhoA activity. RhoA, on the other hand, is a central mediator of actomyosin contractility at the rear where it blocks Rac activity and thus formation of actin-rich protrusions (Byrne et al., 2016).

It remains to be determined how universal the Rac/RhoA antagonism is, and whether there are other factors that have similar opposing activities. For example, in mouse embryonic fibroblasts (MEFs), RhoA activity has been observed in leading protrusions, questioning the concept of mutual inhibition and a rear-specific role of RhoA (Pertz et al., 2006). Expression of a dominant-negative Rac abolished the activation of RhoA in these protrusions but maintained a protrusive phenotype. Although the antagonism between RhoA and Rac, as well as the function of Rac in protrusion formation is therefore still intact, the maintenance of distinct Rac and RhoA domains is likely not sufficient to establish a front-rear axis.

Mechanical forces

In addition to the biochemical networks governing cell polarity, the accompanying changes in cell shape trigger mechanical forces that support and stabilize the polarized cell (Fig. 1C, left). During formation of a protrusion, the plasma membrane has to extend. Like stretching an elastic band, the growing protrusion causes the plasma membrane to unwrinkle, putting the entire cell under immense tension. The increasing membrane tension surpasses the force imposed by actin filaments and antagonizes actin polymerization, thereby constraining any further extension of the leading edge, and blocks formation of secondary protrusions (Houk et al., 2012). Furthermore, an increase in membrane tension supports the retraction of the rear to release strain. Therefore, the interplay between actin polymerization and membrane tension stabilizes the leading edge and supports induction of the rear (Diz-Muñoz et al., 2013).

Step 3: persistent migration

During biological processes that are characterized by major cell migration events, such as embryonic development (Aman and Piotrowski, 2010) or immune response (Hampton and Chtanova, 2019), cells need to move long distances and populate new territories. Yet, in many cases, the absence of external guidance cues begs the question, how can these cells achieve directional migration? At first glance, persistent directionality of cell migration appears incompatible with the stochastic formation of protrusions around the cell periphery. Theoretically, this uncontrolled initiation of movement would lead to an unbiased random migration behavior that is highly inefficient (Viswanathan et al., 1999). However, the observed migratory behavior of single cells *in vitro* in the absence of external guidance cues is notably different and characterized by two phases. First, a cell undergoes a diffusive phase during which it tumbles around its own position, unable to move forward. Eventually, it transitions into a second phase of directional persistence and the cell is able to move along a relatively straight trajectory for an extended period of time (Harris et al., 2012; Maiuri et al., 2015). Such cell behavior is inconsistent with purely random cell movement, and recent data support the involvement of self-organized regulatory networks that reinforce a stable front-rear axis (Begemann et al., 2019; Theisen et al., 2012).

Maintaining directional persistence in the front

The cell front is a highly dynamic structure, undergoing constant cycles of extension and retraction. Upon retraction, the cell has the possibility to redefine its front-rear axis and polarize in a different direction. Therefore, the key to persistent, self-organized migration is to ensure the new lamellipodium is formed in close proximity to the previous one.

Work in *in vitro* cultured fibroblasts has indicated that directional persistence at the front can be regulated through mechanochemical communication between old and new lamellipodia, which is based on the sensing of membrane curvature (Begemann et al., 2019). This effect is mediated by I-BAR domain-containing proteins that bind to regions of negative membrane curvature, such as the inside of a lamellipodium (Millard et al., 2005; Saarikangas et al., 2009). Through signaling to Rac and the Scar/WAVE complex, I-BAR proteins can initiate actin polymerization and hence protrusion extension in mammalian cells (Begemann et al., 2019; Miki et al., 2000). Upwards bending of a lamellipodium upon retraction leads to a change in membrane curvature, which induces the accumulation of I-BAR proteins and local activation of actin polymerization. This causes formation of a nascent lamellipodium directly underneath the retracting one, and thus maintains the same direction of migration (Begemann et al., 2019) (Fig. 2, right).

Despite evidence from mammalian cells for a role of I-BAR proteins in the mechanical regulation of cell migration, it is still unclear how universal this mechanism is. For example, work in *Dictyostelium* indicated that I-BAR proteins are not necessary for protrusion formation and chemotaxis, even in shallow chemokine gradients (Veltman et al., 2011). Whether I-BAR proteins are dispensable, not only for protrusion formation in general but for persistent migration of *Dictyostelium*, in particular in the absence of external guidance cues, has to be further investigated. Nonetheless, these insights indicate that the above-described mechanism might be cell-type specific, and that there could be alternative pathways maintaining directional persistence that have yet to be uncovered.

Maintaining directional persistence in the rear

Like the cell front, the rear is dynamic, as it maintains a constant balance between focal adhesion and retraction. In certain cell types, such as keratinocytes or fibroblasts, after retraction of the lamellipodium, cell polarity is re-initiated with establishment of the rear, rather than the front (Cramer, 2010; Mseka et al., 2007; Rid et al., 2005). Therefore, a full retraction of the rear reverts the cell to a naïve state in which it can initiate polarization in any new direction. However, maintaining a constant level of focal adhesion in the rear while the cell moves forward can stabilize the front-rear axis. This is achieved through a treadmilling mechanism that involves continuous extension of integrin-based focal adhesion sites in the front-facing part of the cell rear and integrin removal in the back (Theisen et al., 2012). In addition, this treadmilling mechanism applies a drag force on the cell front, which has been shown to promote protrusion formation in the opposite direction. Thus, the cell rear can stabilize the directional persistence in the front (Fig. 2, left).

Maintaining directional persistence globally

In addition to local stabilizing mechanisms, persistence in cell migration is also mediated through global feedback loops, which connect front and rear domains. As discussed above, local breaks in

Development (2021) 148, dev191767. doi:10.1242/dev.191767

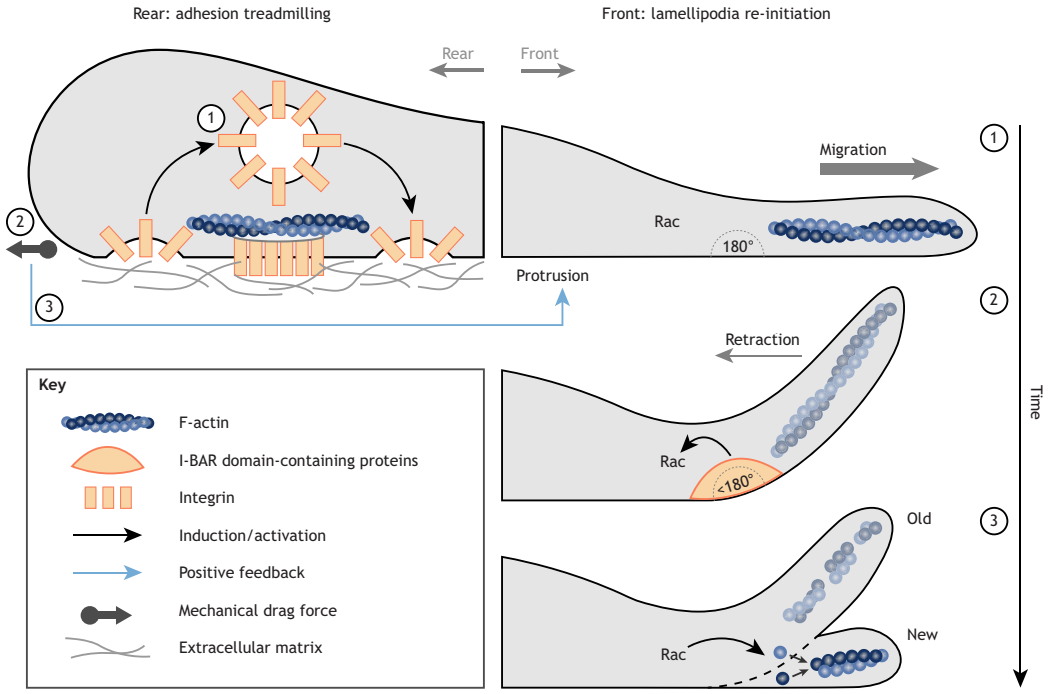

Fig. 2. Directional persistence in self-organized single cell migration. Persistence at the front of an individually migrating cell (right) is maintained through mechanochemical connections between the retracting (old) and the nascent (new) lamellipodium (1-3). Membrane deformations upon retraction are sensed by I-BAR domain-containing proteins and transmitted to Rac signaling (2), inducing actin polymerization and lamellipodia formation at the site of the old lamellipodium (3). Persistence at the rear (left) is maintained through the treadmilling of integrin adhesion sites (1), which prevents complete retraction of the rear. Through this continuous adhesion to the ECM (extracellular matrix), a drag force is constantly applied to the cell rear (2), which stabilizes protrusion formation at the opposite end of the cell (3).

the actin cortex in combination with high global contractility can lead to spontaneous symmetry breaking and the establishment of front-rear polarity (Paluch and Raz, 2013). The local disruption of the actin cortex at the future cell front leads to a local drop of contractility, which initiates the establishment of a front domain and causes actin flows from the region of low to high contractility. Thereby, actin-binding proteins, such as the contractility regulator myosin II, are transported to the opposite end of the cell: the rear domain. This relocalization of molecules connected to actomyosin contractility reinforces cortical flows, leading to a positive-feedback loop that stabilizes the front-rear axis and promotes protrusion (Liu et al., 2015; Ruprecht et al., 2015). Indeed, cell migration assays in various cell types, following different modes of migration, including bleb and lamellipodia based, have demonstrated a causality between cortical flow and migratory persistence, as well as cell migration speed (Maiuri et al., 2015; Yolland et al., 2019).

Migration as a cell collective

Within an organism, cells often do not migrate individually, but rather move in a collective manner to shape tissues or populate new areas (Scarpa and Mayor, 2016; Weijer, 2009). As previously described (Shellard and Mayor, 2019), there are two modes of collective cell migration. In one mode, cells within the collective polarize individually but depend on communication and interaction with other cells in the cluster for efficient migration, e.g. as seen in axial mesendoderm in zebrafish (Dumortier et al., 2012). In the other mode, the cell collective moves as a supracellular unit characterized by an overarching polarity with distinct leader and follower cells, which are dependent on each other and are not able to migrate persistently on their own, as described for the folding of epithelial sheets during ventral furrow formation in *Drosophila* (He et al., 2014). Most cases of collective cell migration, however, seem to combine aspects of both individual and supracellular behavior to different extents, e.g. as observed during the morphogenesis of the *Drosophila* follicular epithelium (Barlan et al., 2017) or *Xenopus* neural crest (NC) migration (Carmona-Fontaine et al., 2008; Shellard et al., 2018). Thus, mechanisms of collective migration should be seen more as a spectrum rather than a dichotomy. In the following section, we explore how the supracellular organization of a migrating cell collective is established, and which mechanisms of single cell migration also apply to a cell collective.

Step 1: defining leaders

Like a single cell, a cell collective usually requires front-rear organization for persistent migration yet faces the particular challenge of establishing an overarching polarity across the entire tissue. This is achieved by defining distinct leader and follower cells with specific morphologies and functions. However, in most cases, these two cell types are highly dynamic, with leader cells being transformed into trailing cells, and vice versa (Richardson et al., 2016; Zhang et al., 2019). Leader cells are typically characterized by mesenchymal properties and extend lamellipodia to the front of the

collective. Follower cells, on the other hand, show increased contractility and actomyosin activity, and thus resemble the rear of a single cell (Mayor and Etienne-Manneville, 2016). Whether follower cells are completely non-migratory and are simply being pulled forward by the leaders or whether they actively contribute force to the cluster migration likely depends on the degree of supracellular organization in the cluster and is still an area of ongoing research. Nonetheless, the establishment of front-rear polarity in a cell collective follows similar principles to those for individual cells and can be achieved through different mechanisms: (1) local activation and global inhibition (or, here, lateral inhibition); (2) mutual inhibition; and/or (3) mechanical forces.

Lateral inhibition

Lateral inhibition is a commonly used mechanism to make cells distinct from their neighbors (Appel et al., 2001; Sato et al., 2016; Sharma et al., 2019; Simpson, 1990; Xia et al., 2019). Lateral inhibition is based on competition between cells, in which a newly defined leader cell prevents the neighboring follower cells from obtaining the same fate (Sjöqvist and Andersson, 2019). This mechanism is employed to define individual leader cells, rather than a leader domain. Therefore, it is commonly used during branching morphogenesis, as seen in angiogenesis or *Drosophila* tracheal branching, in which a single leader cell needs to be established *de novo* within an existing tissue to induce a new branch site (Jakobsson et al., 2010; Llimargas, 1999).

At the molecular level, lateral inhibition is based on Notch signaling. In the example of angiogenic sprouting, a prospective leader cell is triggered through activation of vascular endothelial growth factor receptor (VEGFR) signaling that induces a series of cell-intrinsic feedback loops mediated by the atypical tetraspanin TM4SF18 (Page et al., 2019) to amplify its activity. VEGFR signaling induces the expression and thereby presentation of the Notch ligand Dll4 at the cell surface. Ligand binding to neighboring cells triggers the Notch signaling pathway in these cells, which inhibits VEGFR expression and thereby keeps the neighbors in a follower state (Jakobsson et al., 2010; Page et al., 2019; Tammela et al., 2011) (Fig. 1A, right).

Mutual inhibition

During lateral inhibition, leader cells suppress neighboring cells from adopting the same fate, which leads to the establishment of a single leader cell. As such, lateral inhibition is unable to establish larger leader and follower domains characteristic for supracellular collectives. Mutual inhibition, on the other hand, applies the same concept in both directions and has been observed to establish larger leader and follower domains, as described in the lateral line primordium (LLP) of zebrafish larvae (Aman and Piotrowski, 2008). Here, mutual inhibition is mediated through Wnt (leader) and Fgf (follower) signaling (Fig. 1B, right). Wnt signaling in the leading domain induces Fgf ligand while suppressing Fgf receptor expression. Therefore, Fgf ligands diffuse to the Fgf receptor-expressing follower domain. Fgf binding induces the expression of Wnt inhibitor Dkk1, which in turn suppresses leader properties in the follower domain. Moreover, the antagonistic Wnt/Fgf signaling axis establishes the differential expression of two Cxcl12a-responsive G-protein-coupled receptors that are important for guided cell migration. As discussed further below, the chemokine receptor Cxcr4b is restricted to leader cells. A still unknown inhibitor blocks expression of Cxcr4b in the follower domain, while in the leader domain this inhibitor is counteracted by Wnt signaling. The scavenger receptor Cxcr7b, on the other hand, is specific to the follower cells, as it is directly inhibited by Wnt signaling in the leader domain (Aman and Piotrowski, 2008; Lecaudey et al., 2008; Valentin et al., 2007). The resulting interlinked non-autonomous cell signaling network ensures the persistence of distinct cellular properties at the front versus the rear in a migrating cell collective.

Mechanical induction

Similar to individual cell migration, biochemical signaling pathways act in concert with mechanical forces to regulate front-rear polarity in cell collectives. The presence of a cell collective adds an additional layer of complexity, as the force is transmitted between cells and can span several cell diameters. Therefore, the application of a dragging force by one cell onto a neighbor can be propagated through the cell collective and induce lamellipodia formation in the opposite direction in even more distant cells (Theisen et al., 2012; Weber et al., 2012).

This phenomenon has been observed in wound healing assays and shown to induce leader cell formation. According to this model, spontaneous fluctuations within the cell cytoskeleton or structural inconsistencies in the substrate lead to alteration of cell-matrix tension. These changes in tension in turn apply a pulling force to neighboring cells (Vishwakarma et al., 2018), which induces polarization of the cells with the leading edge being directed in the opposite direction. Through cadherin-based adherens junctions between cells across the entire tissue, this tension can be propagated from one cell to the next until it reaches the edge. Therefore, cells at the edge polarize and extend actin-rich protrusions away from the cluster, forming the leading domain. Although the molecular mechanism of how polarization is achieved remains largely unknown, it has been observed that pulling forces at the rear of the cell recruit plakoglobin to its adherens junctions. Plakoglobin mediates binding of keratin intermediate filaments, both of which have been implicated in the subsequent cell polarization (Weber et al., 2012). Plakoglobin has previously been suggested to inhibit the activity of actin polymerization factors Rac and Arp2/3 (Todorović et al., 2010). By blocking Rac and Arp2/3 activity specifically in the rear, plakoglobin can establish a gradient of polymerized actin filaments within the cell, which could thus explain how polarization is achieved (Fig. 1C, right).

In addition to this model, recent studies proposed a mechanism for epithelial wound healing in which polarity is established through a global interplay between ERK/MAPK signaling and tissue mechanics (Aoki et al., 2017; Boocock et al., 2020; Hino et al., 2020) (Fig. 1D). Although the described mechanochemical mechanisms are of importance in mediating the connection between ERK signaling and mechanical forces, in this system unidirectional ERK waves propagating from the wound site through the tissue establish tissue polarity and induce cell migration in the opposite direction.

Step 2: stabilizing leader and follower domains

Once leader cells are defined, the cell collective needs to establish and maintain polarity, with distinct leader and follower domains. Each domain has a distinct role in eventually moving the entire collective forward. A combination of mechanical and biochemical communication between individual cells and between domains ensures that every cell takes on the appropriate role at the right time and in the right place, thereby allowing migration as one unit.

Mesenchymal characteristics in the leader domain

Front-rear polarity has to be maintained throughout migration in order for it to be persistent. Most importantly, leader cell character has to be stabilized within and restricted to the front domain to prevent spreading of the cell cluster. How this is achieved remains the subject

of intense research. Different mechanisms have been described in different systems, although it is currently unclear whether each system has evolved its own way of maintaining the leader domain or whether a combination of mechanisms acts together.

One of the key mechanisms of collective cell migration is contact inhibition of locomotion (CIL), which will be discussed in more detail below. The underlying basis for CIL is that cell-cell contact inhibits protrusion formation at the site of collision (Mayor and Carmona-Fontaine, 2010). Therefore, only cells with at least one free side can acquire mesenchymal character, thus restricting this fate to the outer cells of a collective.

Although CIL partially explains why outer but not inner cells can adopt mesenchymal character, how these characteristics remain restricted to cells at the front of the cluster and inhibited in lateral cells is still largely unclear. Studies in wound healing assays have observed the presence of supracellular actomyosin cables and coinciding RhoA activity, both in the rear and the sides of coherently migrating cell clusters (Reffay et al., 2014). As RhoA activity is known to prevent lamellipodia formation (Byrne et al., 2016), this is a possible explanation for the lack of lamellipodia formation in these regions. However, how these actomyosin cables are established in the first place and whether there is a feedback connection between these cables and lamellipodia formation in the front, and thus a possibility for self-organization, is still unclear.

Contractility in the follower domain

How the rear cells contribute to active forward migration of a collective is still largely unknown. The rear of a single cell is characterized by increased actin-myosin contractility. A similar feature, but organized in a supracellular manner, has been observed in *Xenopus* NC cells (Shellard et al., 2018). Connected through N-cadherin junctions between cells, a supracellular actomyosin cable spans the entire width of the cell cluster along the back. That way, all rear cells contract simultaneously, mimicking one giant cell. This contractility gradient triggers a retrograde flow of peripheral cells from front to back (Shellard et al., 2018), conceptually similar to retrograde membrane flow in single cell migration (see Box 1). To maintain the shape of the cluster, cells in the rear are pushed to intercalate between their frontal neighbors, making their way through the entire tissue until reaching and replacing the leader cells in the front (Shellard et al., 2018). Whether a similar process is in place in other systems or whether there are alternative mechanisms providing contractility in the rear requires further investigation.

Furthermore, a molecular connection between leader and follower domains, that would indicate a self-organization in NC migration, remains to be identified. However, artificial induction of contractility on one side has been shown to induce a leader domain on the opposite site, hinting towards the existence of feedback loops between the two domains (Shellard et al., 2018).

Step 3: providing direction

As discussed above, a single cell that is placed in an environment without external guidance signals can, due to self-organized mechanisms, maintain a certain degree of directional persistence. In a migrating collective, the sheer number of migrating cells provides an additional layer of directionality control, which has been shown to support persistent migration even in the absence of a chemokine gradient. Using two example mechanisms described in different systems, we will explore how cell collectives can maintain directional persistence and what advantages these mechanisms bring to the developing organism.

Contact inhibition of locomotion

Contact inhibition of locomotion (CIL) is a phenomenon in which, upon cell-cell contact, the formation of protrusions is inhibited at the site of collision. As stated above, this assists in polarizing supracellular systems by restricting lamellipodia formation to the edge of the cell cluster. However, CIL, in combination with additional features, such as mutual attraction, has also been shown – through computational modelling approaches – to increase directional persistence (Carmona-Fontaine et al., 2008, 2011) (Fig. 3A).

The outcome of CIL largely depends on cell density. In a dense cluster, all inner cells are tightly attached to neighbors and therefore inhibited to form protrusions at all sides, with the exception of cells at the cluster edge. In collectives with more loosely attached cells that are individually polarized and migratory (as shown in Fig. 3A), colliding cells can re-polarize and extend a new protrusion in the opposing direction until they encounter another cell (Mayor and Carmona-Fontaine, 2010; Roycroft and Mayor, 2016; Stramer and Mayor, 2017). Thus, cells are constantly repelled from the point of highest cell density, which biases their migration towards unpopulated regions. Migration solely based on CIL therefore leads to cell dispersion until the cell density is too low and collision events are not frequent enough to provide any directional bias, e.g. as seen in Cajal-Retzius cells (Villar-Cerviño et al., 2013). Thus, to keep the collective coherent, additional layers of control are required, e.g. physical borders, that can restrict cell dispersion. On a molecular level, though, NC cells have, for example, been shown to additionally express the chemoattractant C3a and the corresponding receptor C3aR, which cause the cells to attract each other. This mutual attraction after repulsion balances out the CIL-caused dispersion of cells and allows for a more efficient and persistent migration (Fig. 3A) (Carmona-Fontaine et al., 2011).

Two different mechanisms have been described to be responsible for CIL. In *Xenopus* neural crest migration (Fig. 3B, left), the planar cell polarity (PCP) pathway is activated locally at the site of collision, leading to a local activation of RhoA. Owing to the accompanying RhoA-induced increase in contractility, a new cell rear is established. As described above, this is sufficient to induce a new cell front at the opposite end, leading to repolarization of the cell (Carmona-Fontaine et al., 2008). An alternative mechanism has been described in head mesoderm of *Drosophila* embryos (Fig. 3B, right), in which CIL depends on transient adhesion between the two colliding cells and subsequent remodeling of the cytoskeleton. Two colliding cells form cadherin-mediated adherens junctions that connect the actin networks of both cells through interacting with the cytoskeleton. This brief fixation blocks retrograde actin flow in both cells and therefore causes the collapse of the destabilized lamellipodium. Furthermore, the collision event disrupts growth of microtubules supporting the leading edge, which have been shown to depolymerize when encountering an immobile object, in this case the colliding cell (Janson et al., 2003; Laan et al., 2008). The role of the microtubules network during CIL is not fully understood; however, it has previously been suggested to mediate the release of the adhesive contact between the two cells (Stramer et al., 2010). Once the adhesion is released, the cortical tension suddenly decreases, which leads to spontaneous contraction of both cells at the collision site and subsequent cell polarization in the opposite direction (Davis et al., 2015).

Self-generated chemokine gradients

One of the most common external guidance cues for directional cell migration is a chemokine gradient. Traditionally, chemokine gradients were thought to be formed through a localized source, as

Development (2021) 148, dev191767. doi:10.1242/dev.191767

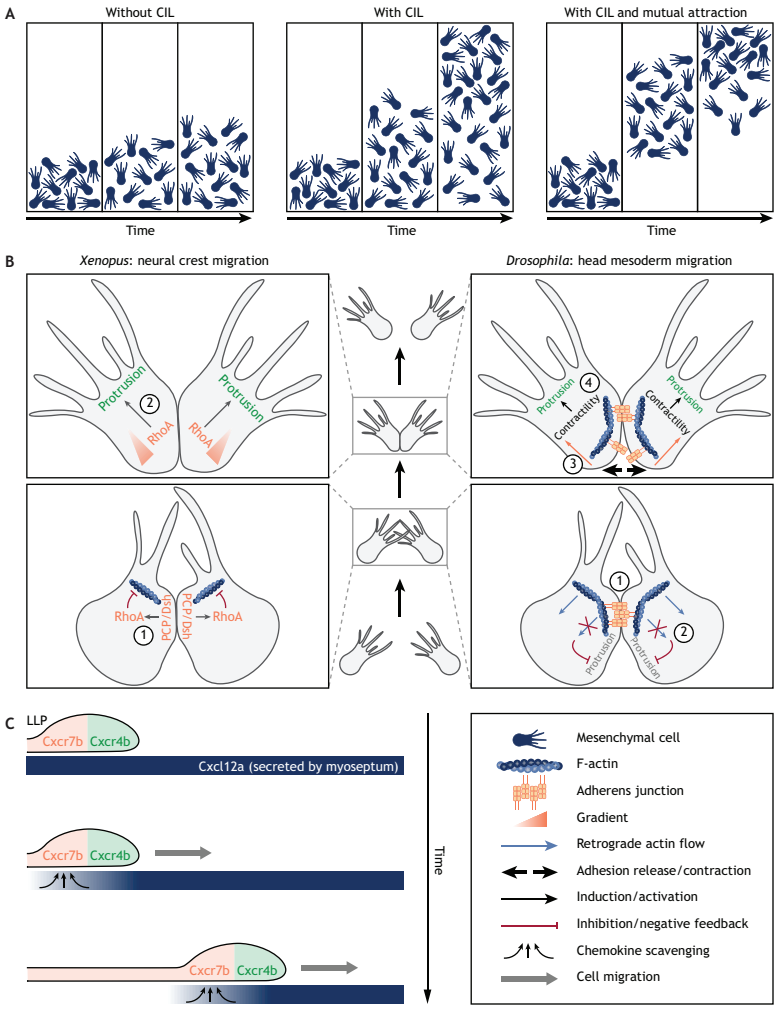

Fig. 3. Directional persistence in self-organized collective cell migration. (A) Collective migration through contact inhibition of locomotion (CIL). Without CIL (left), cells migrate randomly with very little net displacement. With CIL (middle), cells are repelled from regions of highest cell density and spread out. The presence of physical boundaries adds an additional level of directionality by preventing uncontrolled radial dispersion of cells. CIL in combination with mutual attraction between cells (right) allows for collective migration with a directional bias. Adapted from computational modeling of Carmona-Fontaine et al. (2011), where it was published under a CC-BY 4.0 license. (B) In *Xenopus* neural crest cells (left), CIL relies on PCP signaling. Accumulation of PCP factors at the collision site activates RhoA signaling (1) and therefore local cell contractility. The newly established RhoA gradient induces actin polymerization and extension of nascent protrusions away from the site of collision (2). In *Drosophila* head mesoderm (right), CIL is mediated by tethering of the actin cytoskeletons of the colliding cells through adherens junctions at the site of collision (1). This induces an abrupt stop of actin retrograde flow and the collapse of the lamellipodium (2). Release of the adhesion causes spontaneous contractility at the collision site (3), defining the new cell rear, and inducing actin polymerization and protrusion formation at the opposite side of the cell (4). (C) Self-generated gradients. In the environment of a uniformly expressed chemokine, cell collectives can self-generate a chemokine gradient. In the zebrafish lateral line primordium (LLP), the scavenger receptor Cxcr7b removes the uniformly expressed chemokine Cxcl12a in the rear of the tissue. This forms a Cxcl12a gradient that is sensed by Cxcr4b in the front of the tissue, allowing for directed cell migration.

described in primordial germ cell (Doitsidou et al., 2002) or neutrophil migration (de Oliveira et al., 2013). However, recent studies have discovered multiple examples in which a cell collective has the capability to self-generate a gradient from a uniform chemokine distribution, making a pre-formed gradient unnecessary. By breaking down the chemokine itself, the migrating tissue continuously generates a local concentration gradient and can thereby guide its own migration (Tweedy et al., 2016b). This phenomenon was first described in *Dictyostelium* (Sucgang et al., 1997; Tweedy et al., 2016a) and in recent years has been observed *in vivo* for the migration of the LLP in the developing zebrafish larva (Donà et al., 2013; Valentin et al., 2007; Venkiteswaran et al., 2013).

The LLP arises as a cluster of approximately 100-150 cells (Agarwala et al., 2015) behind the developing ear and migrates along the underlying myoseptum on either side of the zebrafish larvae towards the tail tip. Its migration is driven by the chemokine Cxcl12a and its corresponding receptor Cxcr4b. Cxcl12a is secreted by cells of the myoseptum and initially equally distributed along the path of migration (Dalle Nogare and Chitnis, 2017). To generate the guidance cue in the first place, the scavenger receptor Cxcr7b is expressed in the follower domain of the LLP (as discussed above). Cxcr7b binds, internalizes and thereby removes Cxcl12a from the environment, specifically in the rear region. This generates a locally confined yet steep gradient across the LLP. Meanwhile, the front of the LLP expresses Cxcr4b, which reads the self-generated gradient and drives the migration of the LLP towards higher concentrations of the chemokine. Unlike a stationary sink, the Cxcr7b-expressing cells migrate along the gradient together with the entire LLP tissue. Thus, as the tissue migrates, a local gradient is continuously formed and provides a self-generated guidance signal (Donà et al., 2013; Haas and Gilmour, 2006; Valentin et al., 2007; Venkiteswaran et al., 2013) (Fig. 3C).

A self-generating gradient is simple, yet extremely robust, as it does not depend on a pre-defined, precisely shaped gradient. The

establishment of a pre-existing gradient, which usually requires a complex molecular network to define the source, sink, counter gradients, diffusion rates and more is unnecessary. Furthermore, a self-generated gradient provides a higher robustness in navigating through complex environments and allows for guidance over a long distances, whereas pre-existing long-range gradients are usually very shallow and, hence, more difficult to follow (Tweedy and Insall, 2020; Tweedy et al., 2019 preprint). Finally, the self-organizing system can handle a wide range of ligand concentrations and compensate for severe ligand overexpression through receptor turnover, making it a robust and reliable system for a developing organism (Lau et al., 2020; Wong and Gilmour, 2020; Wong et al., 2020).

Conclusions and perspectives

Self-organization is an underlying concept driving both individual and collective cell migration. Within a single cell, individual molecular regulators engage in a complex network of feedback loops that allow symmetry breaking and self-sustained migration. In a collective, each cell forms an individual component of the whole. The interaction between these individuals, whether through physical contact, mechanical forces or cell signaling, establishes an overarching order that allows for collective migration.

In this Review, we have presented general concepts and selected examples that demonstrate the importance of self-organized cell migration during embryonic development. Understanding how self-organization is achieved by migrating cells also has important implications for medical research. Immune cells are some of the most migratory cells in the body and are known to employ mechanisms of self-organization for their movement. Immature T cells, for example, constantly search for antigens and target cells. To this end, they migrate long distances without any directional cues. *In vivo* studies have shown that T cells, in the brain in particular, undergo a Lévy walk: a type of migration that comprises the two phases of motility (diffusive and persistent) we have described above. This mode of migration is mediated through self-organized intrinsic directionality. This enables T cells to reside in a specific location long enough to recognize a potential antigen and to transmit an activating signal, while still covering a sufficiently large area during their search (Harris et al., 2012; Krummel et al., 2016).

This is just one example of the importance of self-organized cell migration for our health and immune response. On the other hand, the advantages of self-organization are also exploited by pathogens and diseases. As such, basic research of cell migration has significantly contributed to understanding the mechanisms of tumorigenesis and metastasis in cancer, and provides valuable input on potential treatment therapies (Chambers et al., 2002; Friedl and Wolf, 2003; Wang et al., 2004). During metastasis, streams of cancer cells delaminate from the primary tumor, migrate away and populate secondary areas within the organism, thereby causing the disease to spread (Friedl and Gilmour, 2009). As cancer cells migrate through different tissue types and organs lacking consistent guidance signals, cancer cells exploit self-organizing mechanisms to drive their own migration. Recent advances in understanding the process of metastasis have shown that it acts via a self-generated gradient of lysophosphatidic acid (LPA), a chemokine of unknown origin, that is present in the tumor environment and broken down by tumor cells (Muinonen-Martin et al., 2014; Susanto et al., 2017). Cancer cells are able to follow this local self-generated gradient and spread out. Preventing cancer cells from egressing from the tumor in the first place would be an efficient treatment to stop the progression of the disease. Therefore, understanding how self-organization provides robust guidance to migrating cancer cells is essential to develop new therapies.

Although self-organized migration is often beneficial for a particular biological system, the underlying complex networks are difficult to decipher or even recognize from a researcher's perspective. Dissecting self-organization requires the combination of biology and physics, including computational modeling and experimental research, cross-disciplinary areas that have only gained significant popularity within the past two decades. As a consequence, the concept of self-organization has long been overlooked in our understanding of cell migration. For many migration events, both in development and disease, initiation and guidance cues remain unclear. Whether self-organizing mechanisms are much more widely used during cell migration events than currently recognized is yet to be determined. Future research in this area could provide exciting answers to many long-standing questions.

Acknowledgements

We thank Elly Tanaka, Edouard Hannezo, Victoria Deneke and Krista Gert for insightful comments on the manuscript.

Competing interests

The authors declare no competing or financial interests.

Funding

Research in the Pauli lab is supported by the Austrian Science Fund (START Projekt Y1031-B28, SFB 'RNA-Deco' F 80) and by the European Molecular Biology Organization-Young Investigators Program, as well as by institutional funding to the Research Institute of Molecular Pathology (IMP) from Boehringer Ingelheim and the Austrian Research Promotion Agency (Österreichische Forschungsförderungsgesellschaft, FFG) (grant FFG-852936).

References

Agarwala, S., Duquesne, S., Liu, K., Boehm, A., Grimm, L., Link, S., König, S., Eimer, S., Ronneberger, O. and Lecaudey, V. (2015). Amotl2a interacts with the hippo effector yap1 and the Wnt/β-catenin effector lef1 to control tissue size in zebrafish. *eLife* **4**, e08201. doi:10.7554/eLife.08201

Albrecht-Buehler, G. (1979). The angular distribution of directional changes of guided 3T3 cells. *J. Cell Biol.* **80**, 53-60. doi:10.1083/jcb.80.1.53

Allan, R. B. and Wilkinson, P. C. (1978). A visual analysis of chemotactic and chemokinetic locomotion of human neutrophil leucocytes. Use of a new chemotaxis assay with Candida albicans as gradient source. *Exp. Cell Res.* **111**, 191-203. doi:10.1016/0014-4827(78)90249-5

Aman, A. and Piotrowski, T. (2008). Wnt/β-catenin and Fgf signaling control collective cell migration by restricting chemokine receptor expression. *Dev. Cell* **15**, 749-761. doi:10.1016/j.devcel.2008.10.002

Aman, A. and Piotrowski, T. (2010). Cell migration during morphogenesis. *Dev. Biol.* **341**, 20-33. doi:10.1016/j.ydbio.2009.11.014

Angelini, T. E., Hannezo, E., Trepat, X., Fredberg, J. J. and Weitz, D. A. (2010). Cell migration driven by cooperative substrate deformation patterns. *Phys. Rev. Lett.* **104**, 168104. doi:10.1103/PhysRevLett.104.168104

Aoki, K., Kondo, Y., Naoki, H., Hiratsuka, T., Itoh, R. E. and Matsuda, M. (2017). Propagating Wave of ERK Activation Orients Collective Cell Migration. *Dev. Cell* **43**, 305-317.e5. doi:10.1016/j.devcel.2017.10.016

Appel, B., Givan, L. A. and Eisen, J. S. (2001). Delta-Notch signaling and lateral inhibition in zebrafish spinal cord development. *BMC Dev. Biol.* **1**, 1-11. doi:10.1186/1471-213X-1-13

Barlan, K., Cetera, M. and Horne-Badovinac, S. (2017). Fat2 and Lar define a basally localized planar signaling system controlling collective cell migration. *Dev. Cell* **40**, 467-477.e5. doi:10.1016/j.devcel.2017.02.003

Barnhart, E., Lee, K. C., Allen, G. M., Theriot, J. A. and Mogilner, A. (2015). Balance between cell-substrate adhesion and myosin contraction determines the frequency of motility initiation in fish keratocytes. *Proc. Natl. Acad. Sci. USA* **112**, 5045-5050. doi:10.1073/pnas.1417257112

Begemann, I., Saha, T., Lamparter, L., Rathmann, I., Grill, D., Golbach, L., Rasch, C., Keller, U., Trappmann, B., Matis, M. et al. (2019). Mechanochemical self-organization determines search pattern in migratory cells. *Nat. Phys.* **15**, 848-857. doi:10.1038/s41567-019-0505-9

Bergert, M., Chandradoss, S. D., Desai, R. A. and Paluch, E. (2012). Cell mechanics control rapid transitions between blebs and lamellipodia during migration. *Proc. Natl Acad. Sci. USA* **109**, 14434-14439. doi:10.1073/pnas.1207968109

Bonabeau, E., Theraulaz, G., Deneubourg, J. L., Aron, S. and Camazine, S. (1997). Self-organization in social insects. *Trends Ecol. Evol.* **12**, 188-193. doi:10.1016/S0169-5347(97)01048-3

Boocock, D., Hino, N., Ruzickova, N., Hirashima, T. and Hannezo, E. (2020). Theory of mechanochemical patterning and optimal migration in cell monolayers. *Nat. Physics* **17**, 267-274. doi:10.1038/s41567-020-01037-7
Brieher, W. M., Hao, Y. K., Ballif, B. A. and Mitchison, T. J. (2006). Rapid actin monomer-insensitive depolymerization of Listeria actin comet tails by cofilin, coronin, and Aip1. *J. Cell Biol.* **175**, 315-324. doi:10.1083/jcb.200603149
Byrne, K. M., Monsefi, N., Dawson, J. C., Degasperi, A., Bukowski-Wills, J. C., Volinsky, N., Dobrzyński, M., Birtwistle, M. R., Tsyganov, M. A., Kiyatkin, A. et al. (2016). Bistability in the Rac1, PAK, and RhoA signaling network drives actin cytoskeleton dynamics and cell motility switches. *Cell Systems* **2**, 38-48. doi:10.1016/j.cels.2016.01.003
Cai, L., Marshall, T. W., Uetrecht, A. C., Schafer, D. A. and Bear, J. E. (2007). Coronin 1B Coordinates Arp2/3 Complex and Cofilin Activities at the Leading Edge. *Cell* **128**, 915-929. doi:10.1016/j.cell.2007.01.031
Callan-Jones, A. C. and Voituriez, R. (2013). Active gel model of amoeboid cell motility. *New J. Phys.* **15**, 025022. doi:10.1088/1367-2630/15/2/025022
Carmona-Fontaine, C., Matthews, H. K., Kuriyama, S., Moreno, M., Dunn, G. A., Parsons, M., Stern, C. D. and Mayor, R. (2008). Contact inhibition of locomotion in vivo controls neural crest directional migration. *Nature* **456**, 957-961. doi:10.1038/nature07441
Carmona-Fontaine, C., Theveneau, E., Tzekou, A., Tada, M., Woods, M., Page, K. M., Parsons, M., Lambris, J. D. and Mayor, R. (2011). Complement fragment C3a controls mutual cell attraction during collective cell migration. *Dev. Cell* **21**, 1026-1037. doi:10.1016/j.devcel.2011.10.012
Chambers, A. F., Groom, A. C. and MacDonald, I. C. (2002). Dissemination and growth of cancer cells in metastatic sites. *Nature Reviews Cancer* **2**, 563-572. doi:10.1038/nrc865
Comer, F. I. and Parent, C. A. (2002). PI 3-kinases and PTEN: how opposites chemoattract. *Cell* **109**, 541-544. doi:10.1016/S0092-8674(02)00765-1
Couzin, I. D. and Krause, J. (2003). Self-organization and collective behavior in vertebrates. *Adv. Study Behav.* **32**, 1-75. doi:10.1016/S0065-3454(03)01001-5
Cramer, L. P. (2010). Forming the cell rear first: Breaking cell symmetry to trigger directed cell migration. *Nat. Cell Biol.* **12**, 628-632. doi:10.1038/ncb0710-628
Dalle Nogare, D. and Chitnis, A. B. (2017). A framework for understanding morphogenesis and migration of the zebrafish posterior Lateral Line primordium. *Mech. Dev.* **148**, 69-78. doi:10.1016/j.mod.2017.04.005
Davis, J. R., Luchici, A., Mosis, F., Thackery, J., Salazar, J. A., Mao, Y., Dunn, G. A., Betz, T., Miodownik, M. and Stramer, B. M. (2015). Inter-cellular forces orchestrate contact inhibition of locomotion. *Cell* **161**, 361-373. doi:10.1016/j.cell.2015.02.015
de Oliveira, S., Reyes-Aldasoro, C. C., Candel, S., Renshaw, S. A., Mulero, V. and Calado, Â. (2013). Cxcl8 (IL-8) Mediates neutrophil recruitment and behavior in the zebrafish inflammatory response. *The Journal of Immunology* **190**, 4349-4359. doi:10.4049/jimmunol.1203266
de Pascalis, C. and Etienne-Manneville, S. (2017). Single and collective cell migration: The mechanics of adhesions. *Mol. Biol. Cell* **28**, 1833-1846. doi:10.1091/mbc.e17-03-0134
Devreotes, P. and Horwitz, A. R. (2015). Signaling networks that regulate cell migration. *Cold Spring Harbor Perspect. Biol.* **7**, a005959. doi:10.1101/cshperspect.a005959
Diz-Muñoz, A., Fletcher, D. A. and Weiner, O. D. (2013). Use the force: Membrane tension as an organizer of cell shape and motility. *Trends Cell Biol.* **23**, 47-53. doi:10.1016/j.tcb.2012.09.006
Doitsidou, M., Reichman-Fried, M., Stebler, J., Köprunner, M., Dörries, J., Meyer, D., Esguerra, C. v., Leung, T. and Raz, E. (2002). Guidance of Primordial Germ Cell Migration by the Chemokine SDF-1. *Cell* **111**, 647-659. doi:10.1016/S0092-8674(02)01135-2
Donà, E., Barry, J. D., Valentin, G., Quirin, C., Khmelinskii, A., Kunze, A., Durdu, S., Newton, L. R., Fernandez-Minan, A., Huber, W. et al. (2013). Directional tissue migration through a self-generated chemokine gradient. *Nature* **503**, 285-289. doi:10.1038/nature12635
Dumortier, J. G., Martin, S., Meyer, D., Rosa, F. M. and David, N. B. (2012). Collective mesendoderm migration relies on an intrinsic directionality signal transmitted through cell contacts. *Proc. Natl. Acad. Sci. USA* **109**, 16945-16950. doi:10.1073/pnas.1205870109
Fets, L., Nichols, J. M. E. and Kay, R. R. (2014). A PIP5 kinase essential for efficient chemotactic signaling. *Curr. Biol.* **24**, 415-421. doi:10.1016/j.cub.2013.12.052
Friedl, P. and Gilmour, D. (2009). Collective cell migration in morphogenesis, regeneration and cancer. *Nat. Rev. Mol. Cell Biol.* **10**, 445-457. doi:10.1038/nrm2720
Friedl, P. and Wolf, K. (2003). Tumour-cell invasion and migration: diversity and escape mechanisms. *Nature Reviews Cancer* **3**, 362-374. doi:10.1038/nrc1075
Fukushima, S., Matsuoka, S. and Ueda, M. (2019). Excitable dynamics of Ras triggers spontaneous symmetry breaking of PIP3 signaling in motile cells. *J. Cell Sci.* **132**, jcs224121. doi:10.1242/jcs.224121
Fuller, D., Chen, W., Adler, M., Groisman, A., Levine, H., Rappel, W. J. and Loomis, W. F. (2010). External and internal constraints on eukaryotic chemotaxis. *Proc. Natl. Acad. Sci. USA* **107**, 9656-9659. doi:10.1073/pnas.0911178107
Gail, M. H. and Boone, C. W. (1970). The locomotion of mouse fibroblasts in tissue culture. *Biophys. J.* **10**, 980-993. doi:10.1016/S0006-3495(70)86347-0
Gerhardt, M., Walz, M. and Beta, C. (2014). Signaling in chemotactic amoebae remains spatially confined to stimulated membrane regions. *J. Cell Sci.* **127**, 5115-5125. doi:10.1242/jcs.161133
Gerstman, B. S. and Chapagain, P. P. (2005). Self-organization in protein folding and the hydrophobic interaction. *J. Chem. Phys.* **123**, 054901. doi:10.1063/1.1990110
Haas, P. and Gilmour, D. (2006). Chemokine signaling mediates self-organizing tissue migration in the zebrafish lateral line. *Dev. Cell* **10**, 673-680. doi:10.1016/j.devcel.2006.02.019
Haeger, A., Wolf, K., Zegers, M. M. and Friedl, P. (2015). Collective cell migration: guidance principles and hierarchies. *Trends Cell Biol.* **25**, 556-566. doi:10.1016/j.tcb.2015.06.003
Hampton, H. R. and Chtanova, T. (2019). Lymphatic migration of immune cells. *Front. Immunol.* **10**, 1168. doi:10.3389/fimmu.2019.01168
Harris, T. H., Banigan, E. J., Christian, D. A., Konradt, C., Wojno, E. D. T., Norose, K., Wilson, E. H., John, B., Weninger, W., Luster, A. D. et al. (2012). Generalized Lévy walks and the role of chemokines in migration of effector $CD8^+$T cells. *Nature* **486**, 545-548. doi:10.1038/nature11098
Harrison, R. G. (1910). The outgrowth of the nerve fiber as a mode of protoplasmic movement. *J. Exp. Zool.* **9**, 787-846. doi:10.1002/jez.1400090405
Hawkins, R. J., Poincloux, R., Bénichou, O., Piel, M., Chavrier, P. and Voituriez, R. (2011). Spontaneous contractility-mediated cortical flow generates cell migration in three-dimensional environments. *Biophys. J.* **101**, 1041-1045. doi:10.1016/j.bpj.2011.07.038
He, L., Wang, X., Tang, H. L. and Montell, D. J. (2010). Tissue elongation requires oscillating contractions of a basal actomyosin network. *Nat. Cell Biol.* **12**, 1133-1142. doi:10.1038/ncb2124
He, B., Doubrovinski, K., Polyakov, O. and Wieschaus, E. (2014). Apical constriction drives tissue-scale hydrodynamic flow to mediate cell elongation. *Nature* **508**, 392-396. doi:10.1038/nature13070
Hino, N., Rossetti, L., Marín-Llauradó, A., Aoki, K., Trepat, X., Matsuda, M. and Hirashima, T. (2020). ERK-Mediated mechanochemical waves direct collective cell polarization. *Dev. Cell* **53**, 646-660.e8. doi:10.1016/j.devcel.2020.05.011
Hoeller, O. and Kay, R. R. (2007). Chemotaxis in the absence of PIP3 gradients. *Curr. Biol.* **17**, 813-817. doi:10.1016/j.cub.2007.04.004
Houk, A. R., Jilkine, A., Mejean, C. O., Boltyanskiy, R., Dufresne, E. R., Angenent, S. B., Altschuler, S. J., Wu, L. F. and Weiner, O. D. (2012). Membrane tension maintains cell polarity by confining signals to the leading edge during neutrophil migration. *Cell* **148**, 175-188. doi:10.1016/j.cell.2011.10.050
Huang, C. H., Tang, M., Shi, C., Iglesias, P. A. and Devreotes, P. N. (2013). An excitable signal integrator couples to an idling cytoskeletal oscillator to drive cell migration. *Nat. Cell Biol.* **15**, 1307-1316. doi:10.1038/ncb2859
Iglesias, P. A. and Devreotes, P. N. (2012). Biased excitable networks: How cells direct motion in response to gradients. *Curr. Opin. Cell Biol.* **24**, 245-253. doi:10.1016/j.ceb.2011.11.009
Insall, R. H. and Weiner, O. D. (2001). PIP3, PIP2, and cell movement - similar messages, different meanings? *Dev. Cell* **1**, 743-747. doi:10.1016/S1534-5807(01)00086-7
Jakobsson, L., Franco, C. A., Bentley, K., Collins, R. T., Ponsioen, B., Aspalter, I. M., Rosewell, I., Busse, M., Thurston, G., Medvinsky, A. et al. (2010). Endothelial cells dynamically compete for the tip cell position during angiogenic sprouting. *Nat. Cell Biol.* **12**, 943-953. doi:10.1038/ncb2103
Janson, M. E., de Dood, M. E. and Dogterom, M. (2003). Dynamic instability of microtubules is regulated by force. *J. Cell Biol.* **161**, 1029-1034. doi:10.1083/jcb.200301147
Kant, I. (1790). Kritik der Urteilskraft. *Lagarde Und Friedrich*.
Karsenti, E. (2008). Self-organization in cell biology: A brief history. *Nat. Rev. Mol. Cell Biol.* **9**, 255-262. doi:10.1038/nrm2357
Kotov, N. A. (2017). Self-assembly of inorganic nanoparticles: Ab ovo. *EPL (Europhysics Letters)* **119**, 66008. doi:10.1209/0295-5075/119/66008
Krummel, M. F., Bartumeus, F. and Gérard, A. (2016). T cell migration, search strategies and mechanisms. *Nature Reviews Immunology* **16**, 193-201. doi:10.1038/nri.2015.16
Laan, L., Husson, J., Munteanu, E. L., Kerssemakers, J. W. J. and Dogterom, M. (2008). Force-generation and dynamic instability of microtubule bundles. *Proc. Natl Acad. Sci. USA* **105**, 8920-8925. doi:10.1073/pnas.0710311105
Lau, S., Feitzinger, A., Venkiteswaran, G., Wang, J., Lewellis, S. W., Koplinski, C. A., Peterson, F. C., Volkman, B. F., Meier-Schellersheim, M. and Knaut, H. (2020). A negative-feedback loop maintains optimal chemokine concentrations for directional cell migration. *Nat. Cell Biol.* **22**, 266-273. doi:10.1038/s41556-020-0465-4
Lecaudey, V., Cakan-Akdogan, G., Norton, W. H. J. and Gilmour, D. (2008). Dynamic Fgf signaling couples morphogenesis and migration in the zebrafish lateral line primordium. *Development* **135**, 2695-2705. doi:10.1242/dev.025981
Lindner, B., García-Ojalvo, J., Neiman, A. and Schimansky-Geier, L. (2004). Effects of noise in excitable systems. *Phys. Rep.* **392**, 321-424. doi:10.1016/j.physrep.2003.10.015

Liu, Y. J., le Berre, M., Lautenschlaeger, F., Maiuri, P., Callan-Jones, A., Heuzé, M., Takaki, T., Voituriez, R. and Piel, M. (2015). Confinement and low adhesion induce fast amoeboid migration of slow mesenchymal cells. *Cell* **160**, 659-672. doi:10.1016/j.cell.2015.01.007

Llimargas, M. (1999). The Notch pathway helps to pattern the tips of the Drosophila tracheal branches by selecting cell fates. *Development* **126**, 2355-2364.

Maiuri, P., Rupprecht, J. F., Wieser, S., Ruprecht, V., Bénichou, O., Carpi, N., Coppey, M., de Beco, S., Gov, N., Heisenberg, C. P. et al. (2015). Actin flows mediate a universal coupling between cell speed and cell persistence. *Cell* **161**, 374-386. doi:10.1016/j.cell.2015.01.056

Matsuoka, S. and Ueda, M. (2018). Mutual inhibition between PTEN and PIP3 generates bistability for polarity in motile cells. *Nat. Commun.* **9**, 1-15. doi:10.1038/s41467-018-06856-0

Mayor, R. and Carmona-Fontaine, C. (2010). Keeping in touch with contact inhibition of locomotion. *Trends Cell Biol.* **20**, 319-328. doi:10.1016/j.tcb.2010.03.005

Mayor, R. and Etienne-Manneville, S. (2016). The front and rear of collective cell migration. *Nat. Rev. Mol. Cell Biol.* **17**, 97-109. doi:10.1038/nrm.2015.14

Meinhardt, H. (1999). Orientation of chemotactic cells and growth cones: models and mechanisms. *J. Cell Sci.* **112**, 2867-2874.

Miao, Y., Bhattacharya, S., Edwards, M., Cai, H., Inoue, T., Iglesias, P. A. and Devreotes, P. N. (2017). Altering the threshold of an excitable signal transduction network changes cell migratory modes. *Nat. Cell Biol.* **19**, 329-340. doi:10.1038/ncb3495

Miki, H., Yamaguchi, H., Suetsugu, S. and Takenawa, T. (2000). IRSp53 is an essential intermediate between Rac and WAVE in the regulation of membrane ruffling. *Nature* **408**, 732-735. doi:10.1038/35047107

Millard, T. H., Bompard, G., Heung, M. Y., Dafforn, T. R., Scott, D. J., Machesky, L. M. and Fütterer, K. (2005). Structural basis of filopodia formation induced by the IRSp53/MIM homology domain of human IRSp53. *EMBO J.* **24**, 240-250. doi:10.1038/sj.emboj.7600535

Molkenthin, N., Mühle, S., Mey, A. S. J. S. and Timme, M. (2020). Self-organized emergence of folded protein-like network structures from geometric constraints. *PLoS ONE* **15**, e0229230. doi:10.1371/journal.pone.0229230

Mseka, T., Bamburg, J. R. and Cramer, L. P. (2007). ADF/cofilin family proteins control formation of oriented actin-filament bundles in the cell body to trigger fibroblast polarization. *J. Cell Sci.* **120**, 4332-4344. doi:10.1242/jcs.017640

Muinonen-Martin, A. J., Susanto, O., Zhang, Q., Smethurst, E., Faller, W. J., Veltman, D. M., Kalna, G., Lindsay, C., Bennett, D. C., Sansom, O. J. et al. (2014). Melanoma cells break down LPA to establish local gradients that drive chemotactic dispersal. *PLoS Biol.* **12**, e1001966. doi:10.1371/journal.pbio.1001966

Nishikawa, M., Hörning, M., Ueda, M. and Shibata, T. (2014). Excitable signal transduction induces both spontaneous and directional cell asymmetries in the phosphatidylinositol lipid signaling system for eukaryotic chemotaxis. *Biophys. J.* **106**, 723-734. doi:10.1016/j.bpj.2013.12.023

O'Neill, P. R., Castillo-Badillo, J. A., Meshik, X., Kalyanaraman, V., Melgarejo, K. and Gautam, N. (2018). Membrane flow drives an adhesion-independent amoeboid cell migration mode. *Dev. Cell* **46**, 9-22.e4. doi:10.1016/j.devcel.2018.05.029

Page, D. J., Thuret, R., Venkatraman, L., Takahashi, T., Bentley, K. and Herbert, S. P. (2019). Positive feedback defines the timing, magnitude, and robustness of angiogenesis. *Cell Reports* **27**, 3139-3151.e5. doi:10.1016/j.celrep.2019.05.052

Paluch, E. K. and Raz, E. (2013). The role and regulation of blebs in cell migration. *Curr. Opin. Cell Biol.* **25**, 582-590. doi:10.1016/j.ceb.2013.05.005

Pertz, O., Hodgson, L., Klemke, R. L. and Hahn, K. M. (2006). Spatiotemporal dynamics of RhoA activity in migrating cells. *Nature* **440**, 1069-1072. doi:10.1038/nature04665

Phillips, J. C. (2009). Scaling and self-organized criticality in proteins I. *Proc. Natl. Acad. Sci. USA* **106**, 3107-3112. doi:10.1073/pnas.0811262106

Ponsinet, V., Baron, A., Pouget, E., Okazaki, Y., Oda, R. and Barois, P. (2017). Self-assembled nanostructured metamaterials. *EPL (Europhysics Letters)* **119**, 14004. doi:10.1209/0295-5075/119/14004

Potel, M. J. and Mackay, S. A. (1979). Preaggregative cell motion in Dictyostelium. *J. Cell Sci.* **36**, 281-309.

Qin, X., Hannezo, E., Mangeat, T., Liu, C., Majumder, P., Liu, J., Choesmel-Cadamuro, V., McDonald, J. A., Liu, Y., Yi, B. et al. (2018). A biochemical network controlling basal myosin oscillation. *Nat. Commun.* **9**, 1-15. doi:10.1038/s41467-017-02088-w

Raynaud, F., Ambühl, M. E., Gabella, C., Bornert, A., Sbalzarini, I. F., Meister, J. J. and Verkhovsky, A. B. (2016). Minimal model for spontaneous cell polarization and edge activity in oscillating, rotating and migrating cells. *Nat. Phys.* **12**, 367-373. doi:10.1038/nphys3615

Recho, P., Putelat, T. and Truskinovsky, L. (2013). Contraction-driven cell motility. *Phys. Rev. Lett.* **111**, 108102. doi:10.1103/PhysRevLett.111.108102

Reffay, M., Parrini, M. C., Cochet-Escartin, O., Ladoux, B., Buguin, A., Coscoy, S., Amblard, F., Camonis, J. and Silberzan, P. (2014). Interplay of RhoA and mechanical forces in collective cell migration driven by leader cells. *Nat. Cell Biol.* **16**, 217-223. doi:10.1038/ncb2917

Renkawitz, J., Kopf, A., Stopp, J., de Vries, I., Driscoll, M. K., Merrin, J., Hauschild, R., Welf, E. S., Danuser, G., Fiolka, R. et al. (2019). Nuclear positioning facilitates amoeboid migration along the path of least resistance. *Nature* **568**, 546-550. doi:10.1038/s41586-019-1087-5

Richardson, J., Gauert, A., Briones Montecinos, L., Fanlo, L., Alhashem, Z. M., Assar, R., Marti, E., Kabla, A., Härtel, S. and Linker, C. (2016). Leader cells define directionality of trunk, but not cranial, neural crest cell migration. *Cell Reports* **15**, 2076-2088. doi:10.1016/j.celrep.2016.04.067

Rid, R., Schiefermeier, N., Grigoriev, I., Small, J. V. and Kaverina, I. (2005). The last but not the least: The origin and significance of trailing adhesions in fibroblastic cells. *Cell Motil. Cytoskelet.* **61**, 161-171. doi:10.1002/cm.20076

Roca-Cusachs, P., Sunyer, R. and Trepat, X. (2013). Mechanical guidance of cell migration: Lessons from chemotaxis. *Curr. Opin. Cell Biol.* **25**, 543-549. doi:10.1016/j.ceb.2013.04.010

Roycroft, A. and Mayor, R. (2016). Molecular basis of contact inhibition of locomotion. *Cell. Mol. Life Sci.* **73**, 1119-1130. doi:10.1007/s00018-015-2090-0

Ruprecht, V., Wieser, S., Callan-Jones, A., Smutny, M., Morita, H., Sako, K., Barone, V., Ritsch-Marte, M., Sixt, M., Voituriez, R. et al. (2015). Cortical contractility triggers a stochastic switch to fast amoeboid cell motility. *Cell* **160**, 673-685. doi:10.1016/j.cell.2015.01.008

Saarikangas, J., Zhao, H., Pykäläinen, A., Laurinmäki, P., Mattila, P. K., Kinnunen, P. K. J., Butcher, S. J. and Lappalainen, P. (2009). Molecular mechanisms of membrane deformation by I-BAR domain proteins. *Curr. Biol.* **19**, 95-107. doi:10.1016/j.cub.2008.12.029

Sasaki, A. T., Janetopoulos, C., Lee, S., Charest, P. G., Takeda, K., Sundheimer, L. W., Meili, R., Devreotes, P. N. and Firtel, R. A. (2007). G protein-independent Ras/PI3K/F-actin circuit regulates basic cell motility. *J. Cell Biol.* **178**, 185-191. doi:10.1083/jcb.200611138

Sato, M., Yasugi, T., Minami, Y., Miura, T. and Nagayama, M. (2016). Notch-mediated lateral inhibition regulates proneural wave propagation when combined with EGF-mediated reaction diffusion. *Proc. Natl. Acad. Sci. U.S.A.* **113**, E5153-E5162. doi:10.1073/pnas.1602739113

Scarpa, E. and Mayor, R. (2016). Collective cell migration in development. *J. Cell Biol.* **212**, 143-155. doi:10.1083/jcb.201508047

Schier, A. F. (2003). Chemokine signaling: rules of attraction. *Curr. Biol.* **13**, R192-R194. doi:10.1016/S0960-9822(03)00122-2

Sharma, P., Saraswathy, V. M., Xiang, L. and Fürthauer, M. (2019). Notch-mediated inhibition of neurogenesis is required for zebrafish spinal cord morphogenesis. *Sci. Rep.* **9**, 1-18. doi:10.1038/s41598-018-37186-2

Shellard, A. and Mayor, R. (2019). Supracellular migration - Beyond collective cell migration. *J. Cell Sci.* **132**, jcs226142. doi:10.1242/jcs.226142

Shellard, A., Szabó, A., Trepat, X. and Mayor, R. (2018). Supracellular contraction at the rear of neural crest cell groups drives collective chemotaxis. *Science* **362**, 339-343. doi:10.1126/science.aau3301

Simpson, P. (1990). *Lateral inhibition and the development of the sensory bristles of the adult peripheral nervous system of Drosophila*.

Sjöqvist, M. and Andersson, E. R. (2019). Do as i say, Not(ch) as i do: lateral control of cell fate. *Dev. Biol.* **447**, 58-70. doi:10.1016/j.ydbio.2017.09.032

Solnica-Krezel, L. and Sepich, D. S. (2012). Gastrulation: making and shaping germ layers. *Annu. Rev. Cell Dev. Biol* **28**, 687-717. doi:10.1146/annurev-cellbio-092910-154043

Sthijns, M. M. J. P. E., Lapointe, V. L. S. and van Blitterswijk, C. A. (2019). Building complex life through self-organization. *Tissue Engineering A* **25**, 1341-1346. doi:10.1089/ten.tea.2019.0208

Stramer, B. and Mayor, R. (2017). Mechanisms and in vivo functions of contact inhibition of locomotion. *Nat. Rev. Mol. Cell Biol.* **18**, 43-55. doi:10.1038/nrm.2016.118

Stramer, B., Moreira, S., Millard, T., Evans, I., Huang, C. Y., Sabet, O., Milner, M., Dunn, G., Martin, P. and Wood, W. (2010). Clasp-mediated microtubule bundling regulates persistent motility and contact repulsion in *Drosophila* macrophages *in vivo*. *J. Cell Biol.* **189**, 681-689. doi:10.1083/jcb.200912134

Sucgang, R., Weijer, C. J., Siegert, F., Franke, J. and Kessin, R. H. (1997). Null mutations of the Dictyostelium cyclic nucleotide phosphodiesterase gene block chemotactic cell movement in developing aggregates. *Dev. Biol.* **192**, 181-192. doi:10.1006/dbio.1997.8720

Susanto, O., Koh, Y. W. H., Morrice, N., Tumanov, S., Thomason, P. A., Nielson, M., Tweedy, L., Muinonen-Martin, A. J., Kamphorst, J. J., Mackay, G. M. et al. (2017). LPP3 mediates self-generation of chemotactic LPA gradients by melanoma cells. *J. Cell Sci.* **130**, 3455-3466. doi:10.1242/jcs.207514

Swaney, K. F., Huang, C.-H. and Devreotes, P. N. (2010). Eukaryotic chemotaxis: a network of signaling pathways controls motility, directional sensing, and polarity. *Annu. Rev. Biophys.* **39**, 265-289. doi:10.1146/annurev.biophys.093008.131228

Takagi, H., Sato, M. J., Yanagida, T. and Ueda, M. (2008). Functional analysis of spontaneous cell movement under different physiological conditions. *PLoS ONE* **3**, e2648. doi:10.1371/journal.pone.0002648

Tammela, T., Zarkada, G., Nurmi, H., Jakobsson, L., Heinolainen, K., Tvorogov, D., Zheng, W., Franco, C. A., Murtomäki, A., Aranda, E. et al. (2011). VEGFR-3 controls tip to stalk conversion at vessel fusion sites by reinforcing Notch signalling. *Nat. Cell Biol.* **13**, 1202-1213. doi:10.1038/ncb2331

Theisen, U., Straube, E. and Straube, A. (2012). Directional Persistence of Migrating Cells Requires Kif1C-Mediated Stabilization of Trailing Adhesions. *Dev. Cell* **23**, 1153-1166. doi:10.1016/j.devcel.2012.11.005
Todorović, V., Desai, B. V., Patterson, M. J. S., Amargo, E. V., Dubash, A. D., Yin, T., Jones, J. C. R. and Green, K. J. (2010). Plakoglobin regulates cell motility through Rho- and fibronectin-dependent Src signaling. *J. Cell Sci.* **123**, 3576-3586. doi:10.1242/jcs.070391
Tweedy, L. and Insall, R. H. (2020). Self-generated gradients yield exceptionally robust steering cues. *Frontiers in Cell and Developmental Biology* **8**, 133. doi:10.3389/fcell.2020.00133
Tweedy, L., Knecht, D. A., Mackay, G. M. and Insall, R. H. (2016a). Self-generated chemoattractant gradients: attractant depletion extends the range and robustness of chemotaxis. *PLoS Biol.* **14**, e1002404. doi:10.1371/journal.pbio.1002404
Tweedy, L., Susanto, O. and Insall, R. H. (2016b). Self-generated chemotactic gradients - cells steering themselves. *Curr. Opin. Cell Biol.* **42**, 46-51. doi:10.1016/j.ceb.2016.04.003
Tweedy, L., Thomason, P. A., Paschke, P. I., Martin, K., Machesky, L. M., Zagnoni, M. and Insall, R. H. (2020). Seeing around corners: cells solve mazes and respond at a distance using attractant breakdown. *Science* **369**, eaay9792. doi:10.1126/science.aay9792
Valentin, G., Haas, P. and Gilmour, D. (2007). The chemokine SDF1a coordinates tissue migration through the spatially restricted activation of Cxcr7 and Cxcr4b. *Curr. Biol.* **17**, 1026-1031. doi:10.1016/j.cub.2007.05.020
van Haastert, P. J. M., Keizer-Gunnink, I. and Kortholt, A. (2007). Essential role of PI3-kinase and phospholipase A2 in Dictyostelium discoideum chemotaxis. *J. Cell Biol.* **177**, 809-816. doi:10.1083/jcb.200701134
Veltman, D. M., Auciello, G., Spence, H. J., Machesky, L. M., Rappoport, J. Z. and Insall, R. H. (2011). Functional analysis of Dictyostelium IBARa reveals a conserved role of the I-BAR domain in endocytosis. *Biochem. J* **436**, 45-52. doi:10.1042/BJ20101684
Veltman, D. M., Lemieux, M. G., Knecht, D. A. and Insall, R. H. (2014). PIP3-dependent macropinocytosis is incompatible with chemotaxis. *J. Cell Biol.* **204**, 497-505. doi:10.1083/jcb.201309081
Venkiteswaran, G., Lewellis, S. W., Wang, J., Reynolds, E., Nicholson, C. and Knaut, H. (2013). Generation and dynamics of an endogenous, self-generated signaling gradient across a migrating tissue. *Cell* **155**, 674. doi:10.1016/j.cell.2013.09.046
Verkhovsky, A. B., Svitkina, T. M. and Borisy, G. G. (1999). Self-polarization and directional motility of cytoplasm. *Curr. Biol.* **9**, 11-20. doi:10.1016/S0960-9822(99)80042-6
Villar-Cerviño, V., Molano-Mazón, M., Catchpole, T., Valdeolmillos, M., Henkemeyer, M., Martínez, L. M., Borrell, V. and Marín, O. (2013). Contact repulsion controls the dispersion and final distribution of Cajal-Retzius cells. *Neuron* **77**, 457-471. doi:10.1016/j.neuron.2012.11.023
Vishwakarma, M., di Russo, J., Probst, D., Schwarz, U. S., Das, T. and Spatz, J. P. (2018). Mechanical interactions among followers determine the emergence of leaders in migrating epithelial cell collectives. *Nat. Commun.* **9**, 1-12. doi:10.1038/s41467-018-05927-6
Viswanathan, G. M., Buldyrev, S. V., Havlin, S., da Luz, M. G. E., Raposo, E. P. and Stanley, H. E. (1999). Optimizing the success of random searches. *Nature* **401**, 911-914. doi:10.1038/44831
Wang, J. and Knaut, H. (2014). Chemokine signaling in development and disease. *Development (Camb.)* **141**, 4199-4205. doi:10.1242/dev.101071
Wang, W., Goswami, S., Lapidus, K., Wells, A. L., Wyckoff, J. B., Sahai, E., Singer, R. H., Segall, J. E. and Condeelis, J. S. (2004). Identification and testing of a gene expression signature of invasive carcinoma cells within primary mammary tumors. *Cancer Res.* **64**, 8585-8594. doi:10.1158/0008-5472.CAN-04-1136
Weber, G. F., Bjerke, M. A. and DeSimone, D. W. (2012). A Mechanoresponsive cadherin-keratin complex directs polarized protrusive behavior and collective cell migration. *Dev. Cell* **22**, 104-115. doi:10.1016/j.devcel.2011.10.013
Wedlich-Soldner, R. and Li, R. (2003). Spontaneous cell polarization: Undermining determinism. *Nat. Cell Biol.* **5**, 267-270. doi:10.1038/ncb0403-267
Weijer, C. J. (2009). Collective cell migration in development. *J. Cell Sci.* **122**, 3215-3223. doi:10.1242/jcs.036517
Wong, M. and Gilmour, D. (2020). Getting back on track: exploiting canalization to uncover the mechanisms of developmental robustness. *Curr. Opin Genet. Dev.* **63**, 53-60. doi:10.1016/j.gde.2020.04.001
Wong, M., Newton, L. R., Hartmann, J., Hennrich, M. L., Wachsmuth, M., Ronchi, P., Guzmán-Herrera, A., Schwab, Y., Gavin, A.-C. and Gilmour, D. (2020). Dynamic buffering of extracellular chemokine by a dedicated scavenger pathway enables robust adaptation during directed tissue migration. *Dev. Cell* **52**, 492-508.e10.
Xia, P., Gütl, D., Zheden, V. and Heisenberg, C. P. (2019). Lateral inhibition in cell specification mediated by mechanical signals modulating TAZ activity. *Cell* **176**, 1379-1392.e14. doi:10.1016/j.cell.2019.01.019
Xiong, Y., Huang, C. H., Iglesias, P. A. and Devreotes, P. N. (2010). Cells navigate with a local-excitation, global-inhibition-biased excitable network. *Proc. Natl. Acad. Sci. USA* **107**, 17079-17086. doi:10.1073/pnas.1011271107
Yam, P. T., Wilson, C. A., Ji, L., Hebert, B., Barnhart, E. L., Dye, N. A., Wiseman, P. W., Danuser, G. and Theriot, J. A. (2007). Actin-myosin network reorganization breaks symmetry at the cell rear to spontaneously initiate polarized cell motility. *J. Cell Biol.* **178**, 1207-1221. doi:10.1083/jcb.200706012
Yamada, K. M. and Sixt, M. (2019). Mechanisms of 3D cell migration. *Nat. Rev. Mol. Cell Biol.* **20**, 738-752. doi:10.1038/s41580-019-0172-9
Yolland, L., Burki, M., Marcotti, S., Luchici, A., Kenny, F. N., Davis, J. R., Serna-Morales, E., Müller, J., Sixt, M., Davidson, A. et al. (2019). Persistent and polarized global actin flow is essential for directionality during cell migration. *Nat. Cell Biol.* **21**, 1370-1381. doi:10.1038/s41556-019-0411-5
Zhang, J., Goliwas, K. F., Wang, W., Taufalele, P. V., Bordeleau, F. and Reinhart-King, C. A. (2019). Energetic regulation of coordinated leader–follower dynamics during collective invasion of breast cancer cells. *Proc. Natl. Acad. Sci. USA* **116**, 7867-7872. doi:10.1073/pnas.1809964116
Zhang, S., Teng, X., Toyama, Y., Saunders Correspondence, T. E. and Saunders, T. E. (2020). Periodic oscillations of myosin-II mechanically proofread cell-cell connections to ensure robust formation of the cardiac vessel II periodic oscillations of myosin-II Mechanically proofread cell-cell connections to ensure robust formation of the cardiac vessel. *Curr. Biol.* **30**, 3364-3377. doi:10.1016/j.cub.2020.06.041

3.2. A self-generated Toddler gradient guides mesodermal cell migration

Authors:

Jessica Stock, Tomas Kazmar, Friederike Schlumm, Edouard Hannezo and Andrea Pauli

Preamble:

This publication investigates the molecular role of Toddler during zebrafish gastrulation and therefore addresses the main aim of this thesis. Using a combination of experimental approaches and computational modeling, we were able to uncover the mechanism that guides mesodermal cell migration to the animal pole during zebrafish gastrulation. We found that Toddler guides mesodermal cells as a self-generated gradient that is formed and sensed by the Apelin receptor, which is expressed in mesodermal cells.

Status:

Posted on bioRxiv (https://www.biorxiv.org/content/10.1101/2021.12.16.472981v1); currently under revision at Science

My contributions:

- Conceiving the study together with Andrea Pauli and Edouard Hannezo
- Performing the experimental work (computational modeling was performed by our collaborator Edouard Hannezo)
- Data analysis for all experiments, except the global cell tracking analysis, which was established by Tomas Kazmar and Friederike Schlumm, yet I was running the final scripts for our data sets
- Writing of the manuscript together with Andrea Pauli and Edouard Hannezo (text and figures, including original draft)

A self-generated Toddler gradient guides mesodermal cell migration

Jessica Stock[1,2], Tomas Kazmar[1], Friederike Schlumm[1], Edouard Hannezo[3]* and Andrea Pauli[1]*

[1] Research Institute of Molecular Pathology (IMP), Vienna Biocenter (VBC), Vienna, Austria

[2] Vienna BioCenter PhD Program, Doctoral School of the University of Vienna and Medical University of Vienna, Vienna, Austria

[3] Institute of Science and Technology Austria (IST), Klosterneuburg, Austria

* corresponding author

Contact details: edouard.hannezo@ist.ac.at, andrea.pauli@imp.ac.at

ABSTRACT

The sculpting of germ layers during gastrulation relies on coordinated migration of progenitor cells, yet the cues controlling these long-range directed movements remain largely unknown. While directional migration often relies on a chemokine gradient generated from a localized source, we find that zebrafish ventrolateral mesoderm is guided by the uniformly expressed and secreted protein Toddler/ELABELA/Apela, acting as a self-generated gradient. We show that the Apelin receptor, which is specifically expressed in mesodermal cells, has a dual role during gastrulation, acting as a scavenger receptor to generate a Toddler gradient, and as a chemokine receptor to sense this guidance cue. Thus, we uncover a single receptor-based self-generated gradient as the enigmatic guidance cue that can robustly steer the directional migration of mesoderm through the complex and continuously changing environment of the gastrulating embryo.

One sentence summary: Aplnr has a dual role to self-generate and sense a Toddler gradient directing mesodermal cells during zebrafish gastrulation.

Keywords: self-organization, gastrulation, self-generated gradient, cell migration, zebrafish

An animal's body plan is first laid out during gastrulation which assembles the three germ layers—mesoderm, endoderm and ectoderm—through the combination of cell migration and differentiation (*1*–*3*). While research throughout the last few decades has provided fundamental insights into how the germ layers are specified (*3*–*6*), our knowledge of the molecular mechanisms that direct their spatial organization is very limited.

In zebrafish embryos, gastrulation starts with Nodal-induced specification and internalization of mesendodermal progenitor cells at the blastoderm margin (*1*, *7*, *8*). Internalized cells subsequently migrate towards the animal pole, giving rise to the mesodermal and endodermal germ layers (*3*, *9*). The molecular guidance, in particular of ventrolateral mesoderm migration, has remained largely unknown across vertebrates. The only factor currently known to be required for this process is the secreted protein Toddler/ELABELA/Apela (*10*, *11*). Toddler is required primarily for mesoderm migration, acting through the Apelin receptor (in zebrafish, Apelin receptor a and b, collectively referred to as Aplnr), a G protein-coupled receptor specifically expressed in mesodermal cells (*10*–*12*). However, how Toddler establishes directional migration during gastrulation has remained unclear.

Here, we show that mesodermal cells provide a dynamic sink to self-generate a Toddler gradient that acts as their elusive guidance cue. We find that the Aplnr is the sole mediator of both Toddler gradient formation and sensing, which unveils a new mode of gradient self-generation in an *in vivo* system. Altogether, our study uncovers a simple yet robust mechanism that guides mesodermal cells through the dynamic and complex environment of a gastrulating embryo.

RESULTS

Toddler acts cell non-autonomously to attract Aplnr-expressing cells

We had previously shown that ventrolateral mesendoderm fails to migrate to the animal pole in *toddler*$^{-/-}$ embryos (*10*), yet the underlying cause remained unclear. To unveil the role of Toddler in mesendodermal cell migration, we first assessed the migratory behavior of mesendodermal progenitors. To this end, we transplanted between one and five marginal cells from a LifeAct-GFP-expressing wild-type or *toddler*$^{-/-}$ donor embryo to an unlabeled, stage- and genotype-matched host embryo and tracked cells after internalization using either light sheet (**Fig. 1A-C, fig. S1, movies S1-S3**) or confocal microscopy (**Fig. 1D-I, fig. S2, movies S4 and S5)**. Consistent with previous observations (*2*, *10*, *13*, *14*), wild-type cells migrated in a directional manner from the margin toward the animal pole, were polarized, and extended actin-rich protrusions toward the animal pole (**Fig. 1A, D-I, fig. S1, movie S1 and 4**). In contrast, internalized *toddler*$^{-/-}$ cells in *toddler*$^{-/-}$ embryos displayed non-directional migration and were often dragged along with epiboly movements due to reduced and

randomly oriented polarity and lamellipodia formation**,** concomitant with an increased frequency of cell blebbing (**Fig. 1B-I, fig. S1 and S2, movies S2-3 and 5**). Given that higher cell density can increase the frequency of blebbing (*15–17*), this transition from actin- to bleb-based protrusions is likely a secondary effect that can be attributed to the increased cell density at the margin in *toddler*$^{-/-}$ mutant embryos. Taken together, these results reveal that, while *toddler*$^{-/-}$ cells are able to migrate in the absence of Toddler, they lack directionality towards the animal pole.

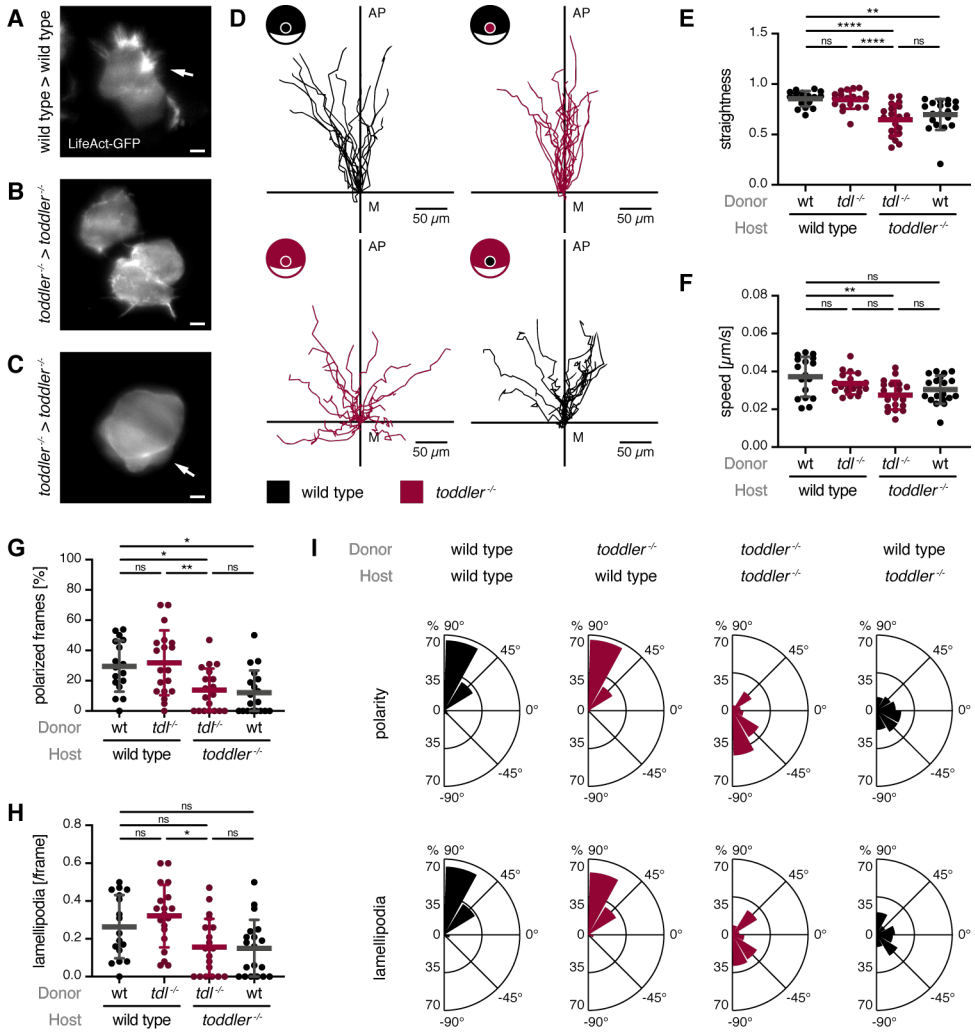

Fig. 1. Toddler acts cell non-autonomously to mediate animal pole-directed polarization and migration of mesendodermal progenitors. Cell transplantation assays to assess the role and cell autonomy of Toddler signaling. LifeAct-GFP-labelled reporter cells (max. 10 cells) were transplanted from the margin of a wild-type or *toddler*$^{-/-}$ donor embryo to the margin of a host embryo of the same or opposite genotype. (A-C) Light sheet microscopy images of representative internalized reporter cells. (A) Wild-type reporter cells in wild-type embryos extending actin-rich lamellipodia (white arrow) towards the animal pole. (B-C) *toddler*$^{-/-}$ reporter cells in *toddler*$^{-/-}$ embryos displaying lack of lamellipodia and polarization (B) or extensive cell blebbing (C, white arrow). Scale bars, 10 µm. (D) Migration tracks of transplanted reporter cells (n = 19 cells for all conditions, except for wild type to wild type transplantation (n = 17)). Cells were tracked for 90 min after internalization using confocal microscopy. Genotypes of donor cells and host embryos are indicated in the embryo scheme

(black: wild type; red: *toddler*$^{-/-}$). x-axis = margin; y-axis = animal-vegetal axis; coordinate origin = start of track. (E) Quantification of track straightness calculated as the net displacement after 90 min divided by the total track length. (F) Quantification of migration speed of cells tracked in (D). (G) Quantification of cell polarity of internalized cells represented as the percentage of frames in which a cell was polarized (see Materials and Methods for classification of polarization). (H) Quantification of lamellipodia represented as average number of lamellipodia detected per frame (see Materials and Methods for classification of lamellipodia). (I) Rose plots showing relative enrichments (percentages) of orientations of polarity and lamellipodia, normalized to the total number of polarity axes or lamellipodia of all cells within the same condition. Data are means ± SD. Significance was determined using one-way ANOVA with multiple comparison; ****, $p < 0.0001$; **, $p < 0.01$; *, $p < 0.05$; n.s., not significant. Rose plots: 90° = animal pole; 0° = ventral/dorsal; -90° = vegetal pole. All graphs are oriented with the animal pole towards the top.

Given that Toddler is a secreted protein (*10*, *11*), we hypothesized that it regulates directional migration of mesodermal progenitors via a cell non-autonomous mechanism. To distinguish cell intrinsic from extrinsic effects, we transplanted marginal cells from wild-type or *toddler*$^{-/-}$ donor embryos into unlabeled, stage-matched host embryos of the opposite genotype. *Toddler*$^{-/-}$ cells placed into a wild-type host embryo were able to migrate directionally, polarize and extend actin-rich protrusions towards the animal pole (**Fig. 1D-I, movie S6**). Wild-type cells in a Toddler-deficient environment, on the other hand, displayed the *toddler*$^{-/-}$ phenotype and failed to migrate directionally away from the margin (**Fig. 1D-I, fig. S2, movie S7**). Combined, these results confirm that Toddler acts cell non-autonomously to mediate the migration of mesendodermal progenitors.

A cell non-autonomous signaling mechanism, as well as the loss of directional migration and polarity in the absence of Toddler indicates that Toddler could act as a chemokine to guide mesodermal cells to the animal pole. As previous efforts to unravel the role of Toddler have led to contradicting results, providing support for a chemoattractant (*18*) as well as a motogen (*10*) function, we revisited this question and assessed the ability of Toddler to attract Aplnrb-expressing cells. Aplnrb-sfGFP-expressing cells from a *toddler*$^{-/-}$ donor embryo transplanted next to a source of Toddler at the animal pole of a stage-matched *toddler*$^{-/-}$ host embryo (**Fig. 2A-B**) displayed directional migration towards a Toddler-expressing source until they made initial contact with and attached to Toddler-expressing cells (**Fig. 2B-E, fig. S3, movie S8**). This cellular behavior is similar to the one described for the previously reported chemokine receptor/ligand pair Cxcr4b/Cxcl12a (*19*). Directional migration was induced robustly over a distance of 100 µm (**Fig. 2C**) and required both the ligand and receptor to be present since the lack of either Toddler in the source or of Aplnr in the migrating cells (knockdown using *aplnra/b* morpholinos) led to the loss of directional migration (**Fig. 2B-E, movie S8**) and reduced contacts between Aplnrb-sfGFP-expressing and Toddler-expressing cells (**fig. S3B, movie S8**). Taken together, these results indicate that Toddler can provide a chemoattractant signal and that Aplnr is necessary as a chemokine receptor to receive the signal.

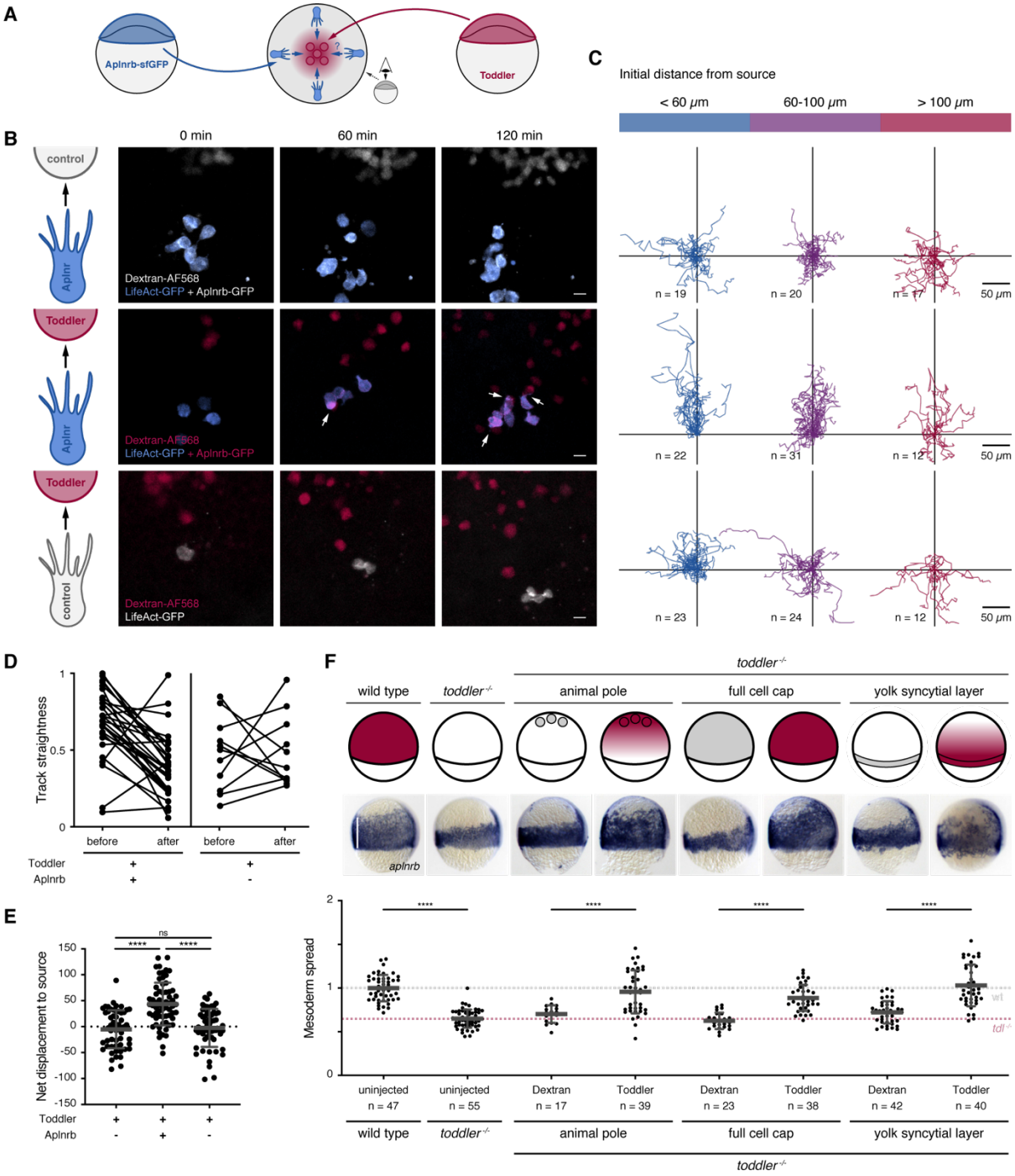

Fig. 2. Aplnr-expressing cells are attracted towards a local source of Toddler. (A) Schematic representation of the experimental set-up to test for Toddler functioning as a chemokine signal for Aplnr-expressing cells. Toddler-expressing cells, red; Aplnrb-expressing cells, blue. (B) Snapshots of a time-laps confocal imaging series assessing ability of Aplnrb-sfGFP-expressing toddler -/- cells to react to an ectopically located Toddler or control source. (Top) Exposure of Aplnr-sfGFP-expressing cells (blue) to Toddler-deficient control cells (grey). n = 56 cells. (Middle) Exposure of Aplnr-sfGFP-expressing cells to Toddler-overexpressing source cells (red). n = 65 cells. White arrows indicate contact between Aplnrb-sfGFP-expressing cells and Toddler source cells. (Bottom) Exposure of cells deficient in Aplnr expression (grey) to Toddler-overexpressing source cells (red). n = 59 cells. (C) Cell tracks corresponding to conditions described in (B). Tracks were grouped by the distance of the cell from the source at the start of imaging (blue: <60 µm, purple: 60-100 µm, red: >100 µm). (D) Quantified track straightness of all Aplnrb-sfGFP-expressing and Aplnr-deficient cells that reach direct cell-cell contact with a

Toddler-expressing source cell. Track straightness was compared before and after contact with the source cell. (E) Quantification of net displacement towards the source. (F) Ectopic expression of Toddler in toddler -/- embryos according to schematic representation of embryos at 75% epiboly (top). Animal pole source: transplantation of Toddler-overexpressing cells to the animal pole of sphere stage toddler -/- embryos; ubiquitous expression: injection of 2 pg toddler mRNA (rescuing concentration) into 1-cell stage toddler -/- embryos; marginal source: injection of 10 pg of toddler mRNA into the yolk syncytial layer of 1k-cell stage toddler -/- embryos. Toddler (red); Dextran control (grey). Mesoderm spread was assessed using in situ hybridization for aplnrb (middle; lateral view, dorsal on the right; white line indicates measurement of ventral mesoderm spread) and quantified relative to the average spread in wild-type embryos (bottom). Data are mean ± SD. Significance was determined using one-way ANOVA with multiple comparison; ****, $p < 0.0001$; **, $p < 0.01$; n.s., not significant. Scale bars, 20 µm. All graphs and images are oriented with the source at the top.

Mesodermal cells are guided by a self-generated Toddler gradient

Our results so far indicate that Toddler can act as a guidance cue that attracts mesodermal cells. In support of this, placing a cluster of Toddler-expressing cells at the animal pole is sufficient to restore animal pole-directed mesoderm migration in *toddler*$^{-/-}$ embryos (**Fig. 2F**). However, in line with previous results (*10*), expression of Toddler throughout the embryo cap, leading to its homogenous distribution, or from the margin (*toddler* mRNA injection into the yolk syncytial layer (YSL) before the onset of gastrulation), causing Toddler to be graded in the opposite direction, are also able to rescue animal pole-directed mesoderm migration in *toddler*$^{-/-}$ embryos (**Fig. 2F**). These results are contrary to typical chemokine models based on concentration gradients formed by a fixed source or sink, and suggest that mesoderm migration during gastrulation requires Toddler, but is largely independent of Toddler's expression site.

Studies in the zebrafish lateral line (*20*, *21*) and *Dictyostelium* (*22*, *23*) have shown that migrating cells can "self-generate" chemokine gradients by locally taking up the chemokine, making them independent of a localized source. To assess quantitatively whether mesodermal cells could self-polarize by locally shaping a Toddler gradient, we turned to computational modeling (see **Materials & Methods**). We simulated the one-dimensional migration of mesodermal cells along the animal-vegetal axis *x* with local cell density *c(x,t)* over time (**Fig. 3A**, see also **fig. S4A-E** for a sensitivity analysis and **Materials & Methods** for details). Cells internalize at the margin (*x=0*), can randomly diffuse (random movements with diffusion coefficient D_c), and migrate directionally according to the local gradient of the Toddler concentration profile *T(x,t)*. Simulation of the Toddler concentration *T(x,t)* along the animal-vegetal axis factored in random Toddler diffusion (with coefficient D_T), baseline degradation (with timescale τ_T), and a sink to remove Toddler that is proportional to the local density of mesodermal cells (under the simplifying assumption that each cell has a constant capacity to remove Toddler, see **Materials & Methods** for details and extensions of the model to more general situations). Importantly, we also took into consideration that the quantity of available Toddler is not a fixed value, as in typical *in vitro* assays of self-generated gradients (*22*, *23*). Indeed, based on single-

cell RNA-seq data (*24*), *toddler* mRNA is expressed ubiquitously throughout the embryo at the onset of gastrulation (**Fig. 3B**) and becomes restricted to non-mesodermal cells during gastrulation (indicated by the mutually exclusive expression patterns of *toddler* and *aplnrb* (**Fig. 3B-C**)). Based on these observations, we infer that Toddler is continuously and homogenously expressed along the animal-margin axis (e.g., by the overlying ectodermal tissue) throughout gastrulation.

To test the core assumptions of the model and constrain its parameters, we first measured the baseline degradation time τ_T of Toddler. To this end, we injected *in vitro* synthesized Toddler peptide into *toddler*$^{-/-}$*, MZoep*$^{-/-}$ double mutant embryos deficient for both Toddler production (*toddler*$^{-/-}$) and the proposed mesodermal Toddler sink (*MZoep*$^{-/-}$) (*25*, *26*). We found that a single time scale can describe Toddler degradation kinetics in *MZoep*$^{-/-}$*, toddler*$^{-/-}$ double mutants, from which we can extract the parameter $\tau_T \approx 2$h (**fig. S4F-G**). Given the known molecular weight of Toddler, we could also estimate its random diffusion to be $D_T \approx 3.10^3 \mu m^2/min$ (a typical value for small diffusible molecules, see (*27*) and **Materials & Methods**). Based on these calculations, locally produced Toddler can propagate up to length scales of $\sqrt{D_T \tau_T} \approx 600\ \mu m$ (the typical size of a zebrafish embryo) in the absence of a mesoderm sink. Altogether, these measurements provided estimates for the key parameters of Toddler dynamics, which we used to make predictions on spatiotemporal dynamics of mesoderm migration.

We simulated wild-type migration in the presence or absence of the mesodermal Toddler sink. The simulation predicted that animal pole-directed migration of mesodermal cells would be abolished in the absence of the sink function if the Toddler gradient was absent (ubiquitous Toddler expression or *toddler*$^{-/-}$) or reversed (preferential Toddler expression at the margin from the YSL) (**Fig. 3D**). With sink function in mesodermal cells, the dynamics depended on one rescaled parameter, namely the product of mesodermal Toddler consumption rate (α) and the coupling between the local slope of the Toddler gradient and the corresponding active mesodermal migration speed (β) (compare **fig. S4A and C, see Materials & Methods**). Introduction of this parameter resulted in local depletion of Toddler at the margin, where mesodermal cells internalize, thus forming a Toddler concentration gradient (**Fig. 3E-F**). The resulting animal pole-directed migration of mesodermal cells sustains the Toddler gradient, with stronger sink function resulting in proportionally faster migration and higher independence of the location of the Toddler source. Thus, in agreement with our experimental findings, the self-generated gradient model suggests that mesodermal cells can shape a gradient from uniform Toddler concentrations (or even from an inverse Toddler gradient, as long as the sink function is strong enough) to direct their migration to the animal pole (**Fig. 3E**). Importantly, the resulting Toddler gradient can be sustained even close to the margin (far from the migratory leading edge) (**Fig. 3F**) due to the continuous production of Toddler.

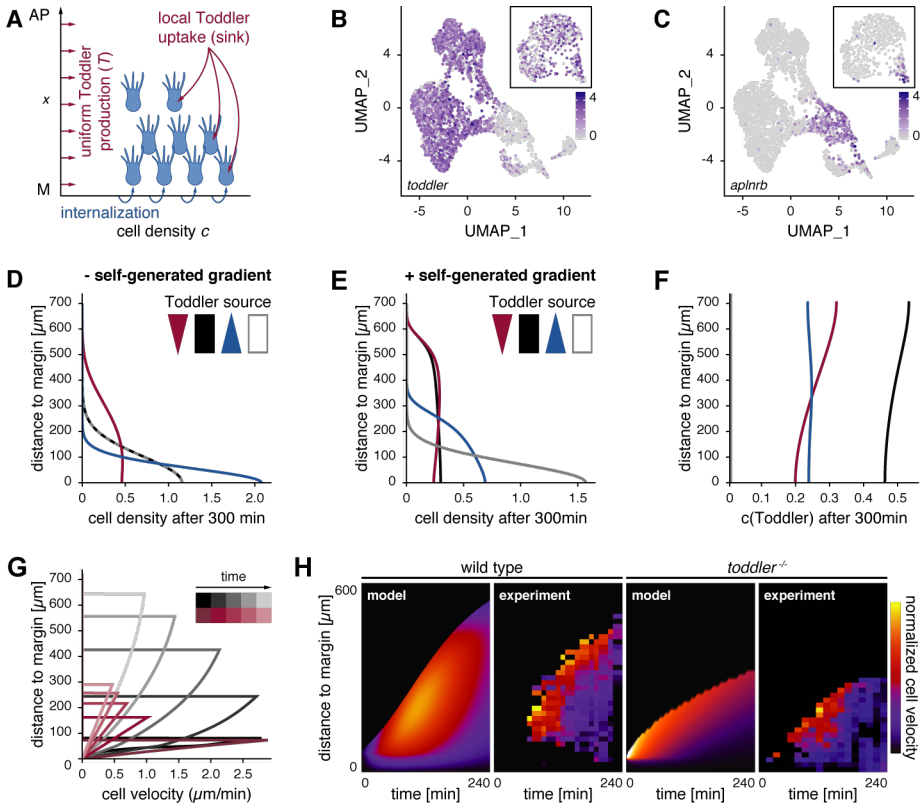

Fig. 3. Computational simulations predict a self-generated Toddler gradient. (A) Schematic representation of the one-dimensional model of mesoderm density and Toddler concentration along the animal-vegetal axis (x = 0 denotes the margin, at which mesodermal cells are added). Toddler (red) is produced uniformly at rate T_0 and is degraded locally by mesoderm cells (blue). Mesodermal cells can move randomly as well as directionally in response to local Toddler gradients. **(B-C)** Uniform manifold approximation and projection (UMAP) clustering of single cells at 60% epiboly based on single cell RNAseq data [24]. Inset depicts UMAP at 30% epiboly. Color-code represents expression levels of *toddler* (B) and *aplnrb* (C) in individual cells, respectively. **(D-E)** Predicted mesoderm density profiles (arbitrary units) after 300 min without (D) or with (E) Toddler uptake by mesoderm cells, for different profiles of Toddler production $T_0(x)$: graded towards the margin (blue), graded towards the animal pole (red), uniform (black) or no production (white/grey). **(F)** Predicted Toddler concentrations (arbitrary units) after 300 min with Toddler uptake by mesodermal cells. Profiles of Toddler productions $T_0(x)$ as described in (D and E). **(G)** Predicted spatiotemporal profiles of mesodermal cell velocities in wild-type (black) and *toddler*$^{-/-}$ embryos (red). **(H)** Predicted (model) and experimental (experiment) kymographs of mesodermal cell migration in wild-type (left) and *toddler*$^{-/-}$ (right) embryos. Experimental data from light-sheet microscopy and tracking of *drl:GFP*-positive cells (N = 7 (wild type) and N = 6 (*toddler*$^{-/-}$) embryos; average number of n = 195 cells tracked per embryo). Color-code represents normalized velocity (yellow: high; dark purple: low).

This model further predicts a distinct pattern of velocities across mesodermal cells, in which cell velocities increase as a function of the distance from the margin but decrease overall as a function of time (**Fig. 3G**). To test this prediction experimentally, we used light sheet microscopy to image transgenic zebrafish embryos expressing *drl:GFP* (*draculin* promoter driving GFP expression), which specifically labels ventrolateral mesoderm during gastrulation (*12*, *28*), injected with *h2b-RFP* mRNA to label all nuclei. This reporter allowed us to identify and track ventrolateral mesodermal cells and their progenitors (see **Materials and Methods** for details). We found that the experimentally

measured average mesodermal cell velocity was indeed highest at the leading edge of the mesodermal cells and decreased overall with the progression of gastrulation (**Fig. 3H**). Therefore, with a single fitting parameter (strength of self-generated directionality as mentioned above, see **Materials & Methods** for details), theoretical predictions could recapitulate the experimental kymographs (**Fig. 3H**). Moreover, the shape of the mesodermal cell density profile along the animal-vegetal axis in wild-type and *toddler*$^{-/-}$ embryos predicted by the model (**fig. S4H**) was also consistent with experimental data (**fig. S4I-J**).

Next, we simulated mesodermal migration dynamics in the absence of Toddler. In this case, the only mode of mesodermal cell movements is random cell motility (with coefficient D_c estimated from short-term measurements of transplanted cell displacements in *toddler*$^{-/-}$ embryos, see **fig. S4K-L**). The model predicted that mesodermal cells migrate approximately half the distance in *toddler*$^{-/-}$ embryos compared to that in wild-type embryos, and that animal pole-directed migration rapidly decreased over time (**Fig. 3G-H**), as expected from a random migration process. Indeed, we found that the migration front of mesodermal cells in *toddler*$^{-/-}$ *tg(drl:GFP)* embryos did not progress as far as in wild-type *tg(drl:GFP)* embryos and had nearly zero net velocity four hours after the onset of internalization (**Fig. 3H**).

In summary, our theoretical predictions, supported by experimental measurements in wild-type and *toddler*$^{-/-}$ embryos, strongly suggests that mesodermal cells are being guided to the animal pole by a self-generated Toddler gradient.

Aplnr-mediated removal of Toddler at the margin self-generates a Toddler gradient

Our hypothesis that mesodermal cells self-generate a Toddler gradient that guides their own migration to the animal pole makes four predictions: First, mesodermal cells are required to locally remove Toddler and thereby mediate the directed migration of individual cells to the animal pole; second, there is a maximal threshold of ligand concentration the system can compensate for; third, Toddler levels in wild-type embryos are highest at the animal pole and lowest at the margin; and fourth, the animal pole-directed migration of mesodermal cells is a phenomenon of collective rather than individual cell migration.

To test the requirement of mesodermal cells as a sink, we transplanted LifeAct-GFP-labelled cells from the margin of a wild-type embryo to the margin of stage-matched host embryos that either possess (wild-type) or lack (*MZoep*$^{-/-}$) the proposed mesodermal sink (**Fig. 4A**). The reporter cells showed directional migration in the wild-type host but lost their directionality and polarity in the *MZoep*$^{-/-}$ host (**Fig. 4B-D, fig. S5A-C, movie S9**), where they formed multiple actin-rich protrusions in various directions (**Fig. 4C, fig. S5A-C, movie S9**), in line with excessive chemokine stimulation from all directions (*29*). To confirm that the absence of a Toddler gradient causes this loss of directional

migration, we engineered a Toddler gradient in *MZoep*$^{-/-}$, *toddler*$^{-/-}$ double mutant embryos by transplanting a cluster of Toddler-expressing cells to the animal pole to establish a local source of Toddler (**Fig. 4A**). This ectopically induced Toddler gradient was indeed able to rescue directional polarization, protrusion formation and migration of wild-type reporter cells towards the animal pole in embryos lacking mesendodermal cells (**Fig. 4B-D, fig. S5A-C**, **movie S9**). Therefore, mesendodermal cells are required to establish a Toddler gradient, which guides them towards the animal pole.

Although only a few examples of self-generated gradients have been described, different mechanisms have been observed to mediate their formation, such as enzymatic chemokine digestion at the cell surface (*22*) or chemokine internalization via a scavenger receptor (*20*, *21*). It has previously been reported that Toddler binds Aplnr-expressing cells (*11*) and induces Aplnr internalization (*10*) (**fig. S6A-C**), which, based on the general mechanism of GPCR-ligand interaction and signaling (*30*), should lead to the concomitant endocytosis and degradation of Toddler, making Aplnr an excellent candidate for the local uptake and thus removal of Toddler. To test this possibility we transplanted individual LifeAct-GFP-labelled wild-type reporter cells to the margin of a sphere-stage *aplnr*^{MO} host embryo, which lacks Aplnr expression (**Fig. 4A**). The reporter cells lost their ability to polarize, lacked the typical animal pole-directed bias in protrusion formation, and failed to migrate towards the animal pole in the *aplnr*^{MO} host, phenocopying their behavior in the *MZoep*$^{-/-}$ host (**Fig. 4B-D, fig. S5A-C**, **movie S10**). These results, together with the chemokine assays presented in **Fig. 2**, establish a dual role for Aplnr in mesodermal cells during zebrafish gastrulation as (1) a scavenger receptor to generate the Toddler gradient by removing it from the environment, and (2) a chemokine receptor to sense the Toddler gradient and direct cell migration.

Self-generated gradients are known to be robust to fluctuations in chemokine levels. However, the limited availability and turnover of the receptor predicts a maximal threshold of ligand concentration the system can compensate for and maintain the balance between ligand and receptor. In light of the dual role of Aplnr, we expanded the computational model described above to account for the Aplnr turnover during Toddler removal. Due to the finite capacity of Aplnr to remove Toddler, the model predicts that, above a threshold level of Toddler, mesodermal migration would become non-directional, resembling *toddler*$^{-/-}$ embryos (**fig. S7A**). It further predicts that these migration defects at high Toddler levels can be rescued by simultaneous overexpression of Aplnr (**fig. S7B**). We confirmed both of these predictions experimentally. Overexpression of Toddler in wild-type embryos caused mesodermal mis-migration phenotypes mimicking *toddler*$^{-/-}$ embryos (**fig. S7C**), as previously observed (*10*). However, simultaneously increasing the number of mesodermal cells (and thereby the level of Aplnr expression in these embryos) by blocking the expression of the Nodal inhibitor Lefty2

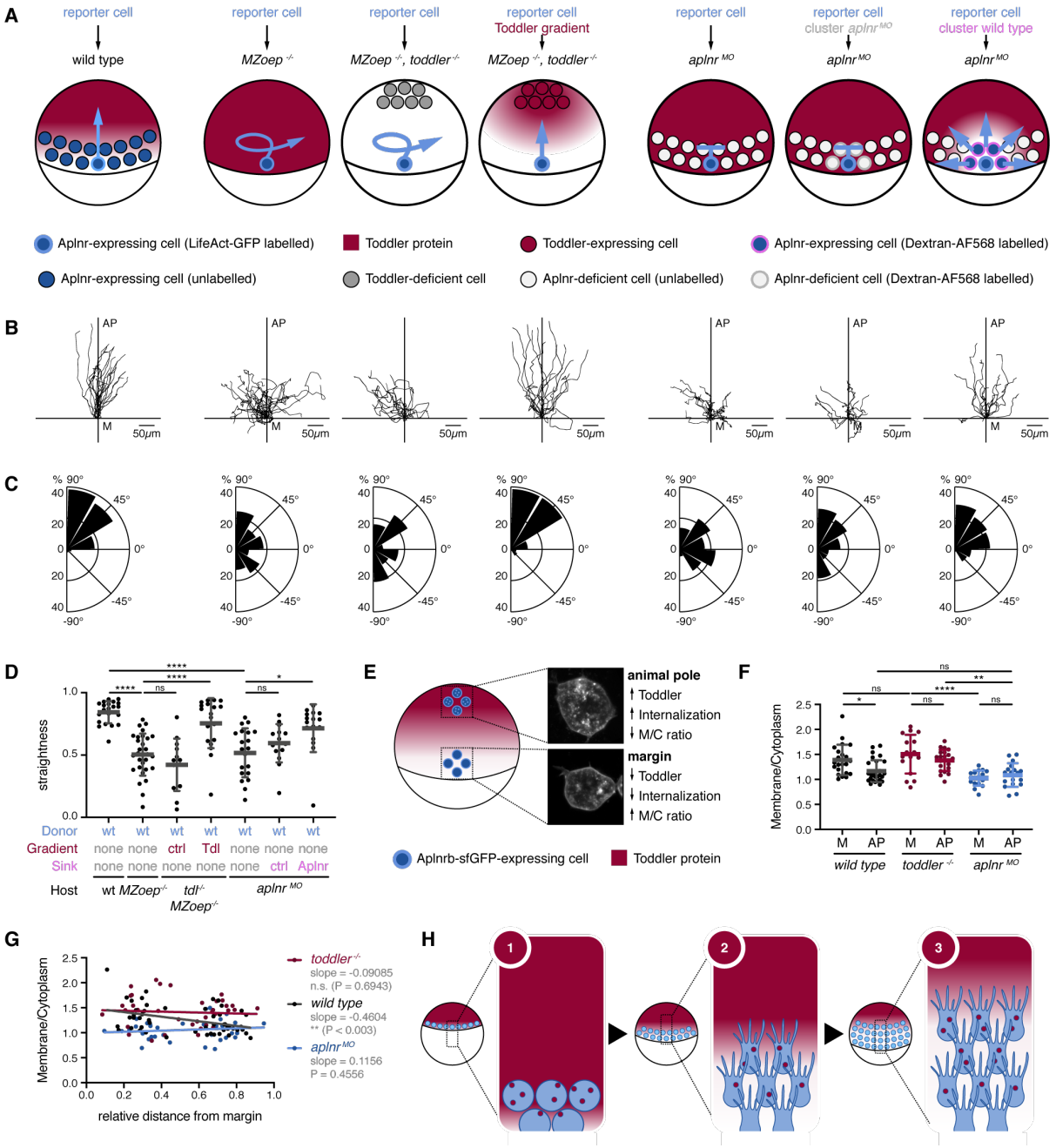

Fig. 4. Aplnr-expressing mesodermal cells are required to establish a Toddler gradient. Cell transplantation assays to test for the necessity of Aplnr-expressing mesodermal cells as a sink for Toddler in the gastrulating embryo. Transplanted LifeAct-GFP-labelled wild-type reporter cells were used as a read-out for the presence and shape of a Toddler gradient. **(A)** Schematic representation of the different scenarios tested. From left to right: (1) Transplantation of reporter cells into a wild-type host embryo (n = 21). (2) Transplantation of reporter cells into an *MZoep* $^{-/-}$ host embryo (n = 22). (3) Transplantation of reporter cells into an *MZoep* $^{-/-}$, *toddler* $^{-/-}$ double mutant host embryo. Additional transplantation of Dextran-AlexaFluor568-labelled control source cells to the animal pole (n = 16). (4) Transplantation of reporter cells into an *MZoep* $^{-/-}$, *toddler* $^{-/-}$ double mutant host embryo. Additional transplantation of Toddler-expressing source cells to the animal pole to simulate presence of a Toddler gradient (n = 15). (5) Transplantation of reporter cells into an *aplnr* ^{MO} embryo (n = 20). (6) Co-transplantation of 1 to 5 reporter cells and a large number of Dextran-AlexaFluor568-labelled Aplnr-deficient control cells into *aplnr* ^{MO} host embryo (n = 15). (7) Co-transplantation of 1 to 5 reporter cells and a large number of Aplnr-expressing cells into *aplnr* ^{MO} host embryos to re-introduce a localized Toddler sink (n = 16). Reporter cell is depicted in dark blue with light blue rim. Expected Toddler gradient is represented in red. Blue arrow

indicates expected migration behavior of the reporter cells. **(B)** Tracks of transplanted reporter cells (order as described in (A)). Cells were tracked for 90 min after internalization. x-axis = margin; y-axis = animal-vegetal axis; coordinate origin = start of track. **(C)** Rose plots showing relative enrichments (percentages) of orientations of polarity, normalized to the total number of polarity axes of all cells within the same condition. 90° = animal pole; 0° = ventral/dorsal; -90° = vegetal pole. **(D)** Quantification of straightness of cell tracks presented in (B). **(E-G)** Detection of a Toddler concentration gradient from margin to animal pole based on Aplnrb-sfGFP internalization. **(E)** Schematic representation of transplantation assay in a wild-type host embryo. Transplantation of Aplnrb-sfGFP-expressing *toddler*$^{-/-}$ cells to the animal pole and margin of the host embryo. Insets display representative confocal images of transplanted cells at animal pole and margin in a wild-type host embryo. **(F)** Quantification Aplnrb-sfGFP internalization levels of marginal and animal pole-located transplanted cells in wild-type (n(margin)=22, n(animal pole)=29), *toddler*$^{-/-}$ (n(margin)=16, n(animal pole)=21) or *aplnr*^{MO} (n(margin)=17, n(animal pole)=18) host embryos, as determined by the ratio of membrane to cytoplasm fluorescence intensity (see Materials and Methods section for details). **(G)** Ratio of membrane to cytoplasm fluorescence intensity of transplanted cells relative to their distance to the margin. P value indicates significance of regression being different to 0 as determined by F test. **(H)** Schematic representation of the self-generated Toddler gradient: (1) Toddler is ubiquitously expressed throughout the embryo cap during zebrafish gastrulation. Mesodermal progenitor cells internalize at the margin and express Aplnr, which acts as a scavenger receptor for Toddler. (2) Aplnr binds and internalizes Toddler, which generates a local Toddler concentration gradient in front of the mesodermal cells, providing a directional cue. (3) Aplnr also acts as a chemokine receptor to sense the self-generated Toddler guidance cue and induces the directed migration of mesodermal cells towards the animal pole, while continuously internalizing Toddler and shaping the local gradient. Data are means ± SD. Significance was determined using one-way ANOVA with multiple comparison; ****, $p < 0.0001$; *, $p < 0.05$; n.s., not significant. All images and graphs are oriented with the animal pole towards the top.

(*31*) restored mesoderm migration in embryos with intermediate levels of Toddler overexpression (5 pg *toddler* mRNA, **fig. S7C**). Taken together, these observations provide independent evidence for Aplnr acting as a scavenger receptor for Toddler and support the model of a self-generated gradient.

Our model of a self-generated gradient predicts Toddler levels to be high at the animal pole and low at the margin due to the local uptake through Aplnr-expressing mesodermal cells. To experimentally confirm this prediction, we aimed at detecting local differences in Toddler levels. Because fluorescently or multi-epitope tagged Toddler is not functional, and because available Toddler antibodies (*11*) are not sensitive enough to detect endogenous Toddler, a direct visualization of the Toddler gradient is currently not feasible, prompting us to use Aplnr internalization (**fig. S6**) as a read-out for the local Toddler concentration. To establish the feasibility of this approach, we first determined the maximal difference that could be expected between the animal pole and margin in wild-type embryos. We assessed maximal and minimal Aplnr internalization levels by measuring the ratio of membrane-localized versus internalized Aplnr in transplanted Aplnrb-GFP-expressing *toddler*$^{-/-}$ cells in the presence of uniformly high Toddler levels (*aplnr*^{MO} host embryos) and in the absence of Toddler (*toddler*$^{-/-}$ host embryos) (**Fig 4E-G and fig. S6D**). This revealed a relatively small yet significant increase in Aplnr-GFP internalization in *aplnr*^{MO} versus *toddler*$^{-/-}$ host embryos. To confirm the presence of a Toddler gradient in wild-type embryos, we transplanted Aplnrb-GFP-expressing cells from a sphere-stage *toddler*$^{-/-}$ host embryo either to margin or to the animal pole at the ventral side

of a shield-stage wild-type host embryo. Consistent with higher levels of Toddler at the animal pole, the level of Aplnr internalization was increased at the animal pole compared to the margin (**Fig. 4E-G and fig. S6D**). Importantly, this local difference in Toddler levels between the animal pole and margin was not detected in either *toddler*$^{-/-}$ or *aplnr*^{MO} host embryos (**Fig. 4E-G and fig. S6D**). Taken together, these results confirm the existence of a Toddler gradient that depends on the sink activity of Aplnr-expressing mesodermal cells.

Finally, migration through self-generated gradients is generally a phenomenon of collective cell migration. Accordingly, the formation of the gradient is predicted to require a sufficient number of cells to locally remove enough chemokine (*32*), as seen by a decrease of animal pole-directed migration in simulations with a reduced number of mesodermal cells (**fig. S5D**). Therefore, we hypothesized that a cluster of Aplnr-expressing cells, but not a single Aplnr-expressing cell, would undergo directional migration in a uniform Toddler environment when transplanted to the margin. To test this hypothesis, we assessed the migratory ability of a small number (up to 10) of LifeAct-GFP-labelled wild-type reporter cells co-transplanted with a large number (more than 50) of Dextran-Alexa568-labelled, Aplnr-expressing (sink^{+}) or Aplnr-lacking (sink^{-}) cells, to the margin of an *aplnr*^{MO} host embryo (**Fig. 4A**). The reporter cells migrated randomly and failed to reach the animal pole when co-transplanted with cells that lacked Aplnr (**Fig. 4B-D, fig. S5A-C**, **movie S10**). However, when the co-transplanted cells expressed Aplnr, the reporter cells displayed increased track straightness, reduced ectopic protrusion formation and increased directional, radial outward-directed polarization (**Fig. 4B-D, fig. S5A-C**, **movie S10**), indicating the presence of a guidance cue. In summary, these results provide evidence that a cluster of Aplnr-expressing cells is sufficient to restore sink activity and directional migration of reporter cells, in line with collective cell migration being a hallmark of self-generated gradients.

DISCUSSION

This study describes a previously unknown, self-generated Toddler gradient, that is formed and sensed by a single molecular mediator, the Apelin receptor, to guide the animal pole-directed migration of ventrolateral mesoderm during zebrafish gastrulation (**Fig. 4H**). Through the global production and local degradation of Toddler, the location of the mesoderm sink defines the directionality of cell migration toward the animal pole, as it both generates and senses a Toddler gradient that is self-sustained and inversely proportional to the mesodermal cell density (**Fig. 4H**).

Different types of self-generated gradients have recently been discovered as powerful guidance mechanisms (*20–22*, *33*). Self-generated chemokine gradients are characterized by one shared feature: Both the function of chemokine gradient formation and sensing are found within the

migrating unit at opposite poles of the tissue (*20*, *21*) or even the same cell, as suggested by theoretical work and studies with cultured cells *in vitro* (*22*). Additional studies based on computational modeling (*34*) or *in vitro* experiments (*35*) have further suggested that removal of the chemokine and sensing of the gradient could be mediated by the same receptor. We provide direct experimental *in vivo* evidence that a GPCR, namely the Aplnr, indeed executes both scavenger and sensor roles, acting as the sole molecular player in generating and sensing the directional cue that guides mesodermal cells to the animal pole. Interestingly, a conceptually similar finding, namely that signaling GPCRs modulate extracellular guidance cues, has been reported for immune cell migration while this study was under review (*36*). The chemokine receptor CCR7 was shown to both sense and self-generate functional CCL19 chemokine gradients *in vitro*, thereby collectively organizing the co-migration of several immune cell types. Together with our study, this highlights the potentially broadly applicable concept of GPCR-mediated self-generated signal gradients in diverse biological contexts.

The use of a self-generated gradient, in particular those based on a single receptor, holds several advantages over a pre-existing gradient for the migration of a dynamic tissue, like the arising mesoderm. First, self-generated gradients can robustly act over long distances (*32*), which is necessary for mesodermal cell migration, with the space from margin to animal pole spanning over 500 µm during zebrafish gastrulation. Secondly, the simple two-component system (here: Aplnr and Toddler) of a single receptor-based self-generated gradient can be easily adjusted to a dynamically changing tissue, and thus circumvents the need to establish stable domains with distinct functions. Instead, the shape of the gradient is determined by the position of the migrating cell front rather than the total size of the tissue. This is particularly beneficial during gastrulation, as the continuous internalization of mesodermal cells and the vegetal pole-directed movement of the margin causes a steady increase in cell number and expansion of tissue size. Finally, while pre-existing gradients require tight regulation of steepness and chemokine concentration along the gradient to ensure reliable cell guidance, self-generated gradients can compensate for changes in length scale (as described above) and chemokine levels by adjusting the rate of chemokine breakdown (*37*). Therefore, self-generated gradients may have evolved to accommodate different architectures of complex migrating tissues by providing the necessary flexibility to adjust to changing environments and migration modes.

Our computational simulations and experimental analyses of mesodermal cell migration patterns are consistent with the formation of a Aplnr-dependent Toddler gradient in wild-type embryos since in the absence of Toddler as a guidance cue mesodermal cell migration was mostly driven by random cell motility. However, it is important to note that *toddler*$^{-/-}$ cells retained some residual bias for migration towards the animal pole (**Fig. 1 and 3-4**). These findings suggest that—at least in the absence of a Toddler–based guidance cue—migration is aided by additional, Toddler-independent

mechanisms, which could include contact inhibition of locomotion (*38*, *39*) or biomechanical forces (*40*, *41*).

Morphogenetic movements during gastrulation across the animal kingdom share common principles. In amniotes, including mouse and human, mesodermal progenitors internalize at the primitive streak before migrating anteriorly as a non-coherent cell sheet (*1*). Previous studies have shown that, while conserved, Toddler and Apelin, the other ligand of Aplnr, are not essential for gastrulation movements in mice (*42*). However, based on the presented advantages and similar nature of morphogenetic movements across species, we hypothesize that self-generated gradients of different or redundant chemokine receptor-ligand pairs could present a universal mechanism underlying the anterior migration of mesodermal progenitor cells in gastrulation, as well as other cell migration events throughout development and physiology.

ACKNOWLEDGMENTS

We thank Karin Aumayer and the team of the biooptics facility at the Vienna Biocenter, in particular Pawel Pasierbek and Tobias Müller, for support with microscopy; Karin Panser, Carina Pribitzer and the animal facility personnel for taking care of zebrafish; Mirjam Binner and Anna Bandura for help with genotyping; Mireia Codina Tobias for her help with establishing the conditions for the Toddler overexpression compensation experiment, Tiago Lubiana Alves for sharing the code for scRNA-Seq analyses; the Heisenberg lab, in particular Diana Pinheiro, for joint lab meetings, discussions on the project and providing the *tg(gsc:CAAX-GFP)* fish line; the Raz lab for providing the Lifeact-GFP plasmid; Angela Andersen, Alex Schier, Carl-Phillip Heisenberg and Elly Tanaka for comments on the manuscript; the entire Pauli lab, in particular Krista Gert and Victoria Deneke, for valuable discussions and feedback on the manuscript.

FUNDING

Work in A.P.'s lab has been supported by the IMP, which receives institutional funding from Boehringer Ingelheim and the Austrian Research Promotion Agency (Headquarter grant FFG-852936), as well as the FWF START program (Y 1031-B28 to A.P.), the Human Frontier Science Program (HFSP) Career Development Award (CDA00066/2015 to A.P.) and Young Investigator Grant (RGY0079/2020 to A.P.), the SFB RNA-Deco (project number F 80 to A.P.), a Whitman Center Fellowship from the Marine Biological Laboratory (to A.P.), and EMBO-YIP funds (to A.P.). This work was supported by the European Union (European Research Council Starting Grant 851288 to E.H.).

AUTHOR CONTRIBUTION

Conceptualization: JS, EH, AP

Methodology: JS

Data analysis: JS

Cell tracking analysis: TK, FS

Computational Modeling: EH

Funding acquisition: AP, EH

Supervision: AP

Writing – original draft: JS

Writing – review & editing: JS, AP, EH

DECLARATION OF INTERESTS

The authors declare no competing interests.

RESOURCE AVAILABILITY

Light sheet imaging data are available upon request.

REFERENCES

1. L. Solnica-Krezel, D. S. Sepich, Gastrulation: Making and Shaping Germ Layers. *Annu. Rev. Cell Dev. Biol*. **28**, 687–717 (2012).
2. L. Solnica-Krezel, Conserved patterns of cell movements during vertebrate gastrulation. *Current Biology*. **15** (2005), , doi:10.1016/j.cub.2005.03.016.
3. L. A. Rohde, C. P. Heisenberg, Zebrafish Gastrulation: Cell Movements, Signals, and Mechanisms. *International Review of Cytology*. **261** (2007), pp. 159–192.
4. D. Pinheiro, C. P. Heisenberg, in *Current Topics in Developmental Biology* (Academic Press Inc., 2020), vol. 136, pp. 343–375.
5. B. Feldman, M. A. Gates, E. S. Egan, S. T. Dougan, G. Rennebeck, H. I. Sirotkin, A. F. Schier, W. S. Talbot, Zebrafish organizer development and germ-layer formation require nodal- related signals. *Nature*. **395**, 181–185 (1998).
6. A. F. Schier, Nodal morphogens. *Cold Spring Harbor perspectives in biology*. **1** (2009), p. a003459.
7. A. F. Schier, W. S. Talbot, Molecular Genetics of Axis Formation in Zebrafish. *Annual Review of Genetics*. **39**, 561–613 (2005).
8. M. L. Williams, L. Solnica-Krezel, Regulation of gastrulation movements by emergent cell and tissue interactions. *Current Opinion in Cell Biology*. **48** (2017), pp. 33–39.
9. C. B. Kimmel, W. W. Ballard, S. R. Kimmel, B. Ullmann, T. F. Schilling, Stages of embryonic development of the zebrafish. *Developmental Dynamics*. **203**, 253–310 (1995).
10. A. Pauli, M. L. Norris, E. Valen, G. L. Chew, J. A. Gagnon, S. Zimmerman, A. Mitchell, J. Ma, J. Dubrulle, D. Reyon, S. Q. Tsai, J. K. Joung, A. Saghatelian, A. F. Schier, Toddler: An embryonic

signal that promotes cell movement via apelin receptors. *Science*. **343** (2014), doi:10.1126/science.1248636.

11. S. C. Chng, L. Ho, J. Tian, B. Reversade, ELABELA: A hormone essential for heart development signals via the apelin receptor. *Developmental Cell*. **27**, 672–680 (2013).
12. M. L. Norris, A. Pauli, J. A. Gagnon, N. D. Lord, K. W. Rogers, C. Mosimann, L. I. Zon, A. F. Schier, Toddler signaling regulates mesodermal cell migration downstream of Nodal signaling. *eLife*. **6** (2017), doi:10.7554/elife.22626.
13. P. J. Keller, A. D. Schmidt, J. Wittbrodt, E. H. K. Stelzer, Reconstruction of zebrafish early embryonic development by scanned light sheet microscopy. *Science*. **322**, 1065–1069 (2008).
14. R. H. Row, J. L. Maître, B. L. Martin, P. Stockinger, C. P. Heisenberg, D. Kimelman, Completion of the epithelial to mesenchymal transition in zebrafish mesoderm requires Spadetail. *Developmental Biology*. **354**, 102–110 (2011).
15. Y. Belotti, D. McGloin, C. J. Weijer, Effects of spatial confinement on migratory properties of Dictyostelium discoideum cells. *Communicative and Integrative Biology*. **14**, 5–14 (2021).
16. M. Bergert, S. D. Chandradoss, R. A. Desai, E. Paluch, Cell mechanics control rapid transitions between blebs and lamellipodia during migration. *Proceedings of the National Academy of Sciences*. **109**, 14434–14439 (2012).
17. V. Venturini, F. Pezzano, F. C. Castro, H. M. Häkkinen, S. Jiménez-Delgado, M. Colomer-Rosell, M. Marro, Q. Tolosa-Ramon, S. Paz-López, M. A. Valverde, J. Weghuber, P. Loza-Alvarez, M. Krieg, S. Wieser, V. Ruprecht, The nucleus measures shape changes for cellular proprioception to control dynamic cell behavior. *Science*. **370** (2020), doi:10.1126/SCIENCE.ABA2644/SUPPL_FILE/ABA2644_VENTURINI_SM.PDF.
18. C. S. Helker, A. Schuermann, C. Pollmann, S. C. Chng, F. Kiefer, B. Reversade, W. Herzog, The hormonal peptide Elabela guides angioblasts to the midline during vasculogenesis. *eLife*. **4** (2015), doi:10.7554/elife.06726.
19. H. Blaser, S. Eisenbeiss, M. Neumann, M. Reichman-Fried, B. Thisse, C. Thisse, E. Raz, Transition from non-motile behaviour to directed migration during early PGC development in zebrafish. *Journal of Cell Science*. **118**, 4027–4038 (2005).
20. G. Venkiteswaran, S. W. Lewellis, J. Wang, E. Reynolds, C. Nicholson, H. Knaut, Generation and dynamics of an endogenous, self-generated signaling gradient across a migrating tissue. *Cell*. **155**, 674 (2013).
21. E. Donà, J. D. Barry, G. Valentin, C. Quirin, A. Khmelinskii, A. Kunze, S. Durdu, L. R. Newton, A. Fernandez-Minan, W. Huber, M. Knop, D. Gilmour, Directional tissue migration through a self-generated chemokine gradient. *Nature*. **503**, 285–289 (2013).
22. L. Tweedy, D. A. Knecht, G. M. Mackay, R. H. Insall, Self-Generated Chemoattractant Gradients: Attractant Depletion Extends the Range and Robustness of Chemotaxis. *PLoS Biology*. **14**, e1002404 (2016).
23. L. Tweedy, O. Susanto, R. H. Insall, Self-generated chemotactic gradients - cells steering themselves. *Current Opinion in Cell Biology*. **42** (2016), pp. 46–51.
24. J. A. Farrell, Y. Wang, S. J. Riesenfeld, K. Shekhar, A. Regev, A. F. Schier, Single-cell reconstruction of developmental trajectories during zebrafish embryogenesis. *Science*. **360**, eaar3131 (2018).
25. A. F. Schier, S. C. Neuhauss, K. A. Helde, W. S. Talbot, W. Driever, The one-eyed pinhead gene functions in mesoderm and endoderm formation in zebrafish and interacts with no tail. *Development*. **124**, 327–342 (1997).

26. K. Gritsman, J. Zhang, S. Cheng, E. Heckscher, W. S. Talbot, A. F. Schier, The EGF-CFC protein one-eyed pinhead is essential for nodal signaling. *Cell*. **97**, 121–132 (1999).
27. P. Müller, K. W. Rogers, B. M. Jordan, J. S. Lee, D. Robson, S. Ramanathan, A. F. Schier, Differential diffusivity of nodal and lefty underlies a reaction-diffusion patterning system. *Science*. **336**, 721–724 (2012).
28. C. Mosimann, D. Panáková, A. A. Werdich, G. Musso, A. Burger, K. L. Lawson, L. A. Carr, K. R. Nevis, M. K. Sabeh, Y. Zhou, A. J. Davidson, A. Dibiase, C. E. Burns, C. G. Burns, C. A. Macrae, L. I. Zon, Chamber identity programs drive early functional partitioning of the heart. *Nature Communications*. **6**, 1–10 (2015).
29. P. Devreotes, A. R. Horwitz, Signaling networks that regulate cell migration. *Cold Spring Harbor Perspectives in Biology*. **7** (2015), doi:10.1101/cshperspect.a005959.
30. N. J. Pavlos, P. A. Friedman, GPCR Signaling and Trafficking: The Long and Short of It. *Trends in Endocrinology and Metabolism*. **28** (2017), pp. 213–226.
31. A. L. van Boxtel, J. E. Chesebro, C. Heliot, M. C. Ramel, R. K. Stone, C. S. Hill, A Temporal Window for Signal Activation Dictates the Dimensions of a Nodal Signaling Domain. *Developmental Cell*. **35**, 175–185 (2015).
32. L. Tweedy, R. H. Insall, Self-Generated Gradients Yield Exceptionally Robust Steering Cues. *Frontiers in Cell and Developmental Biology*. **8**, 133 (2020).
33. A. Shellard, R. Mayor, Collective durotaxis along a self-generated stiffness gradient in vivo. *Nature 2021*, 1–5 (2021).
34. J. M. Haugh, Deterministic model of dermal wound invasion incorporating receptor-mediated signal transduction and spatial gradient sensing. *Biophysical Journal*. **90**, 2297–2308 (2006).
35. C. Scherber, A. J. Aranyosi, B. Kulemann, S. P. Thayer, M. Toner, O. Iliopoulos, D. Irimia, Epithelial cell guidance by self-generated EGF gradients. *Integrative biology : quantitative biosciences from nano to macro*. **4**, 259–269 (2012).
36. J. Alanko, M. C. Ucar, N. Canigova, J. Stopp, J. Schwarz, J. Merrin, E. Hannezo, M. Sixt, *bioRxiv*, in press, doi:10.1101/2022.02.22.481445.
37. M. Wong, L. R. Newton, J. Hartmann, M. L. Hennrich, M. Wachsmuth, P. Ronchi, A. Guzmán-Herrera, Y. Schwab, A. C. Gavin, D. Gilmour, Dynamic Buffering of Extracellular Chemokine by a Dedicated Scavenger Pathway Enables Robust Adaptation during Directed Tissue Migration. *Developmental Cell*. **52**, 492-508.e10 (2020).
38. C. Carmona-Fontaine, H. K. Matthews, S. Kuriyama, M. Moreno, G. A. Dunn, M. Parsons, C. D. Stern, R. Mayor, Contact inhibition of locomotion in vivo controls neural crest directional migration. *Nature*. **456**, 957–961 (2008).
39. A. Roycroft, R. Mayor, Molecular basis of contact inhibition of locomotion. *Cellular and Molecular Life Sciences*. **73**, 1119–1130 (2016).
40. E. Hannezo, C. P. Heisenberg, Mechanochemical Feedback Loops in Development and Disease. *Cell*. **178** (2019), pp. 12–25.
41. C. P. Heisenberg, Y. Bellaïche, Forces in tissue morphogenesis and patterning. *Cell*. **153** (2013), p. 948.
42. L. Freyer, C. W. Hsu, S. Nowotschin, A. Pauli, J. Ishida, K. Kuba, A. Fukamizu, A. F. Schier, P. A. Hoodless, M. E. Dickinson, A. K. Hadjantonakis, Loss of Apela Peptide in Mice Causes Low Penetrance Embryonic Lethality and Defects in Early Mesodermal Derivatives. *Cell Reports*. **20**, 2116–2130 (2017).

43. M. Smutny, Z. Ákos, S. Grigolon, S. Shamipour, V. Ruprecht, D. Čapek, M. Behrndt, E. Papusheva, M. Tada, B. Hof, T. Vicsek, G. Salbreux, C. P. Heisenberg, Friction forces position the neural anlage. *Nature Cell Biology*. **19**, 306–317 (2017).
44. X. X. I. Zeng, T. P. Wilm, D. S. Sepich, L. Solnica-Krezel, Apelin and Its Receptor Control Heart Field Formation during Zebrafish Gastrulation. *Developmental Cell*. **12**, 391–402 (2007).
45. I. C. Scott, B. Masri, L. A. D'Amico, S. W. Jin, B. Jungblut, A. M. Wehman, H. Baier, Y. Audigier, D. Y. R. Stainier, The G Protein-Coupled Receptor Agtrl1b Regulates Early Development of Myocardial Progenitors. *Developmental Cell*. **12**, 403–413 (2007).
46. A. Agathon, B. Thisse, C. Thisse, Morpholino knock-down of Antivin1 and Antivin2 upregulates nodal signaling. *Genesis*. **30**, 178–182 (2001).
47. S. Paskaradevan, I. C. Scott, The Aplnr GPCR regulates myocardial progenitor development via a novel cell-non-autonomous, G i/o protein-independent pathway. *Biology Open*. **1**, 275–285 (2012).
48. J. Zhang, W. S. Talbot, A. F. Schier, Positional Cloning Identifies Zebrafish one-eyed pinhead as a Permissive EGF-Related Ligand Required during Gastrulation. *Cell*. **92**, 241–251 (1998).
49. T. Y. C. Tsai, M. Sikora, P. Xia, T. Colak-Champollion, H. Knaut, C. P. Heisenberg, S. G. Megason, An adhesion code ensures robust pattern formation during tissue morphogenesis. *Science*. **370**, 113–116 (2020).
50. A. Shindo, A. Audrey, M. Takagishi, M. Takahashi, J. B. Wallingford, M. Kinoshita, Septin-dependent remodeling of cortical microtubule drives cell reshaping during epithelial wound healing. *Journal of Cell Science*. **131** (2018), doi:10.1242/jcs.212647.
51. K. Jaqaman, D. Loerke, M. Mettlen, H. Kuwata, S. Grinstein, S. L. Schmid, G. Danuser, Robust single-particle tracking in live-cell time-lapse sequences. *Nature Methods*. **5**, 695–702 (2008).
52. R. Jonker, A. Volgenant, A shortest augmenting path algorithm for dense and sparse linear assignment problems. *Computing*. **38**, 325–340 (1987).
53. F. Pedregosa, G. Varoquaux, A. Gramfort, V. Michel, B. Thirion, O. Grisel, M. Blondel, P. Prettenhofer, R. Weiss, V. Dubourg, J. Vanderplas, A. Passos, D. Cournapeau, M. Brucher, M. Perrot, É. Duchesnay, Scikit-learn: Machine Learning in Python. *Journal of Machine Learning Research*. **12**, 2825–2830 (2011).
54. S. van der Walt, J. L. Schönberger, J. Nunez-Iglesias, F. Boulogne, J. D. Warner, N. Yager, E. Gouillart, T. Yu, Scikit-image: Image processing in python. *PeerJ*. **2014**, e453 (2014).
55. I. Kasa, A Circle Fitting Procedure and its Error Analysis. *IEEE Transactions on Instrumentation and Measurement*. **IM–25**, 8–14 (1976).
56. C. Thisse, B. Thisse, High-resolution in situ hybridization to whole-mount zebrafish embryos. *Nature Protocols*. **3**, 59–69 (2008).
57. L. Ho, S. Y. X. Tan, S. Wee, Y. Wu, S. J. C. Tan, N. B. Ramakrishna, S. C. Chng, S. Nama, I. Szczerbinska, Y. S. Chan, S. Avery, N. Tsuneyoshi, H. H. Ng, J. Gunaratne, N. R. Dunn, B. Reversade, ELABELA Is an Endogenous Growth Factor that Sustains hESC Self-Renewal via the PI3K/AKT Pathway. *Cell Stem Cell*. **17**, 435–447 (2015).
58. T. Jin, Gradient sensing during chemotaxis. *Current Opinion in Cell Biology*. **25**, 532–537 (2013).
59. N. A. Hill, D. P. Häder, A Biased Random Walk Model for the Trajectories of Swimming Micro-organisms. *Journal of Theoretical Biology*. **186**, 503–526 (1997).

60. P. Recho, A. Hallou, E. Hannezo, Theory of mechanochemical patterning in biphasic biological tissues. *Proceedings of the National Academy of Sciences of the United States of America*. **116**, 5344–5349 (2019).
61. L. Tweedy, P. A. Thomason, P. I. Paschke, K. Martin, L. M. Machesky, M. Zagnoni, R. H. Insall, Seeing around corners: Cells solve mazes and respond at a distance using attractant breakdown. *Science*. **369** (2020), doi:10.1126/science.aay9792.

Science
AAAS

Supplementary Materials for

A self-generated Toddler gradient guides mesodermal cell migration

Jessica Stock[1,2], Tomas Kazmar[1], Friederike Schlumm[1], Edouard Hannezo[3]* and Andrea Pauli[1]*

Correspondence to: edouard.hannezo@ist.ac.at, andrea.pauli@imp.ac.at

This PDF file includes:

Materials and Methods

Figs. S1 to S7

Captions for Movies S1 to S10

Other Supplementary Materials for this manuscript include the following:

Movies S1 to S10

MATERIALS AND METHODS

Ethical statement

All fish experiments were conducted according to Austrian and European guidelines for animal research and approved by the Amt der Wiener Landesregierung, Magistratsabteilung 58 - Wasserrecht (animal protocols GZ: 342445/2016/12 and MA 58-221180-2021-16).

Zebrafish husbandry

Zebrafish (*Danio rerio*) were raised according to standard protocols (28°C water temperature, 14/10 hour light/dark cycle). TLAB fish were generated by crossing AB and natural variant TL (Tupfel Longfin) zebrafish and used as wild type for all experiments. *MZoep*$^{-/-}$ (*26*) and *toddler*$^{-/-}$ (*10*) double mutant, as well as *tg(drl:gfp)* (*28*), *toddler*$^{-/-}$ lines and *tg(gsc:CAAX-GFP)* (*43*) wild-type lines were generated by crossing the two respective lines.

Genotyping of mutants

Genotyping of *toddler*$^{-/-}$ (*10*) and *MZoep*$^{-/-}$ (*26*) mutants was performed by PCR amplification. As previously published (*10*), the *toddler* PCR amplicon (toddler_gt_F and toddler_gt_R) was digested with RsaI as the mutation destroys the corresponding restriction site. Detection of digest product (wild type: 192 + 318 nt, *toddler*$^{-/-}$: 510 nt) was performed using standard gel electrophoresis with 4% agarose gels. The *oep* PCR amplicon (oep_gt_F and oep_gt_R) was digested with Tsp45I as the mutation introduces the respective restriction site. Detection of the digested product (wild type: 300 nt, *oep*$^{-/-}$: 150 + 150 nt) was performed using standard gel electrophoresis with 4% agarose gels.

Injection of mRNAs and morpholinos into zebrafish embryos

Capped mRNAs for *toddler, oep, aplnrb, aplnrb-sfgfp, lifeact-gfp, human h2b-bfp, human h2b-rfp* and *f'bfp* were transcribed from linearized plasmids using the SP6, T7 or T3 mMessage machine kit (Ambion), according to manufacturer's protocol. All mRNAs were injected into 1-cell stage embryos unless indicated otherwise. All plasmids were previously described (Table S1).

Double knockdown of *aplnra* and *aplnrb*, as well as knockdown of *lefty2* were performed using morpholino (MO) injection as previously described (*10*, *44–47*). Briefly, 0.5 and 1 ng of MOs against *aplnra* (cggtgtattccggcgttggctccat; GeneTools) and *aplnrb* (cagagaagttgtttgtcatgtgctc; GeneTools) respectively or 12.5 ng of MO against *lefty2* (agctggatgaacagagccatgac; GeneTools) were injected into 1-cell stage embryos. A control MO (cctcttacctcagttacaatttata; GeneTools) was used at equivalent concentrations.

Table 1 | List of plasmids

Plasmid	mRNA	Restriction/Polymerase	Source
AP242	toddler	BglII/SP6	Pauli et al., 2014
R013	oep	NotI/T7	Zhang et al., 1998
AP552	aplnrb	EcoRV/T7	Pauli et al., 2014
AP606	aplnrb-sfgfp	BglII/SP6	Pauli et al., 2014
R160	lifeact-gfp	XbaI/T3	Raz Lab
R203	human h2b-bfp	EcoRV/SP6	Tsai et al., 2020
R009	human h2b-rfp	NotI/SP6	https://www.addgene.org/53745/
R202	f'bfp	EcoRV/SP6	Shindo et al., 2018

Table 2 | List of primers

Primer name	Sequence
toddler_gt_F	CGACAGAATTTATCGTCTGAGGAAC
toddler_gt_R	TGAAAGTTACATTGGGTTAGAAAGC
oep_gt_F	AGGCCCTCGAGATAAATAACA
oep_gt_R	ACAGCAAACATCAAGAACCTG

Live cell imaging

Light sheet microscopy

For light sheet microscopy, four embryos were mounted in 0.6% low-melt agarose in 1XPBS in glass capillaries (Brand, 20 µL). The capillary was placed in the heated (27°C), with fish water filled sample chamber of a Zeiss Z1 light sheet microscope. The two most suitably oriented embryos were imaged. To assess morphology and migration behavior of wild-type and *toddler*$^{-/-}$ cells, four successfully transplanted embryos (only one genotype per experiment) were mounted. The two embryos that had the best orientation (animal pole straight up or down + lateral orientation + transplanted cells in the center of the frame at the margin) were selected for imaging. Time laps series of Z-stacks were taken from both embryos over 5 hours (from sphere stage to end of gastrulation) with a 20x objective.

For global cell tracking experiments, wild-type *tg(drl:gfp)* or *toddler*$^{-/-}$ *tg(drl:gfp)* embryos were injected with 100 pg *h2b-rfp* mRNA at the 1-cell stage and mounted at sphere stage. The 0.6% low-melt agarose was supplemented with fluorescent beads (1:1000, TetraSpeck™ microspheres, 0.2 µm, fluorescent blue/green/orange/dark red, Invitrogen #T7280) that were used to adjust the light sheet

offset and stabilize the imaging sequence. Four embryos were mounted, and the two most ideally oriented embryos (animal pole up or down) were selected for imaging. Time laps series of Z-stacks were taken from both embryos over 8 hours with a 10x objective. At 24 hours post fertilization, z-stacks from four positions around the embryo were acquired (0°, 90°, 180° and 270° in reference to the position of the time course imaging) to determine the location of dorsal and ventral sides within the embryo. Finally, 6 z-stacks of 1000 z-slices were acquired with lasers turned off (used to remove background during subsequent data analysis). Raw light sheet data was converted to tiff files. For cell morphology analyses, the data was binned 4x in xy to allow for better data handling. The region of interest (internalizing migrating cell) was identified in binned images and automatically cropped (in x/y/z and time) in the raw data, using a custom-made app (https://drive.google.com/drive/folders/1183kxnarTEyb1-4Otzyh0RlQhEnHO8Oo?usp=sharing). Cropped imaging files were analyzed as described below.

Table 3 | Settings for light sheet microscopy

	Cell morphology	**Cell tracking**
Magnification/Objective	20x water immersion	10x water immersion
Laser	488 (6%) and 561 (5%)	499 (5%) and 561 (5%)
Exposure time	30 ms	30 ms
Illumination	Dual sided illumination with online fusion	Dual sided illumination with online fusion
Image size	439.1x439.1 µm; 1920x1920 px	772.85x772.85 µm; 1200x1200 px
Z-stack	50 to 80 slices (depending on embryo), 2 µm interval	150 slices, 1.774 µm interval
Time series	500 time points, 30 sec intervals	700 time points, 42 sec intervals

Table 4 | Settings for confocal microscopy

	Transplantation experiments	**Aplnrb-GFP internalization**
Magnification/Objective	10x (air)	20x (air)
Laser	405, 488 and 561	405, 488 and 561
Pinhole	4 AU (120 µm)	1 AU (32 µm)
Averaging	2x	8x
Image size	14.19x14.09 mm; 20467x20322 px	319.45x319.45 µm; 1024x1024 px

Z-stack	9 slices (120 µm)	21 slices (20 µm)
Time series	72 time points (25 for chemokine assays), 5 min interval	Not applicable

Confocal microscopy

For confocal imaging, embryos were mounted in the desired orientation in a drop of 0.8% low-melt agarose in 1XPBS on round glass bottom dishes (ibidi). Agarose drops were left to harden before dishes were filled with E3 medium (5 mM NaCl, 0.17 mM KCl, 0.33 mM $CaCl_2$, 0.33 mM $MgSO_4$, 10^{-5}% Methylene Blue). Time laps movies of z-stacks were acquired on an inverted LSM800 Axio Observer (Zeiss) with temperature incubation (27°C) for 6 hours. To assess Aplnrb-GFP internalization, z-stacks for each embryo were taken for only one time point at sphere stage (**fig. S6A-C**) or shield stage (**Fig. 4E-G and fig. S6D**).

Transplantation assays

Cellular phenotype

To assess cell migration behavior of individual cells after internalization, donor embryos were injected with 100 pg *lifeact-gfp* mRNA. For light sheet imaging experiments only, host embryos were injected with 100 pg *h2b-rfp* mRNA. Between 1 and 5 cells were taken from the marginal region of donor embryos at sphere stage and transplanted to the margin of stage- and genotype-matched host embryos. At dome stage, embryos were mounted laterally with transplanted cells facing the glass dish and imaged on a confocal microscope or mounted in a glass capillary for light sheet microscopy and imaged as described above. For light sheet microscopy individual frames were acquired in 1 min intervals, while for confocal microscopy individual frames were acquired 5 min intervals. Analysis of the cellular phenotype (see below for details) confirmed that, except for slight differences in cell speed, results were consistent between light sheet and confocal data. The differences in cell speed likely stem from the lower time-resolution in confocal imaging that can not fully resolve all fluctuations in the migratory tracks and therefore might lead to an underestimation of the actual distance travelled by the cell in 5 min.

Cell autonomy

To assess the cell autonomy of Toddler signaling, embryos were prepared, and transplantations performed as described above. Donor and host embryos were stage-matched but of opposite genotypes (transplantation of wild type into *toddler*$^{-/-}$ and vice versa). Imaging and subsequent analysis were performed blindly.

Chemokine assay

All embryos used for the chemokine assay were *toddler*$^{-/-}$. Donor^{receptor} embryos were injected at the 1-cell stage with 150 pg *lifeact-rfp* mRNA only (control) or in combination with 200 pg *aplnrb-sfGFP* mRNA. Donor^{ligand} embryos were injected at the 1-cell stage with 100 pg Dextran-AlexaFluor488 only (control) or in combination with 100 pg *toddler* mRNA. Host embryos were injected at the 1-cell stage with 150 pg *h2b-bfp* mRNA. Embryos were left to develop until sphere stage. 50-100 cells were taken from donor^{ligand} embryos and transplanted to the animal pole of stage-matched host embryos. 1-10 cells were taken from donor^{receptor} embryos and transplanted to the host embryo at positions surrounding the animal pole. Embryos were mounted on the animal pole and imaged as described above.

Localized Toddler source

Animal pole expression of Toddler was achieved by transplantation assays. Donor embryos were injected at the 1-cell stage with 100 pg Dextrane-AlexaFluor488 only (controls) or in combination with 200 pg *toddler* mRNA. Dextrane-AlexaFluor488 was used to trace successful injection and transplantation. At sphere stage, 50 to 100 cells were taken from donor embryos and transplanted to animal pole of stage-matched *toddler*$^{-/-}$ host embryos. For uniform expression of Toddler, 100 pg Dextran-AlexaFluor488 only (controls) or in combination with 2 pg of *toddler* mRNA were injected into 1-cell stage *toddler*$^{-/-}$ embryos. To achieve marginal expression, 100 pg Dextrane-AlexaFluor488 only (controls) or in combination with 10 pg *toddler* mRNA were injected into the yolk syncytial layer of 1k-cell stage embryos. Embryos were collected for in situ hybridization (see below) at 75% epiboly.

Sink removal

To test for sink function of mesendodermal cells and scavenger function of Aplnr, wild-type donor embryos were injected with 100 pg *lifeact-gfp* mRNA at the 1-cell stage. Host embryos were either untreated (*MZoep* $^{-/-}$) or injected with *aplnr* MOs to inhibit *aplnr* mRNA translation in wild-type embryos. 1 to 5 donor cells were taken from the margin at sphere stage and transplanted to the margin of a stage-matched host embryo. Transplantations of more than 10 cells were excluded from analysis to avoid the possibility of sink re-introduction. Embryos were mounted laterally with transplanted cells facing the objective and imaged using confocal microscopy as described above.

Toddler gradient

To assess the sufficiency of a Toddler gradient to guide cell migration in the absence of mesendodermal cells, transplantations were performed using *MZoep*$^{-/-}$*, toddler*$^{-/-}$ double mutant host embryos. Wild-type donor^{reporter} embryos were injected with 100 pg *lifeact-GFP* mRNA at the 1-cell stage. *MZoep*$^{-/-}$, *toddler*$^{-/-}$ double mutant donor^{source} embryos were injected at the 1-cell stage with 200 pg Dextran-AlexaFluor568 only (controls) or in combination with 200 pg *toddler* mRNA. 50 to 100

cells of donor^{source} cells were transplanted to the animal pole of a sphere stage host embryo. Subsequently, 1 to 5 LifeAct-GFP positive donor^{reporter} cells were transplanted to the margin of the same host. Embryos were mounted laterally with transplanted cells facing the objective and imaged using confocal microscopy as described above.

Single vs. collective cell migration

To generate a sink of Aplnr-expressing cells by transplantation, donor^{reporter} wild-type embryos were injected with 100 pg *lifeact-gfp* mRNA at the 1-cell stage. For donor^{sink}, *tg(gsc:caax-gfp)* embryos were injected with 100 pg Dextran-AlexaFluor568 at the 1-cell stage. These embryos were used since they allow to identify and exclude the dorsal region at transplantation. Host and donor^{sink} embryos were injected with 0.5 ng of *aplnra* MO and 1 ng of *aplnrb* MO. At late dome stage, 50 cells from the ventral margin of donor^{sink} embryos followed by 5 to 10 cells from the margin of donor^{reporter} embryos were taken into the same needle and transplanted to the margin of stage-matched host embryos. Embryos were mounted laterally with transplanted cells facing the objective and imaged as described above. Imaging and subsequent analysis were performed blindly.

Detection of Toddler gradient through Aplnrb-sfGFP internalization levels

To assess Aplnrb-sfGFP internalization levels depending on the cell position along the animal-vegetal axis within the embryo, host embryos (wild type or *toddler-/-*) were either left untreated or injected with 0.5 ng of *aplnra* MO and 1 ng of *aplnrb* MO, as indicated. Donor *toddler*$^{-/-}$ embryos were laid 2 hours after host embryos and injected with 200 pg of Aplnrb-sfGFP mRNA and 200 pg of Dextrane. Once the host embryos reached shield stage, up to 20 cells were transplanted from the sphere-staged donor embryo to two positions within a single host embryo, the ventral margin and the animal pole. Embryos were left to recover for 15 min before being mounted laterally in 0.8% low-melt agarose with transplanted cells facing the objective and imaged as described above.

Imaging analysis

Protrusions and polarity

Cells of interest for analysis were identified in the time-laps movies based on several criteria:

(i) Ventral or lateral position in the host embryo: Cells that were transplanted to the dorsal side (as indicated by visible convergence and extension movements as well as the formation of somites at the end of the time-laps) were excluded from the analysis.

(ii) Only internalized cells were analyzed. Internalization was identified by a cell's position in the z-dimension (lower cell layer) and a change in direction that indicates the transition from vegetally directed epiblast to animally directed hypoblast cell movement.

(iii) Sufficiently long cell tracks: Analysis of a cell had to be possible for at least 15 (light sheet; ≙30min) or 12 (confocal; ≙1h) time frames. Every cell that divided, moved out of frame or overlapped with another transplanted cell within this time window was excluded from analysis.

(iv) Analysis was performed before ~70% epiboly (before the onset of convergence and extension movements).

Protrusions were distinguished based on the LifeAct-GFP signal of polymerized actin and defined by the following characteristics:

(i) Lamellipodia: actin-mesh that expands several µm in width; wide protrusion that extends beyond the cell body.

(ii) Filopodia: thin actin strings that extend from the cell body.

(iii) Bleb: actin-free (marked by cytoplasmic, dispersed LifeAct-GFP), round membrane extension with polymerized actin at its base.

Each cell was analyzed from the time of internalization until one of the 4 criteria above was no longer applicable. In some cases, a cell divided shortly after internalization, therefore, analysis was started 10 (light sheet) or 2 (confocal) time frames (≙10min) after division to exclude mitosis-induced cell rounding and loss of polarity. Length and angle (in reference to animal pole) of protrusions were measured in ImageJ. A straight line through the center of the protrusion was drawn from the base (border to cell body) to the tip of the protrusion. A cell was counted as polarized if it was elongated and actin polymerization and protrusion formation was restricted to one side only, with additional protrusions (filopodia only) allowed within a 45° angle to either side. Protrusions were measured and counted for every cell in each time frame. Protrusion rate (protrusion/min) was calculated by normalizing the sum of all protrusions for one cell to the length of the time course (for light sheet) or the number of time frames (for confocal). To quantify orientation of polarization and protrusions, the numbers of angles within every 30° were counted and normalized to the total number of the same protrusion/polarity within the same genotype. As the position of dorsal and ventral in these embryos was not specifically determined, the left and right side of the resulting 360° rose plot were combined to be collectively counted as dorsal/ventral orientation.

Cell tracks

Cell tracks were obtained from maximum intensity projections of the cell of interest using tracking tools in Imaris (Imaris x64 9.7.2). First, time laps movies were corrected for epiboly movements to represent the cell movement relative to epiboly in the final cell tracks. In all confocal imaging data sets except for the Toddler/Aplnr chemokine assay (**Fig. 2 and fig. S3**), epiboly movement was determined by manually tracking the vegetal pole-directed progression of the margin in the brightfield images. The cell tracks were then corrected based on the resulting 'epiboly track'. In the light sheet data sets (**fig. S1**) and the chemokine assay (**Fig. 2 and fig. S3**), epiboly movements were determined by automatically tracking (Imaris) H2B-RFP or H2B-BFP labelled cell nuclei, respectively. The tracks of 3-5 nuclei that were successfully tracked throughout the entire time course were used as a reference for correction of the data sets. Cells of interest in all confocal data (**Fig. 1-2 and 4, fig. S2-3 and S5-6**)

and light sheet data in **Fig. 1** and **fig. S1** were manually tracked. Final tracks were exported and assembled using Adobe Illustrator. Average speed was calculated by dividing track length by track duration. Track straightness was calculated by dividing displacement by track length. Net displacement to the source was determined by measuring the vertical distance between start and end point of the track. The end point of the track was either the point at which the cell first made contact with the source, or, if no contact was made, after 2 hours of imaging.

Global cell tracking

Global cell tracking of all nuclei in the acquired light sheet microscopy data (**Fig. 3 and fig. S4**) was based on the approach of Jaqaman et al (*51*). To this end, detected nuclei were greedily interconnected into short tracklets, which were then merged to form the final tracks. The interconnection of both the detected nuclei and tracklets was computed by solving a linear assignment problem using LAPMOD, a sparse variant of the Jonker & Volgenant linear assignment solver (*52*). Very short tracklets of less than 3 time points were pruned. New tracklets were not allowed to form within a sphere with a radius of 10 µm. Maximum allowed displacement between consecutive time points was set to 10 µm. Gaps between tracklets no longer than 3 time points were closed if the maximum displacement per time point stayed below a threshold of 10 µm.

The nuclei were detected using a multi-scale Laplacian of Gaussian filter (5 scales between 1 and 2.5 micron) after preprocessing the imaging data using the following operations: (1) A per-pixel mean image was computed and used for background subtraction to simplify cell tracking; noise and outliers were removed below and above the 50th and 99.99th percentile of intensity. (2) Working in the log domain, the volumes were downsampled 2x along x- and y-coordinates to obtain close-to-isotropic spacing; a 7x7 px median filter was applied for all z-planes independently. (3) Furthermore, to simplify the tracking, the sequence was stabilized using a translation transformation that was estimated at each time point from the locations of the beads around the embryo using RANSAC. In particular, aligning was started at a reference point, and bead locations were always pre-aligned at the current time point using past transformation; the beads locations fed into RANSAC estimation were selected as mutual nearest neighbors after this pre-alignment.

The global cell tracking was implemented in Python (https://drive.google.com/drive/folders/12Q36RQGpzItsEP4bC3OKYiWuM53ZC7sv?usp=sharing) using OpenCV, scikit-image and scikit-learn (48, 49). The tracker was optimized to take advantage of a SLURM-based computation cluster, however, the implementation also allows running locally on a single computer, however, the runtime might be prohibitive.

For visualization and analysis of the trajectories (https://drive.google.com/drive/folders/1GRgfTBL03aOvJ6FsMxBItVcMB6h2_cZc?usp=sharing), a

sphere was fitted to the extracted nuclei locations (*55*), with latitude and longitude coordinates and the radial distance from the center of the embryo. The reference sphere was aligned with the animal and vegetal pole matching the north and south pole, respectively. Afterwards the animal-vegetal axis and the dorsoventral axis were interactively recovered. This brought all the experiments into a common reference frame and allowed for simpler interpretation.

Cell internalization was determined by calculating each cell's frame-by-frame difference in radius at the margin. The minimum of the average changes indicated a peak of internalization movements, which occurred between 30% and 50% epiboly in all datasets. This was used to align the recordings in developmental timing.

To isolate the tracks of mesodermal cells, nuclei colocalizing with the Drl:GFP signal were identified. In relation to the background fluorescence, a cell was considered Drl:GFP marker positive with a green fluorescence level higher than 96% of all measurements (z-score 1.8) for at least 50 frames.

The animal-to-vegetal pole velocity was measured specifically for ventrolateral mesoderm cells. This was calculated by the change in distance relative to the margin over a moving window of 10 min (14 frames). The distance to margin is the difference in latitude between the position of the cell and the position of the margin at the corresponding time point.

Detection of a Toddler gradient via Aplnrb-sfGFP internalization levels

Using Fiji, a mask was generated for each Aplnrb-sfGFP-positive cell, encompassing the entire cell area (including cytoplasm and membrane) by manually outlining the cells ($mask^{full}$). Each mask was than reduced by 1.25 µm around the entire circumference. The resulting reduced mask represented the cytoplasmic area ($mask^{cyto}$). $Mask^{cyto}$ was then subtracted from $mask^{full}$, resulting in a consistently 1.25µm thick band as a mask for the membrane ($mask^{membr}$). The mean fluorescent intensity was measured within $mask^{membr}$ and $mask^{cyto}$, and the ratio ($mask^{membr}/mask^{cyto}$) was calculated as a proxy for Aplnrb-sfGFP internalization levels in each cell.

Compensation of Toddler overexpression

Overexpression of Toddler was achieved at different levels by injecting 0 pg (water control), 5 pg or 10 pg of *toddler* mRNA into 1-cell stage wild-type embryos. Half of the embryos of each batch were additionally injected with *lefty2* MO to enhance Nodal signaling and thus increase the number of mesodermal cells. Embryos were collected for in situ hybridization at 75% epiboly (see below).

In situ hybridization

In situ hybridization was performed as previously described (*56*). Briefly, wild-type and *toddler*$^{-/-}$ embryos were fixed at 75% epiboly in 3.7% FA overnight and hybridized with a DIG-labelled antisense probe against *aplnrb* (*10*). After BCIP/NBT/Alkaline-phosphatase-staining, embryos were dehydrated in Methanol and imaged in BB/BA on a Stemi 305 steromicroscope (Zeiss).

To quantify the mesoderm migration phenotype, embryos were imaged laterally at 75% epiboly. The spread of *aplnrb*-positive cells was measured in ImageJ on the ventral side and normalized to the distance between margin and animal pole to account for differences in epiboly progression between individual embryos. Data was normalized to the average spread in wild-type embryos.

To assess the mesodermal cell density profile of embryos, the gray values for a 100-pixel wide rectangle from animal pole to margin were measured using ImageJ and inverted (0=white, 255=black). Values for all 100 pixels in one row were averaged. The lowest value measured along the animal-margin axis was subtracted as background, and measurements were normalized to the highest value (=1). All background-subtracted pixel values were plotted as position along the animal-margin axis (margin=0, animal pole=1).

Internalization of Aplnr

To assess Aplnrb-GFP internalization in the absence of Toddler or upon Toddler overexpression (**fig. S6A-C**), *toddler* $^{-/-}$ embryos were injected at the 1-cell stage with 100 pg *f'bfp* mRNA and 50 pg *aplnrb-sfgfp* mRNA. At the 32-cell stage, 100 pg Dextrane-AlexaFluor568 only (controls) or in combination with 100 pg *toddler* mRNA were injected into a single blastomere. Embryos were left to develop until sphere stage and then mounted on the animal pole and imaged as described above. To quantify Aplnrb-GFP internalization, cell outlines were manually traced in ImageJ based on the f'BFP signal. Mean fluorescence intensity of Aplnrb-GFP was measured for membrane and cytoplasm and multiplied with the membrane and cytoplasmic area, respectively. The ratio of total membrane and cytoplasmic signal was used as a measure of the internalization rate.

Toddler half-life assessment

To measure the half-life time of Toddler protein, *MZoep* $^{-/-}$*, toddler* $^{-/-}$ embryos were collected and left to develop until 30% epiboly. At 30% epiboly, 1 µg of Toddler peptide (GL Biochem: DKHGTKHDFLNLRRKYRRHN**C**PKKR**C**LPLHSRVPFP, cysteine residues in bold were crosslinked according to (*57*)) was injected into the cell cap. 10 cell caps were collected every 30 min for 3 hours through manual removal of yolk and flash-frozen in liquid nitrogen.

Western blotting was performed according to standard protocols. Briefly, embryo caps were supplemented with 10 µL of 2x Laemmli buffer and boiled for 5 min at 95°C. SDS-PAGE was performed using Any kD™ Mini-PROTEAN® TGX™ Precast Protein Gels (BioRad), loading 10 embryo caps per lane. Blotting was performed using a wet-blot system (BioRad). Protein detection was achieved using the following antibodies: anti-Toddler (rabbit, 1:500, provided by the Reversade Lab (*11*)) and anti-tubulin (mouse, 1:10000, Sigma-Aldrich T6074).

Computational modeling

Here, we provide additional details for the modelling of self-generated Toddler gradients during zebrafish gastrulation.

Position of the problem

We write the conservation equation for the concentration of mesoderm cells $m(x,t)$ and secreted Toddler $T(x,t)$ as a function of time t and position x along the animal-vegetal axis (where $x = 0$ is the position of the margin, and where we restrict ourselves to a one-dimensional description thanks to the radial symmetry of the problem):

$$\begin{cases} \partial_t m = D_m \partial_{xx} m - \partial_x m v \\ \partial_t T = D_T \partial_{xx} T + \dfrac{T_0(x) - T - \alpha m T}{\tau_T} \end{cases}$$

In this description, mesodermal cell concentration can change from i) free diffusion and ii) directional motion at speed v, while Toddler concentration can change from i) free diffusion, ii) production (from ectoderm cells), iii) intrinsic degradation and iv) mesoderm consumption. We have denoted D_m and D_T as the diffusion coefficient of mesoderm cells (in the absence of directed motion) and Toddler molecules, respectively, $T_0(x)$ as the target concentration of Toddler (which can be spatially modulated) in the absence of any mesoderm consuming it, τ_T as the timescale of intrinsic Toddler degradation and α as the consumption rate of Toddler from mesoderm cells (larger density of mesoderm cells signifying more receptor density for Toddler degradation – note that this implicitly assumes that receptor density per cell is constant, an assumption that we relax below). For this equation we must additionally specify a dependency between directed cell migration velocity v and Toddler concentration. How cells sense gradients is an area of active study, and different non-linear as well as adaptative responses have been uncovered in particular while interpreting GPCR signalling gradients (see for instance review by Jin (*58*)). Here, we explored two simple limits of gradient sensing: $v = \beta \partial_x T$ (i.e. cells move up an *absolute* gradient of Toddler) or $v = \beta \frac{\partial_x T}{T}$ (i.e. cells move up a *relative* gradient in Toddler) - with β denoting in each case the strength of the coupling. We also note that this equation makes the important approximation (which we will come back to below in **fig. S3C**) that Toddler gradients only impacts the average "advective" velocity of cells v and not their random motility coefficient D_m. This is a coarse-grained description which can be made because the cell velocity in response to a Toddler gradient does not necessarily require a Toddler-dependent change of the instantaneous cell speed, but can arise from a partial bias in their random walk that is caused by a more persistent directionality in cell polarity triggered by the local Toddler gradient. Similarly, in our 1D model the velocity v (in the x direction) is proportional to the gradient of Toddler. In a 2D model, this proportional relationship could have different origins, as both the absolute velocity V and the polarity angle θ need to be considerd, while in our case only the projection along the x direction

$v = V\ sin\theta$ matters for the problem at hand. For instance, the gradient could either act directly on the absolute velocity V or only on reorienting the polarity angle θ (*59*) although both result in changes in the 1D velocity v.

Finally, we specify boundary and initial conditions for this problem at the margin: the Toddler protein and mesodermal cells cannot escape at the margin, leading to no-flux boundary conditions $\partial_x T(x = 0) = 0$ and $\partial_x m(x = 0) = 0$. While the initial conditions for Toddler are largely irrelevant and given its continuous production simplest defined as $T(x, 0) = T_0$, they are key for mesoderm specification. We therefore first assume that the mesodermal cell number is fixed and initially concentrated very close to the margin: $m(x, 0) = M_0\delta(x, 0)$.

Key length and timescales in the problem

From these equations, two natural scales emerge: a time scale τ_T, which represents the timescale of Toddler turnover, and a length scale $L = \sqrt{D_T\tau_T}$, which represents the distance at which Toddler produced by a localized source is degraded. This is, for instance, important during our rescue experiments, during which we place Toddler-expressing cells at the animal pole (**Fig. 4A**, forth from the right): Toddler is predicted to decay exponentially from the source cell location, at a length scale of L.

Parameter constraints, fitting and non-dimensionalization

A number of parameters can be constrained in this model. Toddler diffusion in particular can be calculated from the size of the Toddler molecule (around 4 kDa) from the Stokes-Einstein relationship. For instance, Lefty, Cyclops or Squint, which have around 10 times the molecular weight of Toddler (and thus are expected to have 2-3 times the hydrodynamical radius) were shown to have free diffusion coefficients in zebrafish embryos of $D_T \approx 20\ \mu m^2.s^{-1}$ (*27*). Therefore, we can estimate that for Toddler $D_T \approx 50\ \mu m^2.s^{-1}$ or $D_T \approx 3.10^3 \mu m^2.min^{-1}$. To estimate the time scale τ_T of Toddler degradation, we have made use of *MZoep*$^{-/-}$, *toddler*$^{-/-}$ double mutant embryos, which are devoid of both endogenous Toddler production and mesoderm-induced Toddler degradation. We injected 1 µg of Toddler peptide and performed a time course analysis of Toddler degradation (**fig. S4F-G**). This showed a roughly exponential decay, as predicted by our linear model, and from which we could extract $\tau_T \approx 120$ min (**fig. S4F-G**). We also compared this exponential to a linear fit $1 - t/t_T$, and used Akaike Information Criterion to see whether this was a more likely model. However, the comparison favored the exponential fit (Difference in AICc of 1.475). Interestingly, this value is in the same order of magnitude as Lefty, Cyclops or Squint during early zebrafish embryo morphogenesis (*27*). Together, this predicts a length scale for Toddler propagation of $L = \sqrt{D_T\tau_T} \approx 600\ \mu m$, which, interestingly, is of comparable scale to the embryo itself. Note that modelling the full complexity of diffusion in a cell-fluid mixture would give rise to slightly different prefactors (up to a factor 2) (*60*),

though, consistent with previous work on self-generated gradients, this would have little quantitative impact on the global dynamics of mesendoderm migration, as a change in diffusion by orders of magnitude would be required to give qualitatively different dynamics (*61*). Taken together, this length scale is consistent with the ability of marginal cells to sense Toddler-expressing cells far away at the animal pole, and to restore animal pole-directed migration as demonstrated in the experiments of **Fig. 2F and 4**.

Next, we examined the movements of *toddler*$^{-/-}$ cells transplanted into a *toddler*$^{-/-}$ background. As these cells show no measurable directed motion ($v = 0$), we reasoned we could use these experiments to constrain the value of free cell diffusion D_m. We found that these cells diffused on a length scale of approximately $25\ \mu m$ from the margin during the 30 min of the timescale (**fig. S4K-L**), leading us to a rough estimate of $D_m \approx 20\ \mu m^2.min^{-1}$.

Once we rescale all time scales by τ_T, all length scales by L:

$$\begin{cases} \partial_t m = \dfrac{D_m}{D_T}\partial_{xx} m - \dfrac{\beta}{D_T}\partial_x(m\partial_x T) \\ \partial_t T = \partial_{xx} T + T_0 - T - \alpha m T \end{cases}$$

Note that this neglects advective terms in the Toddler equation (for instance cell/fluid movements transporting Toddler). This is a safe assumption given the order of magnitude difference between the two. Estimating a Peclet number yields $Lv/D_T \approx 0.04$, so that free diffusion is largely dominant. We can further rescale Toddler by its maximal concentration T_0, and mesoderm by its initial total amount M_0 leading to

$$\begin{cases} \partial_t m = \dfrac{D_m}{D_T}\partial_{xx} m - \dfrac{\beta T_0}{D_T}\partial_x(m\partial_x T) \\ \partial_t T = \partial_{xx} T + 1 - T - \alpha M_0 m T \end{cases}$$

Thus, in addition to the length and time scales (which have been independently measured), this shows that the problem now only depends on 3 rescaled parameters: the relative diffusion coefficients of mesoderm and Toddler $\frac{D_m}{D_T}$ (which is strongly constrained by our measurements, and found to be very small), the rescaled consumption of Toddler from mesoderm αM_0, and the rescaled coupling from Toddler gradient to directed mesoderm speeds $\frac{\beta T_0}{D_T}$. These two last parameters are harder to independently measure and should therefore be considered as fitting parameters in the theory.

Importantly, however, analysis of the system of equations above finds that these last two parameters can largely be coarse-grained into a single one, with their product being the most relevant parameter: this is because α controls how strong of a gradient of Toddler is created, and β how strongly this gradient is interpreted, so that high α – low β and low α – high β give rise to similar velocities. Numerical simulations keeping the product $\alpha\beta$ constant, but changing each by several orders of magnitude confirmed this (see **fig. S4C** where we multiply β by 5 and divide α by 5, giving nearly

identical results to **fig. S4A**), although this effect would break down at very high α (when mesoderm consumption of Toddler would be so strong that the Toddler concentration reaches values close to zero).

Another approximation of the model that we wished to verify was that the random motility of cells (represented by the diffusion coefficient D_m) was unaffected by the local Toddler gradient. To verify this, we quantitatively analyzed the experiments in which cells with or without Aplnr were transplanted at a distance from Toddler-secreting or Toddler-deficient cells (**Fig. 2A-C**). We quantified the average displacement of cells over 15 min, either in the direction of the source (y-axis) or perpendicular to it (x-axis), and generated probability distributions for each case. As expected from a purely random and diffusive process in the x-direction, all three conditions displayed Gaussian distributions in step size centered around zero average displacement (**fig. S3C**). Importantly, the standard deviation (proportional to D_m) was nearly identical in all three cases, arguing that random motility is unaffected by either the presence of a Toddler gradient or Apelin receptor expression. Interestingly, when looking at the same distribution in the y-direction (towards the source), we found again that the standard deviation of the displacement was comparable between conditions (and also to its value in the x-direction, as expected from a random walk, **fig. S3C**). The only difference for the Toddler-Apelin receptor pair was that the best-fit Gaussian distribution was not centered around 0, but instead around a non-zero average velocity value of $0.3\ \mu m/min$ – as expected for a biased random walk and our model in which Toddler gradients only act on the advective velocity *v* (**fig. S3C**, see legends for detailed statistics and fitting).

Finally, although the model as defined above assumes that all cells internalize at the same time (initial Delta function at x=0 in the initial condition $m(x,0) = M_0\delta(x,0)$), the experimental situation is more gradual, with numbers of internalizing cells showing a broad temporal peak with typical variance σ of an hour (*13*). This can easily be taken into account by assuming that the initial condition is now zero mesoderm cells $m(x,0) = 0$, but adding a gradual source term in the conservation equation for mesoderm cells: $\partial_t m = \frac{D_m}{D_T}\partial_{xx} m - \frac{\beta T_0}{D_T}\partial_x(m\partial_x T) + I(x,t)$, where $I(x,t)$ is the spatio-temporal dynamics of internalization. Thus, we take in the simulations $I(x,t) = M_0 H(l-x)e^{-\frac{t^2}{2\sigma^2}}$: internalization only occurs close to the margin (represented by a Heaviside function decaying at $l = 50\ \mu m$), and on timescales $\sigma = 1h$ (*13*). Although these are the parameters that we show in **Fig. 3**, we also ran simulations with the previous initial condition (synchronous internalization of all mesendoderm cells) and found very similar results for both wild type and *toddler*$^{-/-}$ simulations (see **fig. S4A-E**).

Thus, in the following, we only fit $\alpha\beta$ in the theory (simulations from main text are made for $\alpha M_0 = 1$). $\alpha\beta$ is essentially proportional to the speed of migrating cells up a self-generated gradient. As we found an average speed of $v \approx 0.08\ \mu m/min$, this means $\alpha\beta \approx 10^4$ in our unit simulations.

With the model fully parametrized in this manner, we turned to its predictions on a number of non-trivial features, such as the spatiotemporal density/velocity profiles of mesoderm migration in wild type and *toddler*$^{-/-}$ mutant, or transplantation assays (**Fig. 3, S5D, S7A,B**).

Model predictions

We first consider the case of *toddler*$^{-/-}$, in which directed cell migration is negligible ($v = 0$). Because the margin constitutes a hard boundary, internalized cells are expected to still migrate upwards to some degree according to a diffusive process with coefficient D_m. Given our estimate of D_m from short-term trajectories, we thus asked how much cells were predicted to travel by pure diffusion (1D along the animal-vegetal axis) in the Δt=3.5 hours between internalization and the 75% epiboly stage. These simulations predicted around 200 µm, compared to 600 µm for wild type (**fig. S4H**). To confirm these predictions experimentally, we measured the intensity profiles of mesoderm markers (*aplnrb*) by *in situ* hybridization assays in *toddler*$^{-/-}$ compared to the wild-type embryos along the animal-vegetal axis as a proxy for the mesoderm concentration (**fig. S4I-J**). We found that the mesoderm concentration profile in *toddler*$^{-/-}$ embryos decayed around twice as fast as in wild-type embryos. It is important to note that uncertainty in the exact diffusion coefficient of mesoderm cells, or the possibility of small, residual, non-zero directionality in the migration of *toddler*$^{-/-}$ cells could explain the slightly stronger phenotype in the model.

In the presence of self-generated gradients, the system organizes into a travelling-wave solution, as expected from the literature (*23*), where cells adopt a non-zero net polarity/velocity towards the animal pole, as observed experimentally (**Fig. 2B-C,E**). Although this self-organized collective migration is robust to the details of the parameters, such as the effective diffusion length scale *L* for Toddler, such parameters do have an effect on the detailed spatiotemporal profiles of mesoderm migration. For very local Toddler diffusion (small L), only a few cells at the very edge sense the self-generated gradient, which causes them to initially migrate very fast (see **fig. S4D** for a simulation with $\tau_T = 10\ s$, so that the length scale L is around 20 µm, i.e. the cell size). However, this creates a concentration gradient of mesoderm cells, which in turn causes a concentration gradient of Toddler, which does not stem from diffusion, but rather the differential degradation of Toddler caused by the spatial differences in mesoderm density. Thus, cells can still migrate in a self-generated manner, although the cellular density gradient is more pronounced than the “front-like” solutions shown in **Fig. 3** (limit of large effective Toddler diffusion relevant here as the length scale L is of the order of the embryo size as described above).

Comparing these predictions to our tracking data of mesoderm cells (marked by *drl:GFP*) undergoing migration towards the animal pole after internalization, we found similar qualitative features, with cells at the edge displaying the largest velocity, which decreased both as a function of time and distance from the edge. More quantitatively, we compared kymographs for the cellular velocity as a function of position, which equals the distance from margin and time (**Fig. 3H**). It is important to note that in the kymographs we show the total effective cell velocity as measured by cell tracking, which represents the sum of the advective velocity and the diffusive flux, which can have directional contribution in the presence of a density gradient. The total flux of cells reads as $J_{tot} = m\beta\partial_x T - D_m\partial_x m$, in which the first term is the advective contribution proportional to the local Toddler gradient, and the second is the diffusive flux. We thus define $v_{tot} = J_{tot}/m = \beta\partial_x T - D_m\partial_x m/m$ as the total average velocity of mesodermal cells at position *x*, which is plotted in **Fig. 3H**. Importantly, while we predict that the contribution of diffusion is rather small compared to advection (see **fig. S4E** for a simulation with zero mesendoderm free diffusion, $D_m = 0$) in wild type, the latter becomes dominant in *toddler*$^{-/-}$, in which advection is close to zero.

Effect of number of transplanted cells on the resulting dynamics

As discussed in the main text, the mechanism of self-generated gradients that we propose relies on a collective effect, for which the number of cells at the margin matters as it dictates the strength of gradient-shaping. To further explore the effect of sink function and cell number, we refined the model to include different cell types: regular Aplnr-expressing mesoderm cells $m(x,t)$, which degrade Toddler, and Aplnr-deficient cells which do not degrade Toddler $m_0(x,t)$. The equation on $m(x,t)$ is exactly the same as before, as is the equation on Toddler (only $m(x,t)$ participate in Toddler degradation, while $m_0(x,t)$ does not enter the Toddler equation). The equation on $m_0(x,t)$ reads $\partial_t m_0 = \frac{D_m}{D_T}\partial_{xx} m_0$ (i.e. no directed migration term). As we show in **fig. S5D**, simulating transplants of small numbers of wild-type cells in *aplnr*^{MO} embryos (large m_0 density, low m density) resulted in little migration, while transplants of small numbers of wild-type cells in wild-type density was effectively the same as regular wild-type migration (as transplanted cells are identical to the surroundings). On the other hand, simulating large clusters of wild-type cells in *aplnr*^{MO} embryos (large m_0 density, intermediate m density) resulted in an intermediary phenotype (**fig. S5D**), as seen in the data (**Fig. 4**).

Overexpression of Toddler and Apelin receptor

We next consider the effect of overexpression of Toddler, which has shown to give rise to defects in upward migration (*10*). This is modelled by a change in the baseline production of Toddler T_0:

$$\partial_t T = \partial_{xx} T + T_0 - T - \alpha M_0 m T$$

where previously we had non-dimensionalized the problem to $T_0 = 1$. When considering different T_0, the assumption of absolute vs. relative gradient sensing (resp. $v = \beta\partial_x T$ or $v = \beta\frac{\partial_x T}{T}$) does impact

the resulting prediction: for absolute gradient sensing, the gradient (and thus migration) increases with T_0, whereas it is almost insensitive to T_0 for relative gradient sensing. However, it should be noted that the equation above implicitly assumes that mesoderm cells (via their Apelin receptors) can take up arbitrary amounts of Toddler ligand. Although this may be correct for the wild-type condition, this situation might not generally hold true for overexpression phenotypes, especially as Apelin receptors are internalized with Toddler, which might result in not enough Apelin receptor left on membranes to sense and uptake Toddler. To take this latter feature of GPCR signalling into account, we supplemented the equations above with a conservation equation for the concentration of Apelin receptors within a cell $r(x,t)$:

$$\tau_r \partial_t r + \partial_x (rv) = r_0 - r - \alpha M_0 r T$$

Note that there are no diffusion terms in this equation, as Apelin receptors don't spatially exchange between cells, although they are "transported" spatially together with the movements of mesoderm cells (advective term putting r in the co-moving frame of cells). This first-order equation assumes that there is a baseline equilibrium of Apelin receptor at the membrane (time scale of recycling τ_r, equilibrium concentration r_0), but that each event of Toddler internalization also removes an Apelin receptor. This is the same sink term as in the Toddler equation, now rewritten to depend also on r :

$$\partial_t T = \partial_{xx} T + T_0 - T - \alpha M_0 T r m$$

Note that the latter term also is multiplied by the mesendoderm concentration m, as we have defined $r(x,t)$ as the single-cell concentration of Apelin receptors.

When simulating these equations with $r_0 = 1$ and $\tau_r = 30$ min (although these values had little bearing on the results), we found very similar dynamics as in previous simulations, with Apelin receptor concentration very slightly increased at the back of the mesoderm edge (where Toddler concentration is lower). However, when simulating a 10x increase in Toddler production ($T_0 = 10$), which was close to concentrations previously reported to induce a Toddler overexpression phenotype (*10*) **(fig. S7C),** we found that this now resulted in an impaired migration (**fig. S7A**), which was due to a much lower concentration of r (due to receptor saturation through Toddler binding), and therefore an impairment of gradient formation. The more the Toddler production was increased, the stronger the defect in migration was. However, increasing the production of Apelin receptor r_0 could restore the normal wild-type phenotype (**fig. S7B**). The exact amount of Aplnr to fully compensate for the 10x Toddler overexpression depends on the turnover rate of Apelin receptors; for $\tau_r = 30$ min, $r_0 = 2.25$ was required to restore the normal migration profile from $T_0 = 10$. Interestingly, this closely matches previous experimental observations of an epistatic relationship between Toddler and Apelin receptors (**fig. S7C**).

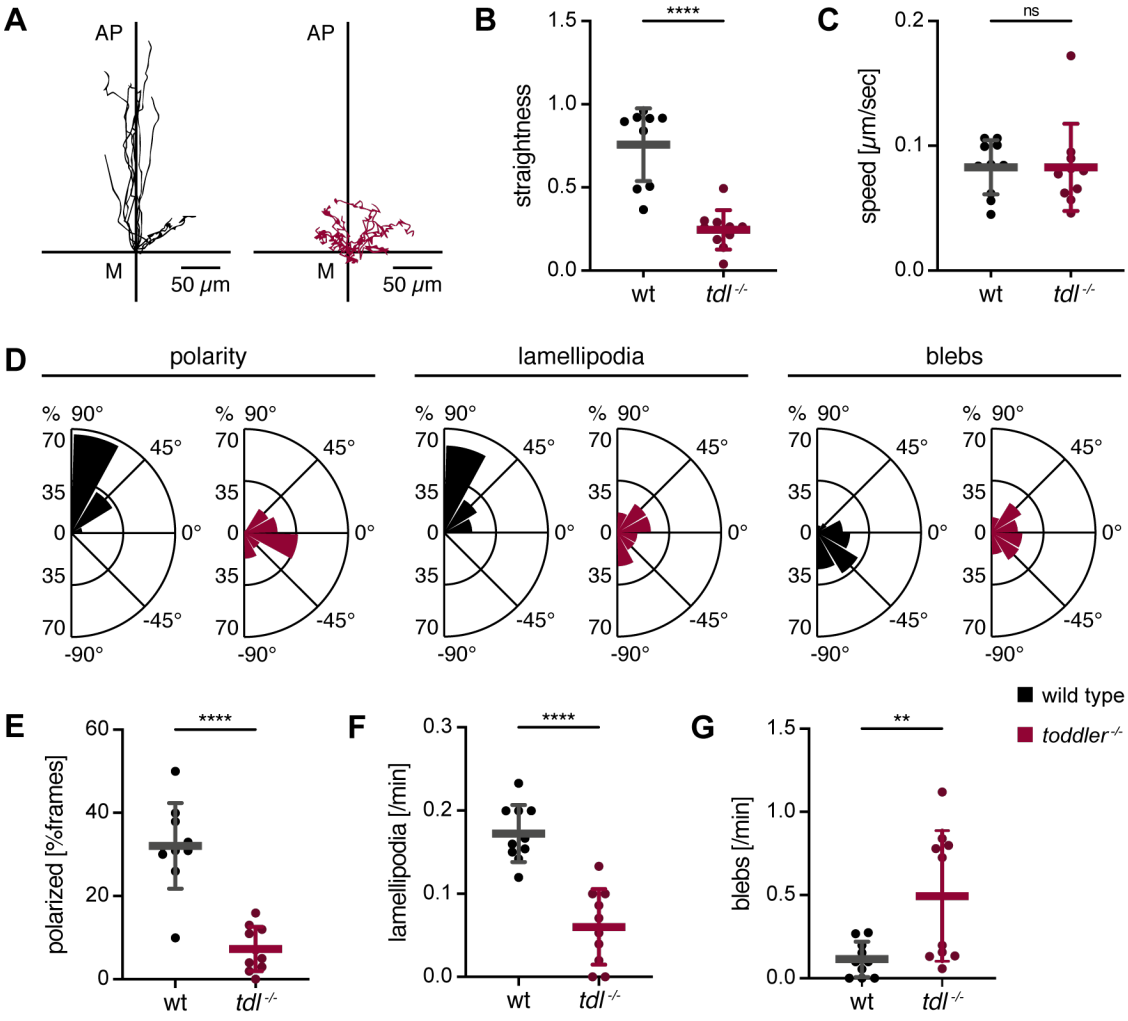

fig. S1. Mesendodermal progenitors are unpolarized and lack animal pole-directed protrusions in the absence of Toddler. Cell transplantation assays to assess the migration behavior of mesendodermal progenitors in the presence versus absence of Toddler signaling using light sheet microscopy. LifeAct-GFP-labelled reporter cells were transplanted from the margin of a wild-type or *toddler*$^{-/-}$ donor embryo to the margin of a stage- and genotype-matched host embryo. **(A)** Tracks of wild-type (left) and *toddler*$^{-/-}$ (right) reporter cells. Cells were tracked for 30 min after internalization. x-axis = margin; y-axis = animal-vegetal axis; coordinate origin = start of track. **(B)** Quantification of track straightness. **(C)** Quantification of migration speed. **(D)** Rose plots showing relative enrichments (percentages) of orientations of polarity, lamellipodia and blebs normalized to the total number of polarity axes or respective protrusions of all cells within the same genotype. **(E)** Quantification of cell polarity represented as the percentage of frames in which a cell was polarized. **(F)** Quantification of lamellipodia. Data represents newly formed lamellipodia per minute. **(G)** Quantification of blebs. Data represents newly formed blebs per minute. Data are means ± standard deviation (SD). Significance was determined using unpaired t test; ****, $p < 0.0001$; **, $p < 0.01$; n.s., not significant. n = 10 cells. Wild type (black); *toddler*$^{-/-}$ (red). Rose plots: 90° = animal pole; 0° = ventral/dorsal; -90° = vegetal pole. All images and graphs are oriented with the animal pole towards the top.

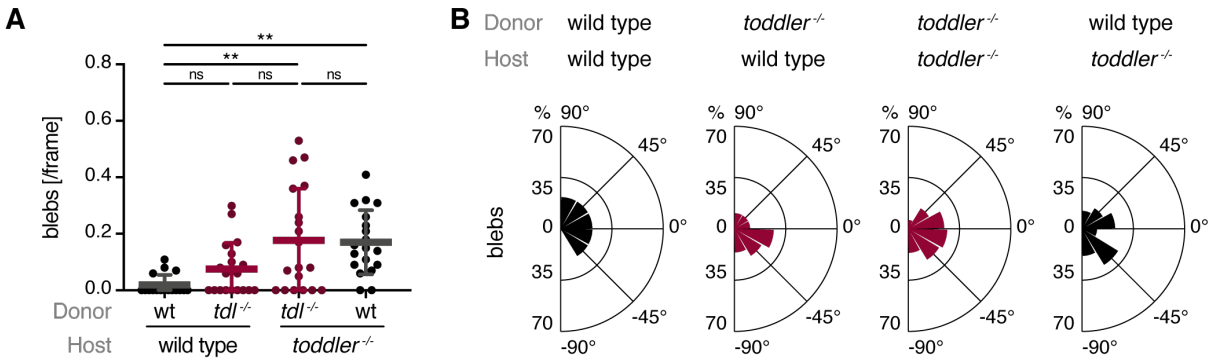

fig. S2. *toddler* $^{-/-}$ cells display an increase in cell blebbing. Cell transplantation assays to assess the cell autonomous or non-autonomous regulation of cell blebbing by Toddler signaling. **(A)** Quantification of blebs represented as the average number of blebs detected per frame (see Materials and Methods for classification of blebs). **(B)** Rose plots showing relative enrichments (percentages) of orientations of blebs, normalized to the total number of blebs of all cells within the same condition. Rose plots: 90° = animal pole; 0° = ventral/dorsal; -90° = vegetal pole. Data are means ± SD. Significance was determined using unpaired t test; **, $p < 0.01$; n.s., not significant.

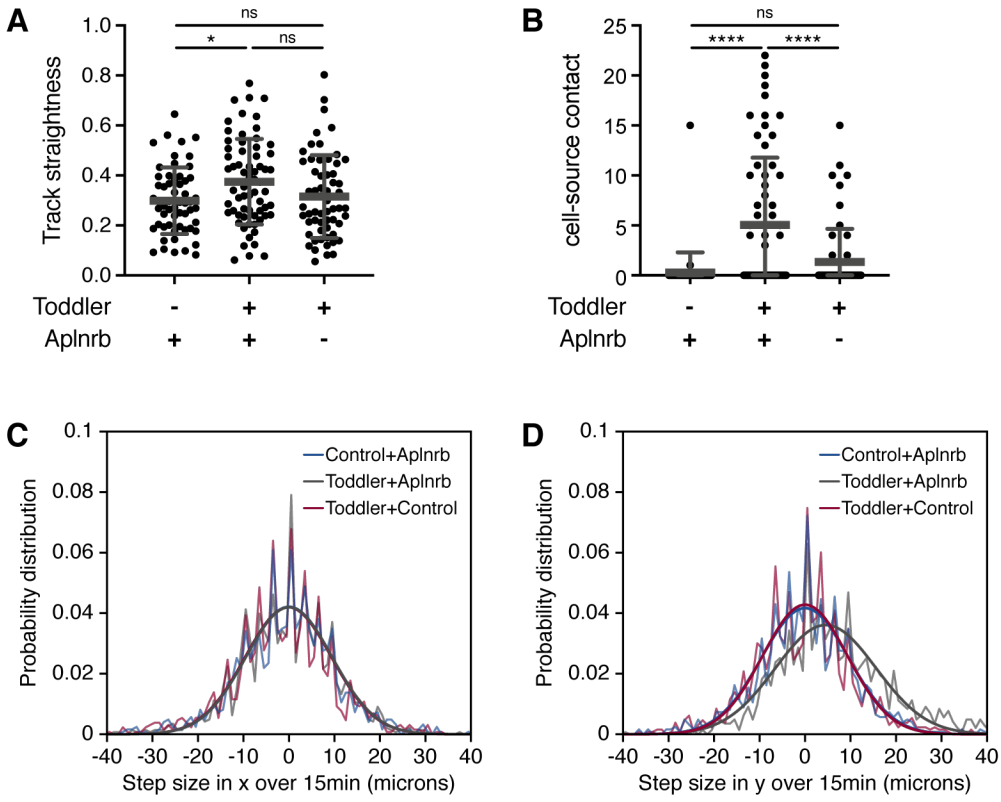

fig. S3. A localized source of Toddler attracts Aplnrb-sfGFP-expressing cells. Assessment of Toddler's ability to act as a chemoattractant for Aplnr-expressing mesodermal cells. **(A)** Track straightness of all cells imaged in Fig. 2B. Track straightness was calculated based on 120 min tracks as displacement divided by track length, irrespective of when the cells encountered the source. **(B)** Quantification of cell-source contact. The longest consecutive streak of frames, in which contact with a Toddler source cell was detected, was plotted for each cell. n = 56, 65 and 59 for the three different conditions, respectively. Data are means ± SD. Significance was determined using one-way ANOVA with multiple comparison; ****, $p < 0.0001$; *, $p < 0.05$; n.s., not significant. **(C-D)** Distribution of step size, defined as distance migrated by cells in the x- (C) and y- (D) directions within 15 minutes (x-direction: left-right movement in respect to the cell-source axis; y-direction: movement towards the source; see **Fig. 2A-C** for schematics and plotting of the trajectories), across all three conditions examined (Aplnrb-sfGFP-expressing cells migrating towards a Toddler-expressing cell, Aplnrb-sfGFP-expressing cells migrating towards a Toddler-negative control cell, Aplnrb-deficient control cells migrating towards a Toddler expressing source). All datasets are well-fitted by Gaussian distribution $P(s) = \frac{e^{-\frac{(s-s_0)^2}{2\sigma^2}}}{\sigma\sqrt{2}}$ (black lines), as predicted from a biased random walk, with the only non-zero bias s_0 occurring in the y-direction for the Aplnrb+Toddler condition. Best-fit variance: $\sigma = 9.50\ \mu m,\ 9{,}49\ \mu m,\ 9.47\ \mu m$ for resp. blue, grey and red datasets in panel C. Best-fit variance: $\sigma = 9.32\ \mu m,\ 11.05\ \mu m,\ 9.57\ \mu m$ for resp. blue, grey and red datasets in panel D, with a best-fit bias $s_0 = 4.55\ \mu m$ for the Toddler+Aplnrb condition.

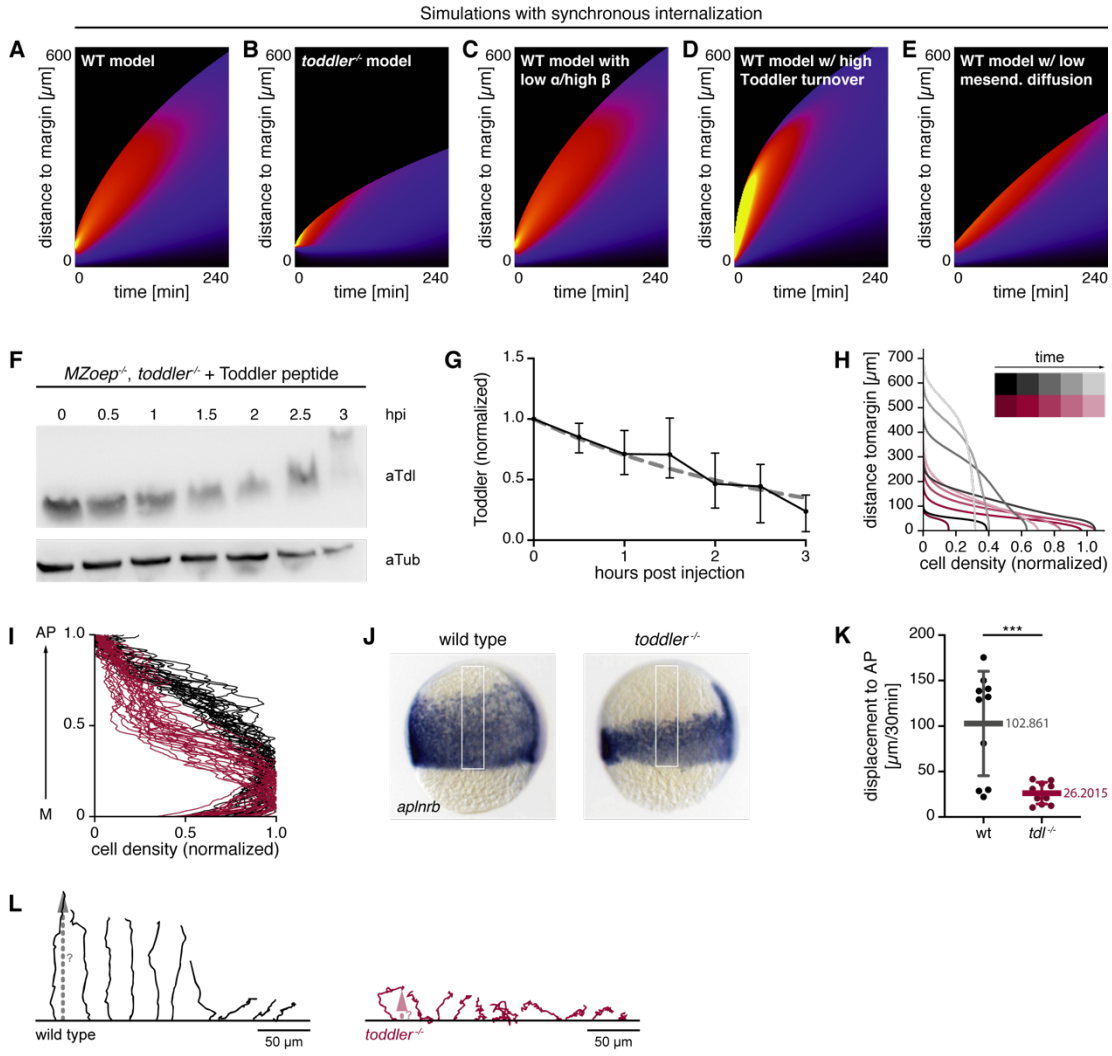

fig. S4. Determination of parameters for computational modeling. (A-E) Kymographs for normalized cellular velocities as a function of time (x-axis) and distance from the margin (y-axis): Sensitivity analysis of the model to different assumptions shown in the case of synchronous internalization from the onset (see Materials & Methods for details). **(A-B)** Simulations with the same simulation parameters as Fig. 4H for WT (**A**) and *toddler*$^{-/-}$ (**B**) embryos but for synchronous internalization, showing qualitatively similar dynamics. **(C)** Simulations keeping the product $\alpha\beta$ constant but multiplying β (coupling between local Toddler gradients and velocity) by 5 and dividing α (sink strength) by 5 gives rise to similar dynamics compared to panel (A). **(D)** Simulations with the same model parameters as (**A**) but with faster Toddler baseline degradation $\tau_T = 10s$, decreasing the range of Toddler gradient propagation. **(E)** Simulations with the same model parameters as (**A**) but with negligible mesendoderm random cell motility $D_m = 0$, giving rise to a smaller range of migration but qualitatively similar velocity profiles. **(F-G)** Assessing Toddler peptide stability in the presence and absence of Aplnr. **(F)** Western Blot analysis of the Toddler peptide degradation rate. *In vitro* synthesized Toddler peptide was injected into *MZoep*$^{-/-}$, *toddler*$^{-/-}$ double mutant embryos. Embryos were collected every 30 min for 3 hours and used for Western Blot analysis, probing for Toddler (aTdl) and alpha-Tubulin (aTub; loading control). **(G)** Quantification of Toddler levels (normalized to Tubulin) at different time points. Dotted line represents exponential fit for degradation curve that were used to calculate Toddler half-life. n=3. **(H-I)** Measurements of cell displacement towards the animal pole to determine Toddler-independent cell velocity in *toddler*$^{-/-}$ embryos. **(H)** Predicted spatiotemporal profile of mesoderm cell densities in the wild-type (grey) and *toddler*$^{-/-}$ (red) condition. **(I-J)** Experimental assessment of mesodermal cell density along the animal-margin axis. **(I)** Quantification of cell density along animal-margin axis in wild-type (black) and *toddler*$^{-/-}$ (red) embryos. n = 25 embryos. **(J)** Images for *in situ*

hybridization for *aplnrb* of a representative wild-type (left) and *toddler*$^{-/-}$ (right) embryo. White box indicates area measured for quantification **(K)** Quantification of the net animal pole (AP)-directed displacement based on tracks in **(I)**. Data are means ± SD. Significance was determined using unpaired t test; ***, $p < 0.001$. **(L)** Individual migration tracks of cells presented in fig. S1. The perpendicular net displacement of each cell from the margin (dotted line) was measured using the end point of each cell track 30 min after internalization. Track start is at the margin. Animal pole is shown towards the top. Wild type (black), *toddler*$^{-/-}$ (red).

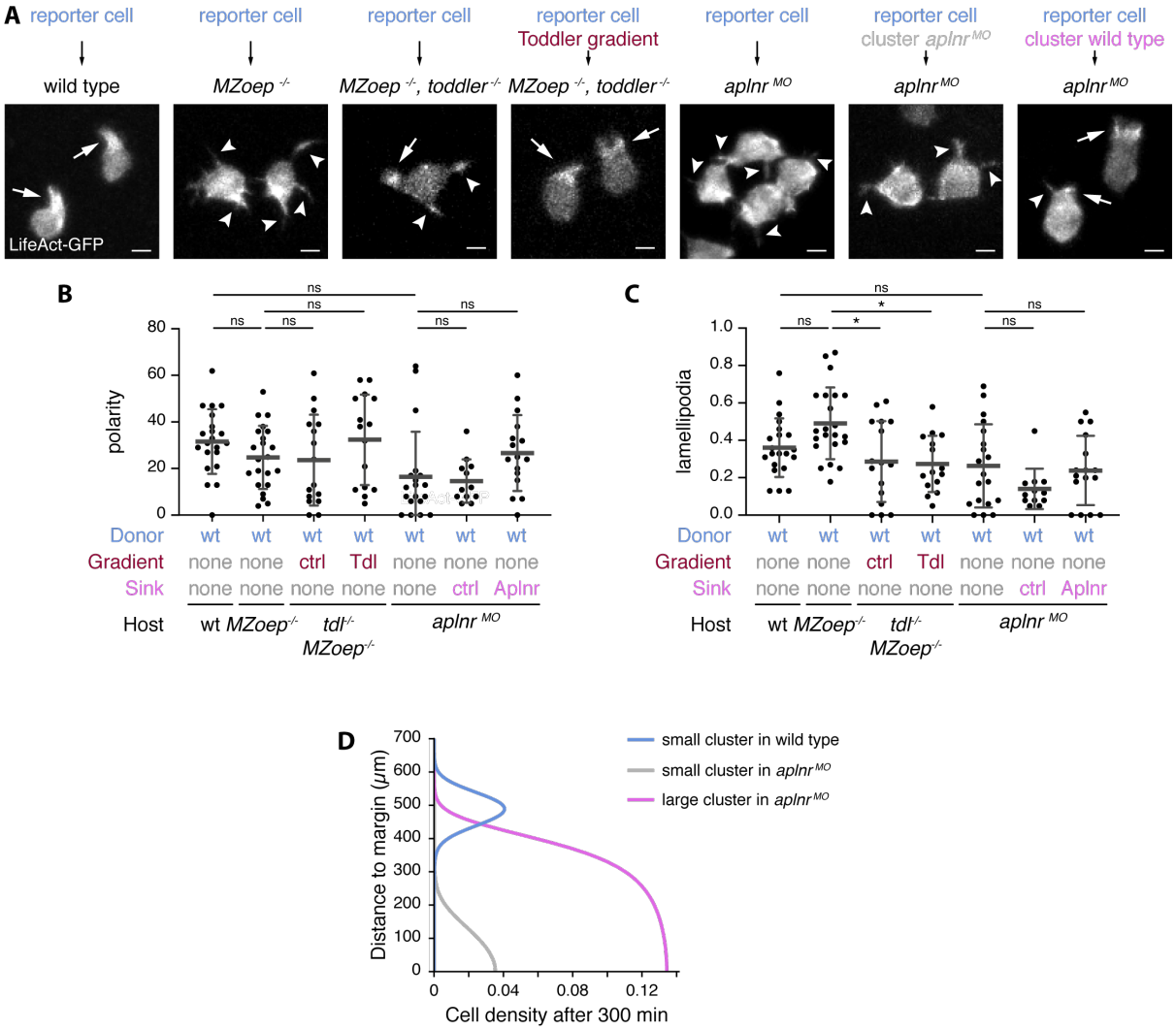

fig. S5. Sink activity of Aplnr-expressing mesodermal cells is required to form a Toddler gradient. (A) Representative confocal images of time-lapse series of transplanted reporter cells in the presence or absence of a mesodermal sink or Toddler gradient, as depicted in **Fig. 4A**. Arrows and arrowheads indicate lamellipodia and filopodia, respectively. **(B)** Quantification of cell polarity of reporter cells from **Fig. 4A-C** represented as percentage of frames in which a cell was polarized. **(C)** Quantification of lamellipodia detected in reporter cells from **Fig. 4A-C** per frame. **(D)** Numerical simulation of scenarios presented in **Fig. 4A** with the same model parameters as in **Figure 3**. Migration of small or large clusters of Aplnr-expressing mesodermal reporter cells, which are able to take up Toddler, was simulated in the presence (wild type) or absence (*aplnr*^{MO}) of Aplnr in host embryos (all other parameters being identical).

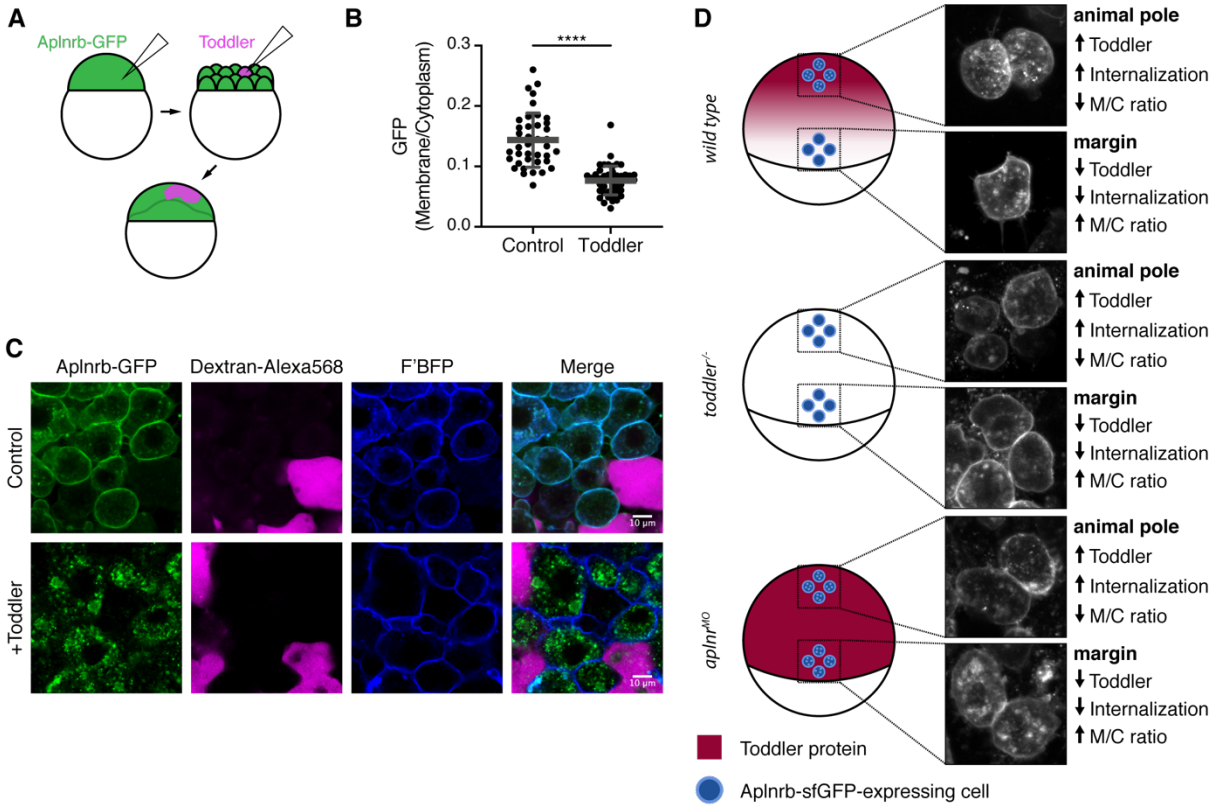

fig. S6. Toddler-induced Aplnrb-sfGFP internalization as a read-out for the Toddler concentration gradient. (A) Schematic representation of experimental set-up. *Aplnrb-GFP* mRNA (green) was injected together with *farnesylated-BFP* mRNA into 1-cell stage embryos to be ubiquitously expressed. Dextran-AlexaFluor568 alone or together with *toddler* mRNA was injected into one blastomere of a 32-cell stage embryo to achieve mosaic expression. **(B)** Quantification of the subcellular localization of Aplnrb-GFP. Data are means ± SD. Significance was determined using unpaired t test; ****, $p < 0.0001$. **(C)** Representative confocal images of Aplnrb-GFP localization in the absence of Toddler (top, n = 32 cells) or under Toddler overexpression conditions (bottom, n = 27 cells). **(D)** Assessment of Aplnrb-sfGFP internalization levels in *toddler*$^{-/-}$ cells transplanted to the animal pole and margin of wild-type (top), *toddler*$^{-/-}$ (middle) and *aplnr*^{MO} (bottom) host embryos. (Left) Schematic representation of transplantation set up and expected Toddler gradient (red) and Aplnrb-sfGFP internalization levels (blue) based on host genotype and position. (Right) Representative images of Aplnrb-sfGFP-expressing *toddler*$^{-/-}$ cells at animal pole and margin in respective host embryos.

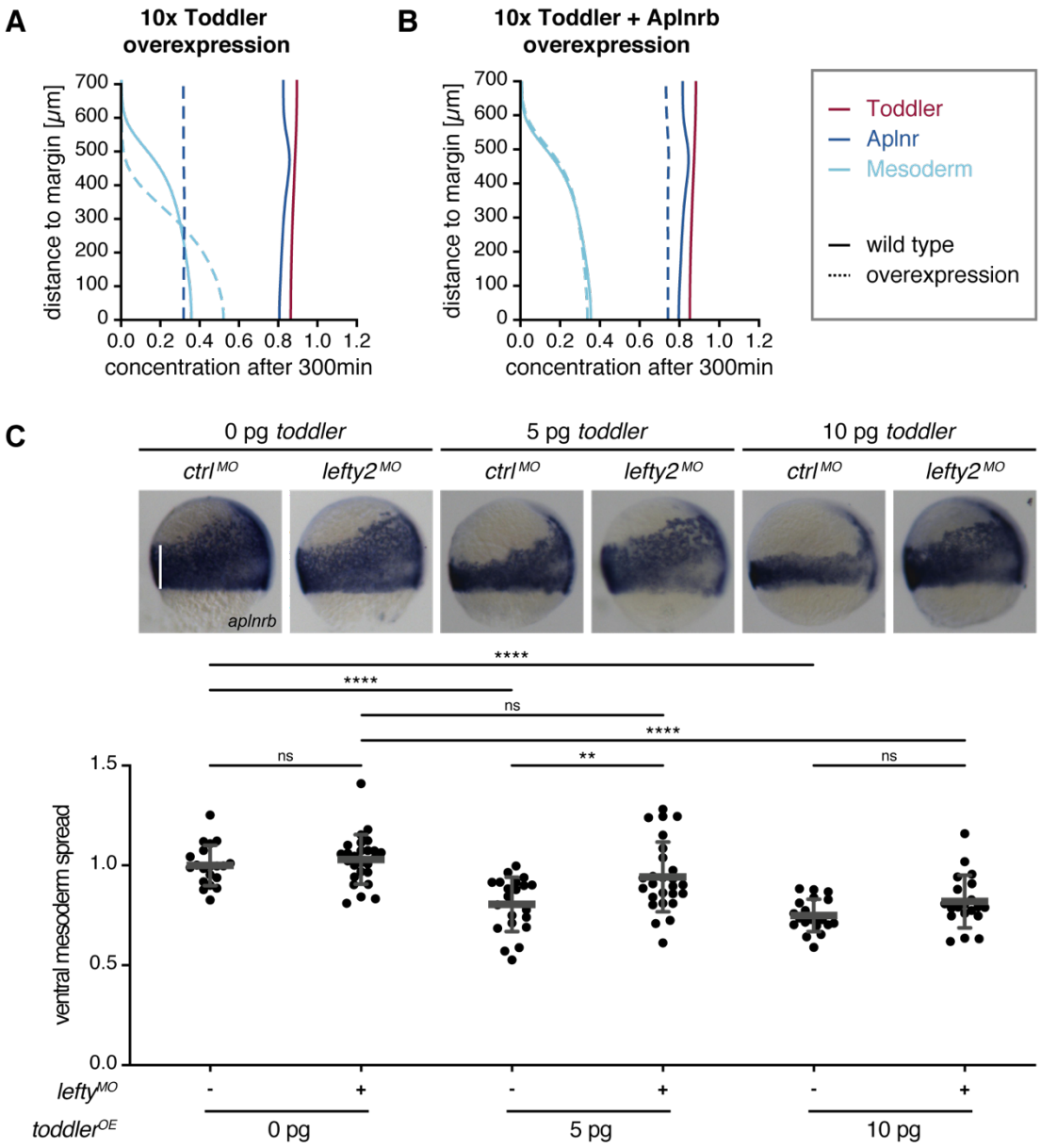

fig. S7. Overexpression of Toddler disrupts self-generated gradient but can be compensated by increasing the number of mesodermal cells. (A) Numerical simulation of mesoderm (light blue) migration upon Toddler (red) overexpression (10-fold, i.e. $T_0 = 10$), assuming a finite capacity of Aplnr (dark blue) to remove Toddler and cells sensing relative Toddler gradients (see Materials and Methods for details). Toddler over-expression causes a decrease in Aplnr concentration, which prevents efficient Toddler gradient formation, resulting in slower mesoderm migration. Unbroken lines represent wild-type scenario, dotted lines depict the changes upon Toddler overexpression. (B) Numerical simulation of mesoderm migration upon Toddler and Aplnr overexpression (same parameters as in (A) for Toddler; Aplnr overexpression by 2.25-fold, see Materials and Methods for details), which rescues normal mesoderm migration. Representation as described in (A). (C) Experimental confirmation of the simulation presented in (A-B). Toddler was overexpressed at different concentrations in wild-type embryos (rescuing concentration of *toddler* mRNA injection into 1-cell stage *toddler*$^{-/-}$ embryos is 2 pg) injected with control or *lefty2* MO to assess the compensation of increased Toddler levels upon increase of mesodermal cells (reducing the levels of the Nodal inhibitor Lefty2 increases the amount of Aplnr-expressing mesodermal cells). (Top) Representative *in situ* hybridization images using *aplnrb* as a probe to detect mesodermal cells. Embryos are shown as lateral views, with dorsal on the right. The white vertical line was used to measure the mesoderm spread from the margin towards the animal pole. (Bottom) Quantification

of the mesoderm spread in each condition relative to the average mesoderm spread in wild-type embryos. Data are means ± SD. Significance was determined using one-way ANOVA with multiple comparison; ****, $p < 0.0001$; **, $p < 0.01$; n.s., not significant.

Supplementary movie legends

Movie S1 | Internalized wild-type cells polarize and extend actin-rich lamellipodia towards the animal pole. Light sheet time-lapse imaging (time interval: 1 min) of LifeAct-GFP-labelled wild-type cells transplanted to the margin of a wild-type host embryo. Establishment of a polymerized actin network and lamellipodia is marked by accumulation of LifeAct-GFP at the front of the cell. The movie starts after cells have successfully internalized, confirming that cells were of either mesodermal or endodermal cell fate, and shows efficient animal-pole directed migration of these cells. Each frame is a maximum intensity projection of a z-stack. Animal pole is to the top. Scale bar, 10 µm.

Movie S2 | Internalized *toddler*$^{-/-}$ cells fail to polarize and fail to form actin-rich lamellipodia. Light sheet time-lapse imaging (time interval: 1 min) of LifeAct-GFP-labelled *toddler*$^{-/-}$ cells transplanted to the margin of a *toddler*$^{-/-}$ host embryo. Cells display a loss of polarization and lamellipodia formation, as well as the formation of ectopic filopodia around the cell periphery. The movie starts after cells have successfully internalized, confirming that cells were of either mesodermal or endodermal cell fate. Cells fail to move towards the animal pole. Each frame is a maximum intensity projection of a z-stack. Animal pole is to the top. Scale bar, 10 µm.

Movie S3 | A subset of internalized *toddler*$^{-/-}$ cells displays an increased blebbing phenotype. Light sheet time-lapse imaging (time interval: 1 min) of LifeAct-GFP-labelled *toddler*$^{-/-}$ cells transplanted to the margin of a *toddler*$^{-/-}$ host embryo, revealing the lack of actin-rich protrusion. Instead, actin-deficient blebs are formed as observed in a subset of analyzed *toddler*$^{-/-}$ cells. The movie starts after cells have successfully internalized, confirming that cells were of either mesodermal or endodermal cell fate. Cells fail to move towards the animal pole. Each frame is a maximum intensity projection of a z-stack. Animal pole is to the top. Scale bar, 10 µm.

Movie S4 | Confocal imaging of internalized wild-type cells. Confocal time-lapse imaging (time interval: 5 min) of LifeAct-GFP-labelled wild-type cells transplanted to the margin of a wild-type host embryo, confirming morphology and animal pole-directed migration observed in movie S1. Each frame is a maximum intensity projection of a z-stack. Animal pole is to the top. Scale bar, 50 µm.

Movie S5 | Confocal imaging of internalized *toddler*$^{-/-}$ cells. Confocal time-lapse imaging (time interval: 5 min intervals) of LifeAct-GFP-labelled *toddler*$^{-/-}$ cells transplanted to the margin of a *toddler*$^{-/-}$ host embryo, confirming morphology and lack of animal pole-directed migration observed in movie S2. Each frame is a maximum projection of a z-stack. Animal pole is to the top. Scale bar, 50 µm.

Movie S6 | *toddler*$^{-/-}$ cells display normal morphology and migration to the animal pole when transplanted into a wild-type host embryo. Confocal time-lapse imaging (time interval: 5 min) of LifeAct-GFP-labelled *toddler*$^{-/-}$ cells transplanted to the margin of a wild-type host embryo. Each frame is a maximum projection of a z-stack. Animal pole is located towards the top. Scale bar, 50 µm.

Movie S7 | Wild-type cells display defects in protrusion formation, polarization and migration to the animal pole when transplanted into a *toddler*$^{-/-}$ host embryo. Confocal time-lapse imaging (time interval: 5 min interval) of LifeAct-GFP-labelled wild-type cells transplanted to the margin of a *toddler*$^{-/-}$ host embryo. Each frame is a maximum projection of a z-stack. Animal pole is located towards the top. Scale bar, 50 µm.

Movie S8 | Aplnr-expressing cells are attracted by a localized source of Toddler. Confocal time-lapse imaging (time interval: 5 min) of Aplnrb-sfGFP-expressing cells reacting to an ectopic Toddler source. Left: Aplnrb-expressing cells (blue) are placed next to a control source (grey). Middle: Aplnr-expressing cells (blue) are placed next to a Toddler-overexpressing source (red). Right: Aplnr-deficient cells (grey) are placed next to a Toddler-overexpressing source (red). Mesodermal and source cells are labelled with LifeAct-GFP and Dextran-AlexaFluore568, respectively. Each frame is a maximum projection of a z-stack. Source is located towards the top. Scale bar, 20 µm.

Movie S9 | Wild-type reporter cells lose directional migration and polarity in *MZoep*$^{-/-}$ host embryos. Confocal time-lapse imaging (time interval: 5 min interval) of wild-type reporter cells (blue) transplanted into *MZoep*$^{-/-}$ embryos to test for the necessity of a mesendodermal Toddler sink. Left: Reporter cells transplanted to the margin of an *MZoep*$^{-/-}$ host embryo, which is deficient of mesendodermal progenitor cells. Middle: Reporter cells transplanted to the margin of an *MZoep*$^{-/-}$, *toddler*$^{-/-}$ double mutant host embryo, which is deficient of mesendodermal progenitor cells and Toddler expression. A control source (grey) was transplanted to the animal pole. Right: Reporter cells transplanted to the margin of an *MZoep*$^{-/-}$, *toddler*$^{-/-}$ double mutant host embryo, which is deficient of mesendodermal progenitor cells and Toddler expression. A Toddler source (red) was transplanted to animal pole to mimic an ectopic Toddler gradient. Segregation of two cell groups, one clearly moving towards the Toddler source and the other one lagging behind, likely stems from the fact that transplanted cells are a mixture of mesodermal (Aplnrb-expressing and Toddler-responsive) and endodermal (Aplnrb-deficient and non-responsive to Toddler) progenitor cells.. Each frame is a maximum projection of a z-stack. Animal pole is located towards the top. Scale bar, 50 µm.

Movie S10 | Wild-type reporter cells lose directional migration and polarity in *MZoep*$^{-/-}$ host embryos. Confocal time-lapse imaging (time interval: 5 min interval) of wild-type reporter cells (blue) transplanted into *aplnr*^{MO} embryos to test for the effect of individual versus collective cell migration in an environment of ubiquitous Toddler levels. Left: Reporter cells transplanted to the margin of an *aplnr*^{MO} host embryo, which forms mesoderm but is deficient in Aplnr expression. Middle: Co-transplantation of reporter cells and a control cluster of Aplnrb-deficient cells (grey) to the margin of an *aplnr*^{MO} host embryo. Right: Co-transplantation of reporter cells and a cluster of Aplnrb-expressing cells (magenta) to the margin of an *aplnr*^{MO} host embryo to mimic sink activity. Each frame is a maximum projection of a z-stack. Animal pole is located towards the top. Scale bar, 50 µm.

3.3. Efforts to directly visualize the Toddler gradient

The presence of various morphogen and chemokine gradients, which are essential for embryonic patterning and/or guidance of cell migration, has long been established in the zebrafish embryo. However, a main challenge that remains for protein gradients in general is their direct visualization. Our discovery of a new chemokine gradient immediately prompted us to tackle this challenge for the self-generated Toddler gradient.

There are three main approaches that are most commonly used to visualize a signaling gradient. First, the signaling protein can be detected via live cell imaging through a fluorescent protein tag. However, large protein tags can often cause steric hindrance that renders the protein non-functional, especially in the case of small signaling proteins, and tagging of genes at their endogenous loci in zebrafish is still not straightforward. Second, the protein could be detected via immunofluorescence (IF) staining using an antibody. This can often be challenging due to low expression levels or unavailability of reliable antibodies. Finally, a reporter can be used to read out the activation of downstream signaling. While the latter is an indirect approach to detect a signaling gradient, it has been used for most successfully visualized morphogen gradients to date. Prominent examples include the Nodal gradient that has been visualized through the detection of phosphorylated Smad2/3 (Harvey and Smith, 2009) or the Cxcl12a gradient through the internalization rate of Cxcr4b (Donà et al., 2013; Venkiteswaran et al., 2013).

Similar to reading out the Cxcl12a gradient via internalization of Cxcr4b, we used the Toddler-dependent internalization of the Apelin receptor to detect differences in the Toddler concentration at the animal pole compared to the margin. This approach confirmed the presence of a Toddler gradient, as described above (page 48, Fig. 4E-G in Stock et al., 2022). While consistent, the differences in Aplnr internalization rate were relatively low. This effect can likely be attributed to the necessity to overexpress Aplnrb-GFP and the mechanical stress caused by cell transplantation, which has previously been suggested to induce Aplnr internalization in a ligand independent way (Kwon et al., 2016), rather than a lack of significant differences in Toddler concentration. Therefore, in an effort to achieve a direct visualization of the Toddler gradient, I took two additional approaches that I am summarizing in the following section.

3.3.1. Toddler detection via antibody

3.3.1.1. Antibody only detects Toddler when overexpressed

We first aimed to detect Toddler directly, using a Toddler-specific antibody. For this purpose, we raised antibodies against the N- and C-terminus of Toddler and tested their specificity using Western Blot analysis. Only the antibody raised against the N-terminal end was able to detect Toddler in

Western blot analysis (Figure 6A). However, this antibody also detected additional proteins (unspecific bands in the Western blot), which prompted us to test the specificity and sensitivity of this antibody in immunofluorescence (IF) assays. We injected different concentrations of *toddler* mRNA into 1-cell stage *toddler*$^{-/-}$ embryos before fixing them at sphere stage. Using our antibody, we were able to specifically detect Toddler in the extracellular space upon *toddler* mRNA injection, while the signal was completely absent in uninjected embryos. However, strong overexpression of at least 100 pg *toddler* mRNA was necessary to reliably detect the Toddler signal (Figure 6B). Given that only 2 pg of *toddler* mRNA are required to rescue *toddler* mutants, we concluded that approximately 50 times the amount of endogenous Toddler would be required to detect it using antibodies.

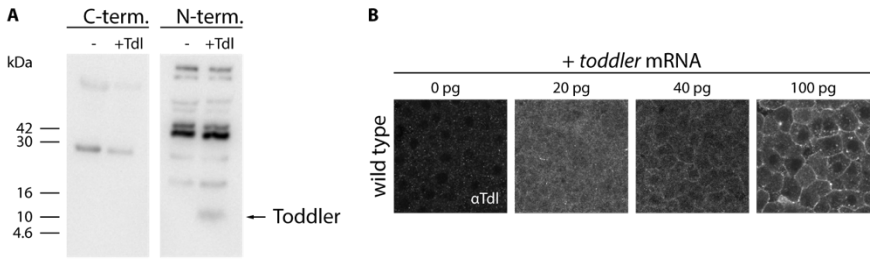

Fig. 6 | Testing the use of a Toddler antibody. (A) Western blot analysis to test the functionality and specificity of Toddler antibodies raised against either the C- or N-terminus of zebrafish Toddler. Only the antibody raised against the N-terminus detects a band of the correct size that is specific to Toddler. (B) Representative images for IF staining of embryos injected with different amounts of *toddler* mRNA. Reliable signal with Toddler antibody can only be achieved when injecting at least 100 pg of *toddler* mRNA at the 1-cell stage.

3.3.1.2. Toddler overexpression phenotype can be compensated by increasing Aplnr levels

As discussed above, overexpression of Toddler leads to a saturation of the available Aplnr (Pauli et al., 2014) and consequently the loss of sink function and therefore the Toddler gradient, which precludes using this approach for visualizing the Toddler gradient. However, we found that a certain level of Toddler overexpression can be compensated for by increasing the number of Aplnr-expressing mesodermal cells and thereby re-establishing the balance between receptor and ligand. By injecting 2.5 ng of lefty2 MO into embryos (which increases Aplnr-expressing mesodermal cells), we were able to compensate for up to 20 pg *toddler* overexpression, as determined by *in situ* hybridization assays, assessing the spread of mesodermal cells (Figure 7).

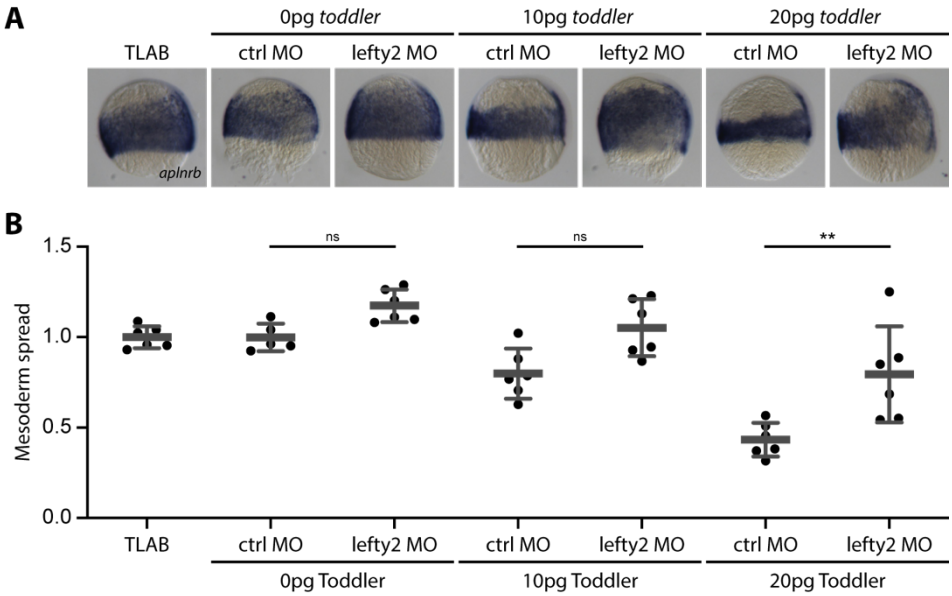

Fig. 7 | Compensation of Toddler overexpression through inhibition of Lefty2. (A) Representative images of *in situ* hybridization on wild-type embryos injected with different amounts of *toddler* mRNA and control or lefty2 MOs, as indicated. (B) Quantification of the ventral mesoderm spread based on *in situ* hybridization images. Data are mean ± SD. Significance was determined using one-way ANOVA with multiple comparison; **, $p < 0.01$; n.s., not significant.

3.3.1.3. Generation of Toddler constructs suited for Tyramide signal amplification (TSA)

While 20 pg *toddler* mRNA is a significant increase in Toddler levels, according to our antibody tests it is still not enough to detect Toddler. We therefore combined our IF approach with Tyramide Signal Amplification (TSA) to additionally increase the signal intensity of the Toddler antibody. Instead of using traditional fluorophore-coupled secondary antibodies, TSA uses a horseradish peroxidase (HRP)-coupled secondary antibody in combination with fluorophore coupled tyramide molecules. In the presence of H_2O_2, HRP converts tyramide into a highly reactive form that binds tyrosine residues in close proximity. Therefore, the higher the number of tyrosine residues in the protein of interest, the higher the signal amplification. The mature Toddler sequence harbors only one Tyrosine residue. Therefore, we introduced two point mutations (R39Y and P44Y) into the Toddler sequence that introduced two additional Tyrosine residues (Figure 8A). This Toddler(2Y) version was fully functional and remained detectable by the Toddler antibody, as assessed by its rescuing ability (Figure 8B) and IF (Figure 8C), respectively.

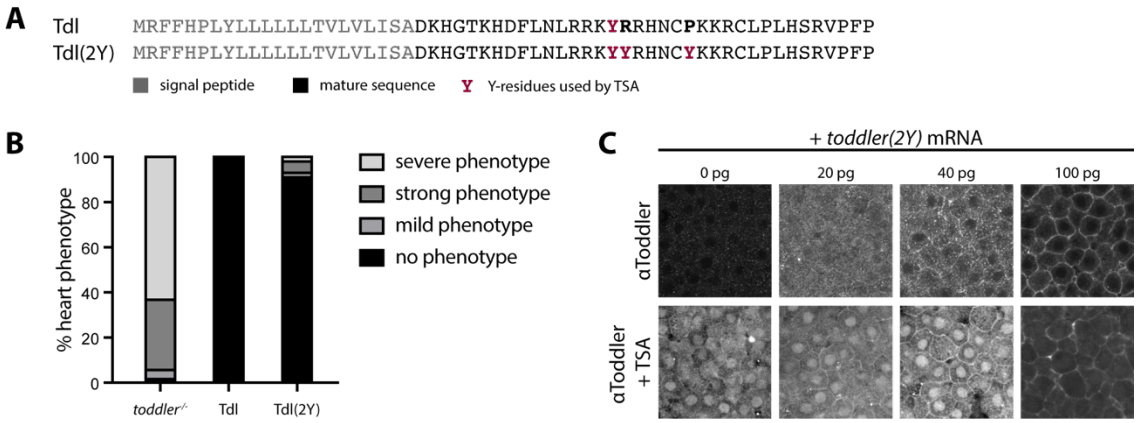

Fig. 8 | Testing the use of TSA-based signal amplification in IF assays for detection of Toddler. (A) Generation of Toddler(2Y) construct harboring two additional Y-residues. (B) *toddler*$^{-/-}$ rescue assay determining the functionality of Toddler(2Y) based on severity of the heart phenotype. (C) IF assays with (top) and without (bottom) TSA kit to amplify signal from the Toddler antibody.

3.3.1.4. Toddler overexpression in combination with signal amplification is not sufficient to reliably detect Toddler

To test the functionality of our approach, we injected *toddler*$^{-/-}$ embryos with different concentrations of *toddler* mRNA, fixed them at sphere stage overnight and then performed antibody staining in combination with the TSA kit, to amplify the signal. Indeed, we were able to detect an extracellular Toddler signal at as low as 20 pg of *toddler* mRNA injection. However, the TSA kit also introduced a significant background signal in the nucleus, in particular in conditions with lower Toddler levels (Figure 8C). As the highest possible level of Toddler overexpression only leads to a very low extracellular signal with severe nuclear background staining, we reasoned that detection and quantification of a Toddler gradient would not be possible with this method.

3.3.2. Detection of Toddler through a protein tag

3.3.2.1. N-terminally HA-tagged Toddler is functional

Previous approaches to visualize the Toddler protein have made use of a C-terminal GFP tag (Pauli et al., 2014). However, this tag rendered the protein non-functional and is therefore not suitable for the visualization of the Toddler gradient, which requires the binding and internalization of Toddler by the Apelin receptor. We reasoned that the size of the GFP tag compared to the small Toddler protein and its position at the highly conserved C-terminus could be interfering with Toddler function. While this excludes live-cell imaging of a fluorescently tagged Toddler as a feasible approach to detect the Toddler gradient, a small protein tag at the less conserved N-terminus of mature Toddler (immediately after the signal peptide cleavage site) might maintain Toddler functionality and allow the use of a better established and more sensitive antibody (Figure 9A). We therefore generated different N-terminally tagged Toddler constructs and tested their functionality. Only the HA-tagged construct

maintained its functionality and was able to rescue the *toddler*$^{-/-}$ phenotype as efficiently as untagged Toddler (Figure 9A-B).

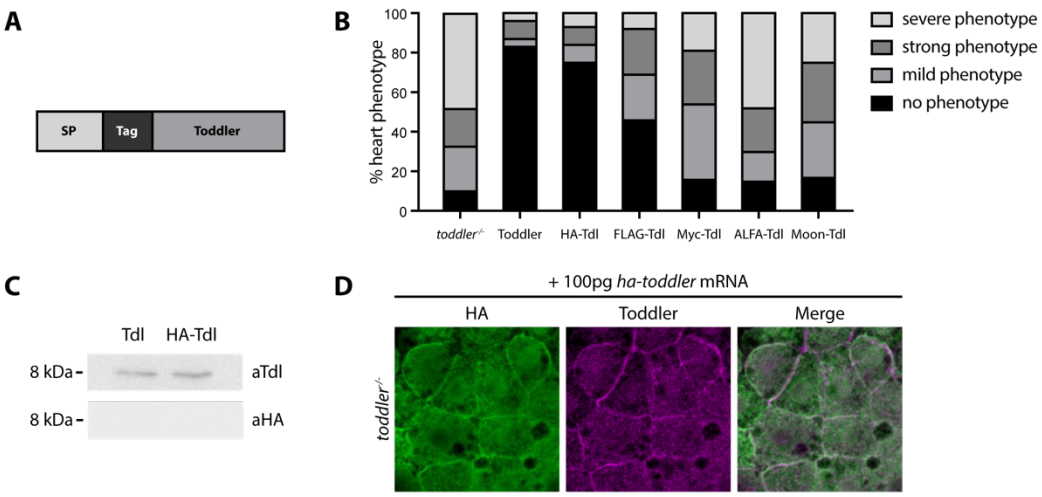

Fig. 9 | Epitope-tagging of Toddler. (A) Schematic representation of tagged Toddler constructs with the tag being inserted after the signal peptide (SP). (B) Testing the functionality of different tagged Toddler constructs based on their ability to rescue the *toddler*$^{-/-}$ phenotype. (C) Western blot analysis of embryos injected either with *toddler* or *ha-toddler* mRNA. Antibodies against Toddler and HA were used to detect HA-Toddler. (D) IF staining of *ha-toddler*-injected embryos using antibodies against Toddler and HA.

3.3.2.2. HA-tag of Toddler cannot be detected in Western blot or immunohistochemistry

To confirm the successful tagging of Toddler, we performed Western blot analysis of embryos injected with either *toddler* or *ha-toddler* mRNA. Using the Toddler antibody, we detected a specific band in both samples. However, the HA antibody was unable to detect a band in either sample (Figure 9C). Furthermore, when performing IF assays on *ha-toddler* injected embryos, HA was detected in the extracellular space but also in the cytoplasm (and more strongly in the cytoplasm than detected with the Toddler antibody) (Figure 9D). Therefore, we cannot exclude that the HA tag might be cleaved off, leading to the maintenance of Toddler's functionality, but preventing us from successfully detecting Toddler with this approach.

3.3.3. Materials and Methods

3.3.3.1. Antibody generation

Antibodies specific to Toddler were generated by immunizing rabbits (Eurogentec) with two *in vitro* synthesized peptides correlating either to the C-terminus (CMPLHSRVPFP) or N-terminus (DKHGTKHDFLNLRRKYRRHNC) of Toddler. The acquired bleeds from multiple rabbits were initially tested on a dot blot for their ability to detect Toddler. The bleeds with the best signal for either peptide were then purified against the C- and N-terminal peptide, respectively. 5 mg of peptide were dissolved in 3 mL of 20 mM Hepes and 1 mM EDTA, before being mixed with 300-310 mg maleimide-activated

POROS and flushed with argon. After 1 hour of incubation and gentle mixing at room temperature the proteins were packed into a column (4.6 x 50 mm) on HPLC using a column packer (Applied Biosystems, buffer: HBS; flow: 10 ml/min for 20-25 min). 5 ml of the antiserum were injected into the column and washed with HBS for affinity purification (monitoring at 280 nm, flow: 7.5 ml/min). Antibodies were eluted using $MgCl_2$-containing buffer (1.5 M $MgCl_2$, 50 mM NaAc, pH 5.2) for a first elution and glycine buffer (0.1 M glycine, 0.1 M NaCl, pH 2.45) for a second elution. Purified antibodies were then dialyzed using HBS buffer, stored in 10% glycerol at 4°C and tested for their reactivity against Toddler using Western blotting.

3.3.3.2. Immunostaining

For immunostaining embryos were fixed overnight in 3.7.% paraformaldehyde (PFA) at 4°C. Embryos were permeabilized the next day for 30 min at room temperature in 0.5% PBS-Tr (0.5% Triton X-100 in PBS). The samples were blocked (1% DMSO, 2% BSA, 5% NGS in PBS-Tr) and incubated overnight with primary antibody against Toddler (rabbit, 1:50, Pauli Lab) or HA (mouse, 1:100, VBC MolBio Services). Samples were washed in 0.1% PBS-Tr and incubated overnight with secondary antibodies coupled to an Alexa Fluor™ 488 or 594 (1:500, Thermo Fisher Scientific). Embryos were washed and mounted in 0.8% low melt agarose and imaged using an inverted LSM800 Axio Observer (Zeiss).

3.3.3.3. Tyramide signal amplification

The TSA kit (Alexa Fluor™ 594 Tyramide SuperBoost™ Kit, Thermo Fisher Scientific, B40925) was used according to the manufacturer's protocol. Briefly, embryos were fixed overnight in 3.7% PFA, washed, blocked, and labelled with the primary antibody as described above. Samples were stained with poly-HRP-conjugated secondary antibody overnight. After washing, embryos were incubated in tyramide working solution for 10 min at room temperature and washed after the reaction was stopped. Embryos were then mounted in 0.8% low melt agarose and imaged using an inverted LSM800 Axio Observer (Zeiss).

3.3.3.4. In situ hybridization

In situ hybridization was performed as described on page 67.

3.3.3.5. Cloning of Toddler constructs (tags and point mutations)

The *toddler* construct encoding the point mutation R39Y was generated through site-directed mutagenesis (Liu and Naismith, 2008), using the previously published PCS2+*toddler* plasmid (Pauli et al., 2014) as template and the primers toddler(R39Y)_SDM_fwd and toddler(R39Y)_SDM_rev. To introduce the second point mutation (P44Y), an additional site-directed mutagenesis was performed on the resulting plasmid using the primers toddler(P44Y)_SDM_fwd and toddler(P44Y)_SDM_rev.

Tagged Toddler constructs were generated by site-directed mutagenesis PCR using the PCS2+*toddler* plasmid as template and the primers listed below.

Table 1| primer sequences for point mutations

primer	sequence
toddler(R39Y)_SDM_fwd	TTGAGGCGGAAATATTACAGACACAACTGC
toddler(R39Y)_SDM_rev	GCAGTTGTGTCTGTAATATTTCCGCCTCAA
toddler(P44Y)_SDM_fwd	CTGCTACAAGAAACGCTGTCTACCT
toddler(P44Y)_SDM_rev	CTTGTAGCAGTTGTGTCTGCGAT

Table 2| primer sequences for tagged Toddler constructs

Tag	primer	Sequence
FLAG	FLAG-toddler_SDM_fwd	CTGGTCCTCATCAGCGCAGATGATTACAAGGATGACGATGACAAGAAACATGGTACAAAACACG
	FLAG-toddler_SDM_rev	CGTGTTTTGTACCATGTTTCTTGTCATCGTCATCCTTGTAATCATCTGCGCTGATGAGGACCAG
Myc	Myc-toddler_SDM_fwd	CTGGTCCTCATCAGCGCAGATGAACAGAAGTTAATAAGCGAAGAAGACTTAAAACATGGTACAAAACACG
	Myc-toddler_SDM_rev	CGTGTTTTGTACCATGTTTTAAGTCTTCTTCGCTTATTAACTTCTGTTCATCTGCGCTGATGAGGACCAG
BC2	BC2-toddler_SDM_fwd	CTGGTCCTCATCAGCGCAGATCCTGATCGCGTGCGCGCCGTGAGCCATTGGAGCAGCAAACATGGTACAAAACACG
	BC2-toddler_SDM_rev	CGTGTTTTGTACCATGTTTGCTGCTCCAATGGCTCACGGCGCGCACGCGATCAGGATCTGCGCTGATGAGGACCAG
ALFA	ALFA-toddler_SDM_fwd	CTGGTCCTCATCAGCGCAGATAGTCGGCTCGAGGAAGAATTGAGGCGCAGGTTGACCGAAAACATGGTACAAAACACG
	ALFA-toddler_SDM_rev	CGTGTTTTGTACCATGTTTTCGGTCAACCTGCGCCTCAATTCTTCCTCGAGCCGACTATCTGCGCTGATGAGGACCAG
Moon	Moon-toddler_SDM_fwd	CTGGTCCTCATCAGCGCAGATAAGAACGAGCAGGAACTGCTGGAGCTGGACAAATGGGCCTCTCTGAAACATGGTACAAAACACG
	Moon-toddler_SDM_rev	CGTGTTTTGTACCATGTTTCAGAGAGGCCCATTTGTCCAGCTCCAGCAGTTCCTGCTCGTTCTTATCTGCGCTGATGAGGACCAG

3.3.3.6. Western blot

Western blot was performed as described on page 68 using antibodies against Toddler (rabbit, 1:250, Pauli Lab) and HA (mouse, 1:1000, VBC MolBio Services).

4. Discussion

During my thesis I focused on understanding the role of Toddler in zebrafish development. Following up on its initial discovery as a key mediator of mesodermal progenitor migration from the margin to the animal pole during gastrulation in zebrafish embryos (Chng et al., 2013; Pauli et al., 2014), my research shed light on the molecular mechanism that is responsible for the directional guidance of mesodermal progenitor cell migration. Considering previous contradicting results supporting either the role of Toddler as a chemokine at later embryonic stages (Helker et al., 2015) or as a motogen during gastrulation (Pauli et al., 2014), we were able to reconcile these discrepancies and show that Toddler acts as a chemokine signal in a self-generated gradient that is mediated by the Apelin receptor.

4.1. A self-generated Toddler gradient guides ventrolateral mesoderm to the animal pole

The conclusion that Toddler acts as a self-generated gradient was based on several lines of evidence. First, Toddler acts in a cell non-autonomous manner, which is characteristic for chemokine signals. Transplantation of *toddler*$^{-/-}$ cells into a wild-type host embryo rescues the migration defect of Toddler-deficient cells. Therefore, the directional migration of mesodermal cells does not require the expression of Toddler in the migrating cells themselves, but rather the presence of Toddler in the extracellular space. Second, a localized Toddler source attracts Aplnrb-expressing but not Aplnr-deficient cells, confirming that Toddler can in fact act as a chemokine and that Aplnr is the corresponding chemokine receptor required to sense the signal. Third, in line with previous studies (Pauli et al., 2014), we showed that, while Toddler does act as a chemoattractant, the direction of mesoderm migration is independent of the location of the Toddler source. This strongly supports our proposed model, as one striking feature of self-generated gradients is the dependence of the direction of cell migration on the location of the sink but not on the location of the ligand source. Fourth, mesodermal cells themselves provide a sink to generate a Toddler gradient. Mesodermal cells are only able to migrate directionally to the animal pole in a collective manner, while individual cells loose directionality in the absence of surrounding mesodermal cells or simply Aplnr-expression in surrounding cells, despite the presence of Toddler. Therefore, we conclude that in addition to its chemokine sensing abilities, Aplnr is also required as a scavenger receptor to locally remove Toddler and generate a gradient that provides a directional cue towards the animal pole. Finally, using the Aplnr internalization rate of transplanted cells as an estimate for surrounding Toddler levels, we were able to detect local differences in Toddler levels at the animal pole compared to the margin in the

presence but not absence of Aplnr-expressing cells, confirming the existence of a self-generated Toddler gradient.

The mode of cell migration and the molecular mechanisms guiding migrating cells must be adapted to the complexity of the surrounding system in which cells migrate. In a 2D *in vitro* setting for example, a pre-defined chemokine gradient arising from a localized source might be the simplest way to guide the migration of cells. However, the complex environment of a gastrulating embryo poses various challenges that could not be overcome with a local source-based gradient, while the dynamic nature of a self-generated gradient can easily adapt. For example, a local source-dependent gradient can only be established over a defined length scale. A self-generated gradient, however, can adjust to a dynamic tissue size and therefore, in the case of zebrafish gastrulation, compensate for the continuous internalization of more mesodermal cells and the vegetal movement of the margin, that increases the size of the mesoderm tissue. Furthermore, unlike other described self-generated gradients that are based on two distinct receptors (e.g. during LLP migration Cxcr4b acts as the sensor and Cxcr7 as the scavenger), we provide evidence for a single receptor-based principle in the case of the Toddler gradient for mesoderm migration. While the LLP for example is a stable and tightly connected tissue that can establish defined domains to perform scavenger and sensing functions (Donà et al., 2013; Venkiteswaran et al., 2013), the dynamic nature and individual migration of mesodermal cells requires each cell to be capable to sense the gradient and steer their own migration.

4.2. Toddler is the main but potentially not only mediator of ventrolateral mesoderm migration

In *toddler*$^{-/-}$ embryos mesodermal cells fail to migrate to the animal pole as they lack their directional guidance cue, which results in the random polarization and migration of mesodermal cells. This establishes Toddler as the main driver of directed mesodermal cell migration. However, even in *toddler*$^{-/-}$ embryos, we observe a residual bias of protrusion formation towards the animal pole. Furthermore, we still detect a small expansion of the mesodermal domain towards the animal pole until three hours after the onset of cell internalization in our global cell tracking data (page 45, Fig 3H in Stock et al., 2022). While not sufficient to guide mesodermal cells, these observations indicate that—at least in the absence of Toddler—additional regulatory pathways may contribute to the animal pole-directed migration of mesodermal cells independently of Toddler and potentially independently of chemokine signals in general.

Contact inhibition of locomotion (CIL) is a well-known mediator of collective cell migration (Carmona-Fontaine et al., 2008; Roycroft and Mayor, 2016). It inhibits the formation of protrusions at cell-cell contacts and thereby steers migration away from regions of high cell density. In our global cell tracking

data of *toddler*$^{-/-}$ embryos, we detect a velocity gradient with the front cells of the mesodermal cell sheet displaying residual velocity towards the animal pole, while cells at the margin migrate less (page 45, Fig. 3H in Stock et al., 2022). This phenomenon could be explained by CIL, as cells at the margin are densely packed and in contact with neighboring cells at all sides, which would inhibit their protrusion formation. Cells at the front, however, have free space towards the animal pole, which would allow for protrusion formation and residual migration towards the animal pole. The effect of CIL should be lost as soon as cells are spread out too much and loose sufficient cell-cell contact. Indeed, this would be in line with the complete loss of mesoderm expansion in *toddler*$^{-/-}$ embryos approximately three hours after the start of cell internalization.

On the other hand, biomechanical forces have been implied in the regulation of cell migration (Hannezo and Heisenberg, 2019; Heisenberg and Bellaïche, 2013). Shear forces from fluids or neighboring cells have been shown to impose directionality on migrating cells. The overlying ectoderm could impose such forces on the mesoderm while continuously moving towards the vegetal pole. This theory is particularly intriguing as Aplnr has been implicated in mediating cell polarization in response to shear forces independently of its ligands (Kwon et al., 2016). It would be interesting in the future to examine the presence of a residual bias in mesoderm migration in embryos lacking Aplnr to determine to which extent additional, Toddler-independent mediators of this migration might still depend on Aplnr.

4.3. Potential signaling pathways downstream of Toddler and Aplnr

Aplnr was previously shown to signal trough G-proteins $G\alpha_{i/o}$ and $G\alpha_{q/11}$, as well as ß-Arrestin in a G protein-independent manner (Chapman et al., 2014). ß-Arrestin is required for the internalization of GPCRs. While functional implications for Aplnr internalization were so far unclear, our model suggests that the removal of receptor-bound Toddler for gradient formation is at least one of the reasons for the internalization of Aplnr. The downstream signaling of Aplnr that is triggered by ß-Arrestin-mediated receptor internalization, such as receptor recycling or degradation, remains to be investigated. This observation prompts a more general question for GPCR signaling on whether the modification of an extracellular signal could be a common feature, that can also be found in other GPCRs in addition to their known intracellular signaling pathways. In fact, recent work by the Sixt lab (Alanko et al., 2022) uncovered a similar mechanism for leukocyte migration in which the receptor CCR7 clears the chemokine CCL19 to generate a gradient while simultaneously sensing the self-generated gradient and mediating directed cell migration. Both of these studies combined, support a so far underappreciated role of GPCRs in modulating extracellular signals through ligand internalization in different biological contexts and organisms.

GPCRs were previously indicated to activate small GTPases, such as Rac and Cdc42, which induce actin polymerization and extension of protrusions (reviewed by Cotton and Claing, 2009). In *toddler*$^{-/-}$ embryos we detect a reduction of actin-rich protrusion formation in mesodermal cells and a loss of directional bias in protrusion formation. As the reduced number of actin-rich protrusions could be explained by an increase in cell-cell contact due to the higher cell density, we speculate that Toddler/Aplnr signaling might not be required for protrusion formation per se, but rather biases the protrusion formation towards the guidance cue, which has recently been described to be a feature of chemokine receptor signaling (Olguin-Olguin et al., 2021). Therefore, a scenario in which Aplnrb recruits small GTPases Cdc42 and Rac, or other mediators of actin polymerization to the site of activation to induce the directional formation of actin-rich protrusions is feasible, however, at this point is lacking experimental evidence.

4.4. Conservation of a self-generated Toddler chemokine gradient in other species

The migration of mesodermal progenitors away from the site of internalization at the blastopore is conserved among vertebrates (Solnica-Krezel, 2005; Solnica-Krezel and Sepich, 2012). Independently of whether the epithelial-mesenchymal-transition of these cells occurs before or after internalization, eventually they all actively migrate in an individual manner. Because this general phenomenon is conserved, it may suggest that the molecular mechanism underlying this characteristic migration behavior might be conserved, too. In fact, Toddler and Aplnr are present and conserved throughout vertebrates. However, recent studies in mice, in which mesodermal progenitors internalize at the primitive streak and subsequently migrate towards the anterior region of the embryo, have shown no obvious defects in gastrulation in the absence of Aplnr or Toddler, Apelin or both (Freyer et al., 2017). This indicates that at least in mice, Toddler and Aplnr are negligible for gastrulation movements. However, this does not exclude the possibility of redundant pathways, or a similar mechanism based on alternative chemokine-receptor pairs, that remain to be investigated.

4.5. Indications for the role of Toddler in other contexts

As described above, despite the lack of obvious gastrulation phenotypes in mice, Toddler is highly conserved among vertebrates (Chng et al., 2013; Pauli et al., 2014) and has been implicated to play a role in other processes. In general, Toddler has been shown to be involved in two main types of biological processes: cell specification and cell migration. Our study supports a major role of Toddler in the regulation of cell migration yet does not negate an additional, potentially Aplnr-independent role of Toddler in cell specification, as for example described in hESCs (Ho et al., 2015).

Regarding the role of Toddler during gastrulation, two main models had previously been proposed. First, the endoderm specification model in which the lack of animal pole-directed migration is an indirect consequence of a defect in endoderm specification resulting in a lower number of endodermal cells (Chng et al., 2013; Deshwar et al., 2016; Norris et al., 2017), and second, the mesendoderm migration model, in which the *toddler*$^{-/-}$ phenotype is caused by a migration defect of mesendodermal cells (Norris et al., 2017; Pauli et al., 2014). Previous work investigating the functionality of Nodal signaling and the importance of endodermal cell number in *toddler*$^{-/-}$ embryos already provided evidence in support of the latter model (Norris et al., 2017). Our study further solidifies that the main, if not the only role of Toddler during gastrulation is the guidance of mesodermal cells, and in consequence endodermal cells, to the animal pole. While we cannot exclude the previously suggested Toddler-independent role of Aplnr in the specification of cardiac progenitors (Deshwar et al., 2016), the defects in heart development in *toddler*$^{-/-}$ embryos could stem from the lack of animal pole-directed migration, preventing mesodermal progenitors to reach the site of cardiac specification.

In addition to animal pole-directed migration, Toddler and Aplnr were also reported to be required for the migration of cardiac progenitors and angioblasts to the dorsal midline (Helker et al., 2015; Zeng et al., 2007). At late gastrulation stages, the expression pattern of *toddler* switches from a uniform to a notochord-specific expression (Pauli et al., 2014), which is consistent with a role for Toddler in attracting Aplnr-expressing cardiac progenitors to the midline, albeit now in the form of a traditional chemokine gradient arising from a localized source at the notochord. It is important to note that the switch in *toddler* expression only occurs several hours after convergence of the mesoderm sets in. Therefore, Toddler is unlikely to be the main chemoattractant that drives convergence of mesoderm cells, but rather supports their migration once they are already near the dorsal midline, which then supersedes a self-generated gradient, as a classical chemokine gradient would be sufficient to cover these smaller distances. Since the switch of the *toddler* expression pattern occurs late during gastrulation, it also remains unclear what stops mesendodermal cells on their way to the animal pole, and what overwrites the Toddler gradient to instead induce their convergence.

Finally, it was reported in mouse cardiac development that Toddler and Aplnr are required in the vascularization of the developing heart (Sharma et al., 2017). In this context it is intriguing to speculate that a similar mechanism as seen in the migration of mesodermal cells could be at play. The coronary vessels are derived from the SV, a pool of progenitor cells that express the Aplnr, while Toddler is expressed in the epicardium, the region that needs to be colonized by the growing vessels. Theoretically, Aplnr-expressing cells could start to locally take up Toddler and thereby self-generate a gradient that allows the cells to spread out until the heart is covered. However, at this point this is

only speculative and experimental evidence needs to be acquired to understand the underlying mechanism.

4.6. Conclusions

With the discovery of a self-generated Toddler gradient, we have answered a long-standing question of developmental biology, explaining how mesodermal cells are guided to the animal pole during zebrafish gastrulation. Toddler is the first characterized guidance cue known to mediate migration of mesodermal progenitors away from the margin after internalization. This study opens several future research avenues. On the one hand, the process of migration away from the site of internalization is highly conserved, which raises the questions whether a similar mechanism, albeit not or only partially mediated by Toddler, could be in effect in other vertebrate species as well. On the other hand, this study highlights the importance and advantage of self-organizing principles, in particular self-generated gradients, to guide the migration of cell collectives in a complex *in vivo* environment and is therefore likely to be involved in other cell migration events in embryonic development, physiology and disease.

5. References

Alanko, J., Ucar, M. C., Canigova, N., Stopp, J., Schwarz, J., Merrin, J., Hannezo, E. and Sixt, M. (2022). Sinking the way: a dual role for CCR7 in collective leukocyte migration. *bioRxiv* 2022.02.22.481445.

Almuedo-Castillo, M., Bläßle, A., Mörsdorf, D., Marcon, L., Soh, G. H., Rogers, K. W., Schier, A. F. and Müller, P. (2018). Scale-invariant patterning by size-dependent inhibition of Nodal signalling. *Nature Cell Biology 2018 20:9* **20**, 1032–1042.

Andrew, N. and Insall, R. H. (2007). Chemotaxis in shallow gradients is mediated independently of PtdIns 3-kinase by biased choices between random protrusions. *Nature Cell Biology* **9**, 193–200.

Armstrong, L., Hughes, O., Yung, S., Hyslop, L., Stewart, R., Wappler, I., Peters, H., Walter, T., Stojkovic, P., Evans, J., et al. (2006). The role of PI3K/AKT, MAPK/ERK and NFκβ signalling in the maintenance of human embryonic stem cell pluripotency and viability highlighted by transcriptional profiling and functional analysis. *Human Molecular Genetics* **15**, 1894–1913.

Attisano, L. and Wrana, J. L. (2002). Signal transduction by the TGF-β superfamily. *Science (1979)* **296**, 1646–1647.

Behrndt, M., Salbreux, G., Campinho, P., Hauschild, R., Oswald, F., Roensch, J., Grill, S. W. and Heisenberg, C. P. (2012). Forces driving epithelial spreading in zebrafish gastrulation. *Science (1979)* **338**, 257–260.

Bensch, R., Song, S., Ronneberger, O. and Driever, W. (2013). Non-directional radial intercalation dominates deep cell behavior during zebrafish epiboly. *Biology Open* **2**, 845–854.

Byrne, K. M., Monsefi, N., Dawson, J. C., Degasperi, A., Bukowski-Wills, J. C., Volinsky, N., Dobrzyński, M., Birtwistle, M. R., Tsyganov, M. A., Kiyatkin, A., et al. (2016). Bistability in the Rac1, PAK, and RhoA Signaling Network Drives Actin Cytoskeleton Dynamics and Cell Motility Switches. *Cell Systems* **2**, 38–48.

Campinho, P., Behrndt, M., Ranft, J., Risler, T., Minc, N. and Heisenberg, C. P. (2013). Tension-oriented cell divisions limit anisotropic tissue tension in epithelial spreading during zebrafish epiboly. *Nature Cell Biology 2013 15:12* **15**, 1405–1414.

Carmany-Rampey, A. and Schier, A. F. (2001). Single-cell internalization during zebrafish gastrulation. *Current Biology* **11**, 1261–1265.

Carmona-Fontaine, C., Matthews, H. K., Kuriyama, S., Moreno, M., Dunn, G. A., Parsons, M., Stern, C. D. and Mayor, R. (2008). Contact inhibition of locomotion in vivo controls neural crest directional migration. *Nature* **456**, 957–961.

Chapman, N. A., Dupré, D. J. and Rainey, J. K. (2014). The apelin receptor: Physiology, pathology, cell signalling, and ligand modulation of a peptide-activated class A GPCR. *Biochemistry and Cell Biology* **92**, 431–440.

Chen, S. R. and Kimelman, D. (2000). The role of the yolk syncytial layer in germ layer patterning in zebrafish. *Development* **127**, 4681–4689.

Chen, Y. and Schier, A. F. (2002). Lefty Proteins Are Long-Range Inhibitors of Squint-Mediated Nodal Signaling. *Current Biology* **12**, 2124–2128.

Chen, H. I., Sharma, B., Akerberg, B. N., Numi, H. J., Kivelä, R., Saharinen, P., Aghajanian, H., McKay, A. S., Bogard, P. E., Chang, A. H., et al. (2014). The sinus venosus contributes to coronary vasculature through VEGFC-stimulated angiogenesis. *Development* **141**, 4500–4512.

Cheng, J. C., Miller, A. L. and Webb, S. E. (2004). Organization and function of microfilaments during late epiboly in zebrafish embryos. *Developmental Dynamics* **231**, 313–323.

Chng, S. C., Ho, L., Tian, J. and Reversade, B. (2013). ELABELA: A hormone essential for heart development signals via the apelin receptor. *Developmental Cell* **27**, 672–680.

Ciruna, B., Jenny, A., Lee, D., Mlodzik, M. and Schier, A. F. (2006). Planar cell polarity signalling couples cell division and morphogenesis during neurulation. *Nature 2006 439:7073* **439**, 220–224.

Conlon, F. L., Lyons, K. M., Takaesu, N., Barth, K. S., Kispert, A., Herrmann, B. and Robertson, E. J. (1994). A primary requirement for nodal in the formation and maintenance of the primitive streak in the mouse. *Development* **120**, 1919–1928.

Cotton, M. and Claing, A. (2009). G protein-coupled receptors stimulation and the control of cell migration. *Cellular Signalling* **21**, 1045–1053.

Deshwar, A. R., Chng, S. C., Ho, L., Reversade, B. and Scott, I. C. (2016). The Apelin receptor enhances Nodal/TGFβ signaling to ensure proper cardiac development. *Elife* **5**,.

Devreotes, P. and Horwitz, A. R. (2015). Signaling networks that regulate cell migration. *Cold Spring Harbor Perspectives in Biology* **7**,.

Diz-Muñoz, A., Krieg, M., Bergert, M., Ibarlucea-Benitez, I., Muller, D. J., Paluch, E. and Heisenberg, C. P. (2010). Control of Directed Cell Migration In Vivo by Membrane-to-Cortex Attachment. *PLOS Biology* **8**, e1000544.

Diz-Muñoz, A., Romanczuk, P., Yu, W., Bergert, M., Ivanovitch, K., Salbreux, G., Heisenberg, C. P. and Paluch, E. K. (2016). Steering cell migration by alternating blebs and actin-rich protrusions. *BMC Biology* **14**, 1–13.

Donà, E., Barry, J. D., Valentin, G., Quirin, C., Khmelinskii, A., Kunze, A., Durdu, S., Newton, L. R., Fernandez-Minan, A., Huber, W., et al. (2013). Directional tissue migration through a self-generated chemokine gradient. *Nature* **503**, 285–289.

Dosch, R., Gawantka, V., Delius, H., Blumenstock, C. and Niehrs, C. (1997). Bmp-4 acts as a morphogen in dorsoventral mesoderm patterning in Xenopus. *Development* **124**, 2325–2334.

Dougan, S. T., Warga, R. M., Kene, D. A., Schier, A. F. and Talbot, W. S. (2003). The role of the zebrafish nodal-related genes squintand cyclops in patterning of mesendoderm. *Development* **130**, 1837–1851.

Dubrulle, J., Jordan, B. M., Akhmetova, L., Farrell, J. A., Kim, S. H., Solnica-Krezel, L. and Schier, A. F. (2015). Response to nodal morphogen gradient is determined by the kinetics of target gene induction. *Elife* **2015**,.

El-Brolosy, M. A. and Stainier, D. Y. R. (2017). Genetic compensation: A phenomenon in search of mechanisms. *PLOS Genetics* **13**, e1006780.

Fan, X., Hagos, E. G., Xu, B., Sias, C., Kawakami, K., Burdine, R. D. and Dougan, S. T. (2007). Nodal signals mediate interactions between the extra-embryonic and embryonic tissues in zebrafish. *Developmental Biology* **310**, 363–378.

Farrell, J. A., Wang, Y., Riesenfeld, S. J., Shekhar, K., Regev, A. and Schier, A. F. (2018). Single-cell reconstruction of developmental trajectories during zebrafish embryogenesis. *Science (1979)* **360**, eaar3131.

Feldman, B., Gates, M. A., Egan, E. S., Dougan, S. T., Rennebeck, G., Sirotkin, H. I., Schier, A. F. and Talbot, W. S. (1998). Zebrafish organizer development and germ-layer formation require nodal-related signals. *Nature 1998 395:6698* **395**, 181–185.

Feldman, B., Dougan, S. T., Schier, A. F. and Talbot, W. S. (2000). Nodal-related signals establish mesendodermal fate and trunk neural identity in zebrafish. *Current Biology* **10**, 531–534.

Freyer, L., Hsu, C. W., Nowotschin, S., Pauli, A., Ishida, J., Kuba, K., Fukamizu, A., Schier, A. F., Hoodless, P. A., Dickinson, M. E., et al. (2017). Loss of Apela Peptide in Mice Causes Low Penetrance Embryonic Lethality and Defects in Early Mesodermal Derivatives. *Cell Reports* **20**, 2116–2130.

Gierer, A. and Meinhardt, H. (1972). A theory of biological pattern formation. *Kybernetik 1972 12:1* **12**, 30–39.

Giger, F. A. and David, N. B. (2017). Endodermal germ-layer formation through active actin-driven migration triggered by N-cadherin. *Proc Natl Acad Sci U S A* **114**, 10143–10148.

Goh, A. M., Lim, C. Y., Chiam, P. C., Li, L., Mann, M. B., Mann, K. M., Menendez, S. and Lane, D. P. (2012). Using targeted transgenic reporter mice to study promoter-specific p53 transcriptional activity. *Proc Natl Acad Sci U S A* **109**, 1685–1690.

Gray, R. S., Roszko, I. and Solnica-Krezel, L. (2011). Planar Cell Polarity: Coordinating Morphogenetic Cell Behaviors with Embryonic Polarity. *Developmental Cell* **21**, 120–133.

Gritsman, K., Zhang, J., Cheng, S., Heckscher, E., Talbot, W. S. and Schier, A. F. (1999). The EGF-CFC protein one-eyed pinhead is essential for nodal signaling. *Cell* **97**, 121–132.

Haas, P. and Gilmour, D. (2006). Chemokine Signaling Mediates Self-Organizing Tissue Migration in the Zebrafish Lateral Line. *Developmental Cell* **10**, 673–680.

Hagos, E. G. and Dougan, S. T. (2007). Time-dependent patterning of the mesoderm and endoderm by Nodal signals in zebrafish. *BMC Developmental Biology* **7**, 1–18.

Hannezo, E. and Heisenberg, C. P. (2019). Mechanochemical Feedback Loops in Development and Disease. *Cell* **178**, 12–25.

Harvey, S. A. and Smith, J. C. (2009). Visualisation and quantification of morphogen gradient formation in the zebrafish. *PLoS Biology* **7**,.

Heisenberg, C. P. and Bellaïche, Y. (2013). Forces in tissue morphogenesis and patterning. *Cell* **153**, 948.

Heisenberg, C. P., Tada, M., Rauch, G. J., Saúde, L., Concha, M. L., Geisler, R., Stemple, D. L., Smith, J. C. and Wilson, S. W. (2000). Silberblick/Wnt11 mediates convergent extension movements during zebrafish gastrulation. *Nature* **405**, 76–81.

Helker, C. S., Schuermann, A., Pollmann, C., Chng, S. C., Kiefer, F., Reversade, B. and Herzog, W. (2015). The hormonal peptide Elabela guides angioblasts to the midline during vasculogenesis. *Elife* **4**,.

Hikasa, H. and Sokol, S. Y. (2013). Wnt Signaling in Vertebrate Axis Specification. *Cold Spring Harbor Perspectives in Biology* **5**, a007955.

Hilger, D., Masureel, M. and Kobilka, B. K. (2018). Structure and dynamics of GPCR signaling complexes. *Nature Structural & Molecular Biology 2017 25:1* **25**, 4–12.

Ho, R. K. and Kimmel, C. B. (1993). Commitment of cell fate in the early zebrafish embryo. *Science (1979)* **261**, 109–111.

Ho, L., Tan, S. Y. X., Wee, S., Wu, Y., Tan, S. J. C., Ramakrishna, N. B., Chng, S. C., Nama, S., Szczerbinska, I., Chan, Y. S., et al. (2015). ELABELA Is an Endogenous Growth Factor that Sustains hESC Self-Renewal via the PI3K/AKT Pathway. *Cell Stem Cell* **17**, 435–447.

Ho, L., van Dijk, M., Chye, S. T. J., Messerschmidt, D. M., Chng, S. C., Ong, S., Yi, L. K., Boussata, S., Goh, G. H. Y., Afink, G. B., et al. (2017). ELABELA deficiency promotes preeclampsia and cardiovascular malformations in mice. *Science (1979)* **357**, 707–713.

Hong, S. K., Jang, M. K., Brown, J. L., McBride, A. A. and Feldman, B. (2011). Embryonic mesoderm and endoderm induction requires the actions of non-embryonic Nodal-related ligands and Mxtx2. *Development* **138**, 787–795.

Jia, S., Ren, Z., Li, X., Zheng, Y. and Meng, A. (2008). smad2 and smad3 Are Required for Mesendoderm Induction by Transforming Growth Factor-β/Nodal Signals in Zebrafish. *Journal of Biological Chemistry* **283**, 2418–2426.

Juan, H. and Hamada, H. (2001). Roles of nodal-lefty regulatory loops in embryonic patterning of vertebrates. *Genes to Cells* **6**, 923–930.

Keegan, B. R., Meyer, D. and Yelon, D. (2004). Organization of cardiac chamber progenitors in the zebrafish blastula. *Development* **131**, 3081–3091.

Keller, P. J., Schmidt, A. D., Wittbrodt, J. and Stelzer, E. H. K. (2008). Reconstruction of zebrafish early embryonic development by scanned light sheet microscopy. *Science (1979)* **322**, 1065–1069.

Kilian, B., Mansukoski, H., Barbosa, F. C., Ulrich, F., Tada, M. and Heisenberg, C. P. (2003). The role of Ppt/Wnt5 in regulating cell shape and movement during zebrafish gastrulation. *Mechanisms of Development* **120**, 467–476.

Kimmel, C. B., Ballard, W. W., Kimmel, S. R., Ullmann, B. and Schilling, T. F. (1995). Stages of embryonic development of the zebrafish. *Developmental Dynamics* **203**, 253–310.

Kotkamp, K., Mössner, R., Allen, A., Onichtchouk, D. and Driever, W. (2014). A Pou5f1/Oct4 dependent Klf2a, Klf2b, and Klf17 regulatory sub-network contributes to EVL and ectoderm development during zebrafish embryogenesis. *Developmental Biology* **385**, 433–447.

Krieg, M., Arboleda-Estudillo, Y., Puech, P. H., Käfer, J., Graner, F., Müller, D. J. and Heisenberg, C. P. (2008). Tensile forces govern germ-layer organization in zebrafish. *Nature Cell Biology 2008 10:4* **10**, 429–436.

Kwon, H. B., Wang, S., Helker, C. S. M., Rasouli, S. J., Maischein, H. M., Offermanns, S., Herzog, W. and Stainier, D. Y. R. (2016). In vivo modulation of endothelial polarization by Apelin receptor signalling. *Nature Communications* **7**, 11805.

Li, R. and Gundersen, G. G. (2008). Beyond polymer polarity: how the cytoskeleton builds a polarized cell. *Nature Reviews Molecular Cell Biology 2008 9:11* **9**, 860–873.

Li, M., Gou, H., Tripathi, B. K., Huang, J., Jiang, S., Dubois, W., Waybright, T., Lei, M., Shi, J. and Zhou, M. (2015). An Apela RNA-Containing Negative Feedback Loop Regulates p53-Mediated Apoptosis in Embryonic Stem Cells. *Cell Stem Cell* **16**, 669–683.

Lin, S., Baye, L. M., Westfall, T. A. and Slusarski, D. C. (2010). Wnt5b-Ryk pathway provides directional signals to regulate gastrulation movement. *Journal of Cell Biology* **190**, 263–279.

Liu, H. and Naismith, J. H. (2008). An efficient one-step site-directed deletion, insertion, single and multiple-site plasmid mutagenesis protocol. *BMC Biotechnol* **8**, 91.

Lord, N. D., Carte, A. N., Abitua, P. B. and Schier, A. F. (2021). The pattern of Nodal morphogen signaling is shaped by co-receptor expression. *Elife* **10**,.

Mayor, R. and Carmona-Fontaine, C. (2010). Keeping in touch with contact inhibition of locomotion. *Trends in Cell Biology* **20**, 319–328.

McCaffrey, L. M. and Macara, I. G. (2012). Signaling pathways in cell polarity. *Cold Spring Harbor Perspectives in Biology* **4**, 1–15.

Meno, C., Gritsman, K., Ohishi, S., Ohfuji, Y., Heckscher, E., Mochida, K., Shimono, A., Kondoh, H., Talbot, W. S., Robertson, E. J., et al. (1999). Mouse Lefty2 and Zebrafish Antivin Are Feedback Inhibitors of Nodal Signaling during Vertebrate Gastrulation. *Molecular Cell* **4**, 287–298.

Miura, T., Luo, Y., Khrebtukova, I., Brandenberger, R., Zhou, D., Thies, R. S., Vasicek, T., Young, H., Lebkowski, J., Carpenter, M. K., et al. (2004). Monitoring early differentiation events in human embryonic stem cells by massively parallel signature sequencing and expressed sequence tag scan. *Stem Cells and Development* **13**, 694–715.

Montague, T. G. and Schier, A. F. (2017). Vg1-nodal heterodimers are the endogenous inducers of mesendoderm. *Elife* **6**,.

Montero, J. A., Carvalho, L., Wilsch-Bräuninger, M., Kilian, B., Mustafa, C. and Heisenberg, C. P. (2005). Shield formation at the onset of zebrafish gastrulation. *Development* **132**, 1187–1198.

Morita, H. and Heisenberg, C. P. (2013). Holding On and Letting Go: Cadherin Turnover in Cell Intercalation. *Developmental Cell* **24**, 567–569.

Müller, P., Rogers, K. W., Jordan, B. M., Lee, J. S., Robson, D., Ramanathan, S. and Schier, A. F. (2012). Differential diffusivity of nodal and lefty underlies a reaction-diffusion patterning system. *Science (1979)* **336**, 721–724.

Myers, D. C., Sepich, D. S. and Solnica-Krezel, L. (2002). Bmp activity gradient regulates convergent extension during zebrafish gastrulation. *Developmental Biology* **243**, 81–98.

Nair, S. and Schilling, T. F. (2008). Chemokine signaling controls endodermal migration during zebrafish gastrulation. *Science* **322**, 89–92.

Neave, B., Holder, N. and Patient, R. (1997). A graded response to BMP-4 spatially coordinates patterning of the mesoderm and ectoderm in the zebrafish. *Mechanisms of Development* **62**, 183–195.

Nornes, S., Tucker, B. and Lardelli, M. (2009). Zebrafish aplnra functions in epiboly. *BMC Research Notes* **2**,.

Norris, M. L., Pauli, A., Gagnon, J. A., Lord, N. D., Rogers, K. W., Mosimann, C., Zon, L. I. and Schier, A. F. (2017). Toddler signaling regulates mesodermal cell migration downstream of Nodal signaling. *Elife* **6**,.

O'Dowd, B. F., Heiber, M., Chan, A., Heng, H. H. Q., Tsui, L. C., Kennedy, J. L., Shi, X., Petronis, A., George, S. R. and Nguyen, T. (1993). A human gene that shows identity with the gene encoding the angiotensin receptor is located on chromosome 11. *Gene* **136**, 355–360.

Ogata, S., Morokuma, J., Hayata, T., Kolle, G., Niehrs, C., Ueno, N. and Cho, K. W. Y. (2007). TGF-β signaling-mediated morphogenesis: modulation of cell adhesion via cadherin endocytosis. *Genes & Development* **21**, 1817–1831.

Olguin-Olguin, A., Aalto, A., Maugis, B., Boquet-Pujadas, A., Hoffmann, D., Ermlich, L., Betz, T., Gov, N. S., Reichman-Fried, M. and Raz, E. (2021). Chemokine-biased robust self-organizing polarization of migrating cells in vivo. *Proc Natl Acad Sci U S A* **118**,.

Paluch, E. K. and Raz, E. (2013). The role and regulation of blebs in cell migration. *Current Opinion in Cell Biology* **25**, 582–590.

Paskaradevan, S. and Scott, I. C. (2012). The Aplnr GPCR regulates myocardial progenitor development via a novel cell-non-autonomous, G i/o protein-independent pathway. *Biology Open* **1**, 275–285.

Pauli, A., Norris, M. L., Valen, E., Chew, G. L., Gagnon, J. A., Zimmerman, S., Mitchell, A., Ma, J., Dubrulle, J., Reyon, D., et al. (2014). Toddler: An embryonic signal that promotes cell movement via apelin receptors. *Science (1979)* **343**,.

Pertz, O., Hodgson, L., Klemke, R. L. and Hahn, K. M. (2006). Spatiotemporal dynamics of RhoA activity in migrating cells. *Nature* **440**, 1069–1072.

Petridou, N. I., Grigolon, S., Salbreux, G., Hannezo, E. and Heisenberg, C. P. (2019). Fluidization-mediated tissue spreading by mitotic cell rounding and non-canonical Wnt signalling. *Nat Cell Biol* **21**, 169–178.

Red-Horse, K., Ueno, H., Weissman, I. L. and Krasnow, M. A. (2010). Coronary arteries form by developmental reprogramming of venous cells. *Nature 2010 464:7288* **464**, 549–553.

Reissmann, E., Jörnvall, H., Blokzijl, A., Andersson, O., Chang, C., Minchiotti, G., Persico, M. G., Ibáñez, C. F. and Brivanlou, A. H. (2001). The orphan receptor ALK7 and the Activin receptor ALK4 mediate signaling by Nodal proteins during vertebrate development. *Genes & Development* **15**, 2010–2022.

Renkawitz, J., Kopf, A., Stopp, J., de Vries, I., Driscoll, M. K., Merrin, J., Hauschild, R., Welf, E. S., Danuser, G., Fiolka, R., et al. (2019). Nuclear positioning facilitates amoeboid migration along the path of least resistance. *Nature* **568**, 546–550.

Ridley, A. J., Schwartz, M. A., Burridge, K., Firtel, R. A., Ginsberg, M. H., Borisy, G., Parsons, J. T. and Horwitz, A. R. (2003). Cell Migration: Integrating Signals from Front to Back. *Science (1979)* **302**, 1704–1709.

Rohde, L. A. and Heisenberg, C. P. (2007). Zebrafish Gastrulation: Cell Movements, Signals, and Mechanisms. *International Review of Cytology* **261**, 159–192.

Roszko, I., Sepich, D. S., Jessen, J. R., Chandrasekhar, A. and Solnica-Krezel, L. (2015). A dynamic intracellular distribution of Vangl2 accompanies cell polarization during zebrafish gastrulation. *Development (Cambridge)* **142**, 2508–2520.

Row, R. H., Maître, J. L., Martin, B. L., Stockinger, P., Heisenberg, C. P. and Kimelman, D. (2011). Completion of the epithelial to mesenchymal transition in zebrafish mesoderm requires Spadetail. *Developmental Biology* **354**, 102–110.

Roycroft, A. and Mayor, R. (2016). Molecular basis of contact inhibition of locomotion. *Cellular and Molecular Life Sciences* **73**, 1119–1130.

Schier, A. F. and Shen, M. M. (2000). Nodal signalling in vertebrate development. *Nature 2000 403:6768* **403**, 385–389.

Schier, A. F. and Talbot, W. S. (2005). Molecular Genetics of Axis Formation in Zebrafish. *Annual Review of Genetics* **39**, 561–613.

Schier, A. F., Neuhauss, S. C., Helde, K. A., Talbot, W. S. and Driever, W. (1997). The one-eyed pinhead gene functions in mesoderm and endoderm formation in zebrafish and interacts with no tail. *Development* **124**, 327–342.

Schneider, S., Steinbeisser, H., Warga, R. M. and Hausen, P. (1996). β-catenin translocation into nuclei demarcates the dorsalizing centers in frog and fish embryos. *Mechanisms of Development* **57**, 191–198.

Scott, I. C., Masri, B., D'Amico, L. A., Jin, S. W., Jungblut, B., Wehman, A. M., Baier, H., Audigier, Y. and Stainier, D. Y. R. (2007). The G Protein-Coupled Receptor Agtrl1b Regulates Early Development of Myocardial Progenitors. *Developmental Cell* **12**, 403–413.

Sepich, D. S., Calmelet, C., Kiskowski, M. and Solnica-Krezel, L. (2005). Initiation of convergence and extension movements of lateral mesoderm during zebrafish gastrulation. *Developmental Dynamics* **234**, 279–292.

Sharma, B., Ho, L., Ford, G. H., Chen, H. I., Goldstone, A. B., Woo, Y. J., Quertermous, T., Reversade, B. and Red-Horse, K. (2017). Alternative Progenitor Cells Compensate to Rebuild the Coronary Vasculature in Elabela- and Apj-Deficient Hearts. *Developmental Cell* **42**, 655-666.e3.

Shi, Y. and Massagué, J. (2003). Mechanisms of TGF-β Signaling from Cell Membrane to the Nucleus. *Cell* **113**, 685–700.

Solnica-Krezel, L. (2005). Conserved patterns of cell movements during vertebrate gastrulation. *Current Biology* **15**,.

Solnica-Krezel, L. and Sepich, D. S. (2012). Gastrulation: Making and Shaping Germ Layers. *Annu. Rev. Cell Dev. Biol* **28**, 687–717.

Stainier, D. Y. R., Raz, E., Lawson, N. D., Ekker, S. C., Burdine, R. D., Eisen, J. S., Ingham, P. W., Schulte-Merker, S., Yelon, D., Weinstein, B. M., et al. (2017). Guidelines for morpholino use in zebrafish. *PLOS Genetics* **13**, e1007000.

Stock, J. and Pauli, A. (2021). Self-organized cell migration across scales – from single cell movement to tissue formation. *Development (Cambridge)* **148**, dev191767.

Sztal, T. E. and Stainier, Y. R. (2020). Transcriptional adaptation: A mechanism underlying genetic robustness. *Development (Cambridge)* **147**,.

Tatemoto, K., Hosoya, M., Habata, Y., Fujii, R., Kakegawa, T., Zou, M. X., Kawamata, Y., Fukusumi, S., Hinuma, S., Kitada, C., et al. (1998). Isolation and Characterization of a Novel Endogenous Peptide Ligand for the Human APJ Receptor. *Biochemical and Biophysical Research Communications* **251**, 471–476.

Theisen, U., Straube, E. and Straube, A. (2012). Directional Persistence of Migrating Cells Requires Kif1C-Mediated Stabilization of Trailing Adhesions. *Developmental Cell* **23**, 1153–1166.

Thisse, C., Thisse, B., Halpern, M. E. and Postlethwait, J. H. (1994). goosecoid Expression in neurectoderm and mesendoderm is disrupted in zebrafish cyclops gastrulas. *Developmental Biology* **164**, 420–429.

Thisse, B., Wright, C. V. E. and Thisse, C. (2000). Activin- and Nodal-related factors control antero–posterior patterning of the zebrafish embryo. *Nature 2000 403:6768* **403**, 425–428.

Tucker, B., Hepperle, C., Kortschak, D., Rainbird, B., Wells, S., Oates, A. C. and Lardelli, M. (2007). Zebrafish Angiotensin II Receptor-like 1a (agtrl1a) is expressed in migrating hypoblast, vasculature, and in multiple embryonic epithelia. *Gene Expression Patterns* **7**, 258–265.

Tweedy, L. and Insall, R. H. (2020). Self-Generated Gradients Yield Exceptionally Robust Steering Cues. *Frontiers in Cell and Developmental Biology* **8**, 133.

Tweedy, L., Knecht, D. A., Mackay, G. M. and Insall, R. H. (2016a). Self-Generated Chemoattractant Gradients: Attractant Depletion Extends the Range and Robustness of Chemotaxis. *PLoS Biology* **14**, e1002404.

Tweedy, L., Susanto, O. and Insall, R. H. (2016b). Self-generated chemotactic gradients - cells steering themselves. *Current Opinion in Cell Biology* **42**, 46–51.

Ulrich, F., Concha, M. L., Heid, P. J., Voss, E., Witzel, S., Roehl, H., Tada, M., Wilson, S. W., Adams, R. J., Soll, D. R., et al. (2003). Slb/Wnt11 controls hypoblast cell migration and morphogenesis at the onset of zebrafish gastrulation. *Development* **130**, 5375–5384.

Ulrich, F., Krieg, M., Schötz, E. M., Link, V., Castanon, I., Schnabel, V., Taubenberger, A., Mueller, D., Puech, P. H. and Heisenberg, C. P. (2005). Wnt11 Functions in Gastrulation by Controlling Cell Cohesion through Rab5c and E-Cadherin. *Developmental Cell* **9**, 555–564.

van Boxtel, A. L., Chesebro, J. E., Heliot, C., Ramel, M. C., Stone, R. K. and Hill, C. S. (2015). A Temporal Window for Signal Activation Dictates the Dimensions of a Nodal Signaling Domain. *Developmental Cell* **35**, 175–185.

van Boxtel, A. L., Economou, A. D., Heliot, C. and Hill, C. S. (2018). Long-Range Signaling Activation and Local Inhibition Separate the Mesoderm and Endoderm Lineages. *Dev Cell* **44**, 179–191.

van Haastert, P. J. M. and Devreotes, P. N. (2004). Chemotaxis: Signalling the way forward. *Nature Reviews Molecular Cell Biology* **5**, 626–634.

Venkiteswaran, G., Lewellis, S. W., Wang, J., Reynolds, E., Nicholson, C. and Knaut, H. (2013). Generation and dynamics of an endogenous, self-generated signaling gradient across a migrating tissue. *Cell* **155**, 674.

Wang, L., Zhang, Y., Qu, H., Xu, F., Hu, H., Zhang, Q. and Ye, Y. (2019). Reduced ELABELA expression attenuates trophoblast invasion through the PI3K/AKT/mTOR pathway in early onset preeclampsia. *Placenta* **87**, 38–45.

Wong, M., Newton, L. R., Hartmann, J., Hennrich, M. L., Wachsmuth, M., Ronchi, P., Guzmán-Herrera, A., Schwab, Y., Gavin, A. C. and Gilmour, D. (2020). Dynamic Buffering of Extracellular Chemokine by a Dedicated Scavenger Pathway Enables Robust Adaptation during Directed Tissue Migration. *Developmental Cell* **52**, 492-508.e10.

Xiong, F., Ma, W., Hiscock, T. W., Mosaliganti, K. R., Tentner, A. R., Brakke, K. A., Rannou, N., Gelas, A., Souhait, L., Swinburne, I. A., et al. (2014). Interplay of Cell Shape and Division Orientation Promotes Robust Morphogenesis of Developing Epithelia. *Cell* **159**, 415–427.

Yamada, K. M. and Sixt, M. (2019). Mechanisms of 3D cell migration. *Nature Reviews Molecular Cell Biology* **20**, 738–752.

Yin, C., Kiskowski, M., Pouille, P. A., Farge, E. and Solnica-Krezel, L. (2008). Cooperation of polarized cell intercalations drives convergence and extension of presomitic mesoderm during zebrafish gastrulation. *Journal of Cell Biology* **180**, 221–232.

Zeng, X. X. I., Wilm, T. P., Sepich, D. S. and Solnica-Krezel, L. (2007). Apelin and Its Receptor Control Heart Field Formation during Zebrafish Gastrulation. *Developmental Cell* **12**, 391–402.

Zhang, C. and Klymkowsky, M. W. (2007). The Sox axis, Nodal signaling, and germ layer specification. *Differentiation* **75**, 536–545.

Zhang, J., Talbot, W. S. and Schier, A. F. (1998). Positional Cloning Identifies Zebrafish one-eyed pinhead as a Permissive EGF-Related Ligand Required during Gastrulation. *Cell* **92**, 241–251.

Zhou, J., Su, P., Wang, L., Chen, J., Zimmermann, M., Genbacev, O., Afonja, O., Horne, M. C., Tanaka, T., Duan, E., et al. (2009). mTOR supports long-term self-renewal and suppresses mesoderm and endoderm activities of human embryonic stem cells. *Proc Natl Acad Sci U S A* **106**, 7840–7845.

Zinski, J., Tajer, B. and Mullins, M. C. (2018). TGF-β Family Signaling in Early Vertebrate Development. *Cold Spring Harbor Perspectives in Biology* **10**, a033274.